Contents lists available at ScienceDirect

Annual Reviews in Control

journal homepage: www.elsevier.com/locate/arcontrol

Review article

Modeling and control of overhead cranes: A tutorial overview and perspectives

Mohammad Rasool Mojallizadeh [a,*], Bernard Brogliato [a], Christophe Prieur [b]

[a] Univ. Grenoble Alpes, INRIA, CNRS, Grenoble INP, LJK, 38000 Grenoble, France
[b] Univ. Grenoble Alpes, CNRS, GIPSA-Lab, 38000 Grenoble, France

ARTICLE INFO

Keywords:
Overhead cranes
Antisway
Underactuation
Control
Modeling

ABSTRACT

This article presents a complete review of the modeling and control schemes for overhead cranes operating in 2D and 3D spaces published to date. The modeling schemes including the pendulum-like models with rigid and flexible links are reviewed and their key characteristics are studied. Subsequently, an overview of the control methods developed for such models is presented. Afterward, a new simulation-oriented model enabling to capture both cables' dynamic and global nonlinearities caused by the pendulation is developed, and different control methods that exist in the literature are evaluated and compared based on this model using numerical experiments. In the end, several research gaps are identified to be considered in future works.

1. Introduction

Overhead cranes (OC) are widely employed in factories and construction sites in order to manipulate heavy objects within the workspace. A typical OC is composed of a cart (trolley) moving on a line or plane. A tool, *e.g.*, a hook, is suspended to the cart through several cables, as shown in Fig. 1 (Ramli, Mohamed, Abdullahi, Jaafar, & Lazim, 2017). Accurate modeling and control of OCs are challenging because of underactuation (Liu & Yu, 2013; Tafrishi, Svinin, & Yamamoto, 2021), and cables' dynamics (Kamman & Huston, 2001; Khalilpour, Khorrambakht, Damirchi, Taghirad, & Cardou, 2021; Lv, Liu, Xia, Ma, & Yang, 2020). Moreover, different types of payloads, swaying around different axes observed in 3-dimensional (3D) operating space, add complexity to the problem. OCs require a precise controller design in order to guarantee an accurate and safe operation. A mathematical model is usually required to design such a controller (Abdel-Rahman, Nayfeh, & Masoud, 2003). Moreover, a realistic model helps to evaluate the controllers' performances using numerical simulations before practical implementations. Hence, mathematical modeling is an unavoidable part of the topic. The OCs are usually modeled based on the pendulum-like models, *i.e.,* single or double-pendulum systems as shown in Fig. 2(a, b) (Ramli et al., 2017). According to the literature, most references deal with the single-pendulum model because of its simplicity. However, in the presence of heavy tools, the single pendulum model is unable to encapsulate the system's behavior since two sway angles appear in the system as shown in Fig. 2(b). A large number of references considered the double-pendulum model to take the tool's effect into account. The modeling has also been tackled from different points of view, including modeling the cables' flexibility (Fig. 2(c)) (d'Andréa Novel, Moyano, & Rosier, 2019), kinematic modeling corresponding to the multi-cable cranes (Arena, Casalotti, Lacarbonara, & Cartmell, 2015), *etc*. The models are then used for the controller design and numerical simulation. The modeling schemes will be deeply reviewed in Section 2.

A control scheme, in this topic, is mainly designed to control the payload position and orientation. Such a controller, in a general classification, is designed based on open-loop, collocated and noncollocated control structures (Ramli et al., 2017). The open-loop control scheme is easy to implement and is designed to avoid excitation of the systems' natural frequencies causing oscillations. Closed-loop methods, on the other hand, are developed to ensure stability and robustness (Damaren, 1999). These control strategies as well as their characteristics will be studied in detail in Section 3.

Reviewing the mentioned modeling and control methods was the topic of some references including the commercial ones available in the market (Ramli et al., 2017). In addition, modeling of several cranes' structures, as well as an introduction to the relevant controllers, have been presented in Abdel-Rahman and Nayfeh (2002). However, choosing and using the most appropriate modeling and control method, for each specific case is still almost impossible without a comprehensive guideline. This issue will be addressed in this study. Compared to other surveys on this subject (see Table 9), the main contributions of this work are as follows:

* Corresponding author.
E-mail addresses: mohammad-rasool.mojallizadeh@inria.fr (M.R. Mojallizadeh), bernard.brogliato@inria.fr (B. Brogliato), Christophe.Prieur@gipsa-lab.fr (C. Prieur).

https://doi.org/10.1016/j.arcontrol.2023.03.002
Received 17 October 2022; Received in revised form 21 February 2023; Accepted 1 March 2023

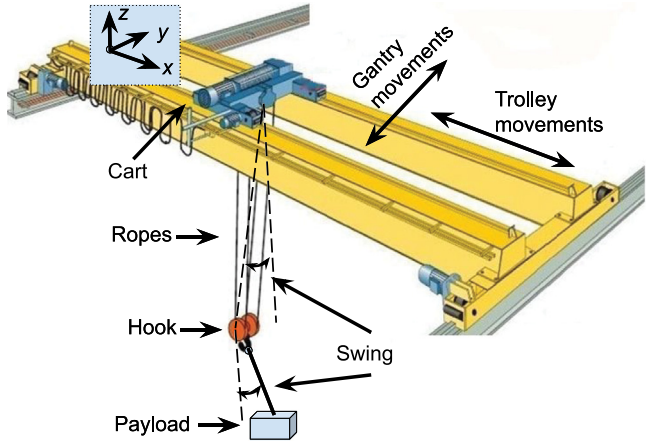

Fig. 1. Schematic diagram of a typical OC in 3D operating space.

- Dynamical models are presented in detail in 2D and 3D operational spaces, for fixed and variable links' lengths, for single-pendulum and double-pendulum systems, and one case with varying mass is treated.
- The control strategies are categorized into several groups, depending on their structure. The structures are then studied to extract their key properties. Subsequently, some controllers from each group have been selected, and comparative analyses are made among them through numerical experiments;
- A toolbox prototype has been developed, using the MATLAB Multibody and Optimization toolboxes, see Section 7.1. It is based on a 20-pendulum model of the cable (both in 2D and 3D operational spaces). As pointed out in Section 8, this is certainly not sufficient to get reliable results in all operating conditions. This is however expected to pave the way toward a more complete toolbox (incorporating, for instance, finite-element cable's models). To the best of the authors' knowledge, it is the first time that such an effort is made to better understand (at least numerically) how controllers behave when applied on more complex models than (2), (3) and (6) below. It also provides a preliminary way to tune the controllers' gains;
- The control methods are evaluated based on the simulation-oriented model enabling to capture both global nonlinearities and local vibrations (within a limited spectrum) observed in OCs due to the cables' flexibility. Hence, it is expected that the numerical simulations based on this model lead to more realistic results compared to the studies where control-oriented models (single and double-pendulum models) are used for the simulations;
- Several research gaps are identified, in the end, and presented as possible topics for future studies.

The remainder of this manuscript is structured as follows. An introduction to the modeling schemes and their properties are presented in Section 2. Subsequently, the control methods introduced in the literature are classified in Section 3. The simulation-oriented model is developed in Section 5. Afterward, the comparisons based on the numerical experiments are then presented in Section 7, and an engineering guideline is provided to enable one to select an appropriate method for each case. In the end, the conclusions are drawn, in Section 8, and several research gaps are identified to be addressed in future studies. Details on the Lagrange dynamics of the 2D and 3D pendulums' models with varying assumptions (constant, variable links' lengths) are given in Appendix A through Appendix F. Appendix G contains some technical computations useful for some control designs. Finally, the computer software developed in this work will be briefly introduced in Appendix H.

2. Review of the mathematical modeling developed for OCs

A summary of the models developed for the OCs are presented in Sections 2.1 to 2.4, and the properties of such models are discussed in Section 2.5. As is well-known (Brogliato, Lozano, Maschke, & Egeland, 2020a), the Lagrange dynamics (or Euler–Lagrange, or Lagrange of the second kind, or Lagrangian control system) of a multibody system can be rewritten as:

$$M(q)\ddot{q} + C(q,\dot{q})\dot{q} + G(q) = Q, \tag{1}$$

where $q \in \mathbb{R}^n$ is a vector of minimal generalized coordinates, $M(q) = M^\top(q)$ is the mass matrix (usually assumed to be $\succ 0$, but it may be $\succcurlyeq 0$ in some cases), $C(q,\dot{q})\dot{q}$ contains centrifugal and Coriolis nonlinear generalized forces, $-G(q) = -\frac{\partial U}{\partial q}$ is the vector of generalized forces that derive from a potential (gravity, elasticity, *etc*). The generalized coordinate q definition varies depending on the modeling assumptions, as well as the vector of generalized forces Q. In the next sections and in the appendix, Lagrange dynamics of several lumped-mass multibody models are presented and discussed.

2.1. Single-pendulum models

Most of the reviewed references used the single-pendulum model for OCs (see Fig. 2(a)). Its dynamical equations are as follows:

$$\begin{cases} (a)\ (m+m_1)\ddot{x} + m_1 l_1 \ddot{\theta}_1 \cos(\theta_1) - m_1 l_1 \dot{\theta}_1^2 \sin(\theta_1) = F - f_r \\ (b)\ m_1 l_1^2 \ddot{\theta}_1 + m_1 l_1 \cos(\theta_1)\ddot{x} + m_1 g l_1 \sin(\theta_1) = 0, \end{cases} \tag{2}$$

where $q = (x,\theta_1)^\top$, m and m_1 represent the cart and payload masses, l_1 is the cable's length, F is the force applied to the cart, f_r is the friction force, g is the gravity constant, θ_1 is the sway angle, and x is the cart position. The references using (2) are listed in Table 2. Remark that (2) can be generalized to the case when the cable's length is variable as follows (Lee, 2004; Sun & Fang, 2014b):

$$\begin{cases} (a)\ (m+m_1)\ddot{x} + m_1 l_1 \ddot{\theta}_1 \cos(\theta_1) + m_1 \ddot{l}_1 \sin(\theta_1) + 2m_1 \dot{l}_1 \dot{\theta}_1 \cos(\theta_1) \\ \quad - m l \dot{\theta}_1^2 \sin(\theta_1) = F - f_r \\ (b)\ m_1 \ddot{l}_1 + m_1 \sin(\theta_1)\ddot{x} - m_1 l_1 \dot{\theta}_1^2 - m_1 g \cos(\theta_1) = F_l \\ (c)\ m_1 l_1^2 \ddot{\theta}_1 + m_1 l_1 \cos(\theta_1)\ddot{x} + 2m l_1 \dot{l}_1 \dot{\theta}_1 + m g l_1 \sin(\theta_1) = 0, \end{cases} \tag{3}$$

where $q = (x, l_1, \theta_1)^\top$, F_l is the force input on the hoisting mechanism (if any: let us remind that l_1 may vary also because of elasticity, see Appendix A). A different choice for q can be made, using the winch mechanism pulley radius and angle of rotation instead of l_1 (Shen, Schatz, & Caverly, 2021). The references considering such a model are indicated by the letter l in the sixth column in Table 2. Following the references presented in Table 5, (2) can be generalized to the 3D operating space as follows (Sun, Fang, & Zhang, 2013; Wu, He, Sun, & Fang, 2014) (see Fig. 3(a) for the notation):

$$\begin{cases} (a)\ (m+m_1)\ddot{x} + m l_1 \ddot{\theta}_x \cos(\theta_x)\cos(\theta_y) - m l_1 \ddot{\theta}_y \sin(\theta_y)\sin(\theta_y) - m l_1 \dot{\theta}_x^2 \sin(\theta_x)\cos(\theta_y) \\ \qquad - 2m l_1 \dot{\theta}_x \dot{\theta}_y \cos(\theta_x)\sin(\theta_y) - m l_1 \dot{\theta}_y^2 \sin(\theta_x)\cos(\theta_y) = F_x - f_{rx} \\ (b)\ (m+m_1)\ddot{y} + m l_1 \ddot{\theta}_y \cos(\theta_y) - m l_1 \sin(\theta_y)\dot{\theta}_y^2 = F_y - f_{ry} \\ (c)\ m l_1 \ddot{x}\cos(\theta_x)\cos(\theta_y) + m l_1^2 \ddot{\theta}_x \cos^2(\theta_y) \\ \quad - 2m l_1^2 \dot{\theta}_x \dot{\theta}_y \sin(\theta_y)\cos(\theta_y) + m g l_1 \sin(\theta_x)\cos(\theta_y) = 0 \\ (d)\ m l_1 \ddot{x}\sin(\theta_x)\sin(\theta_y) - m l_1 \ddot{y}\cos(\theta_y) \\ \quad - m l_1^2 \ddot{\theta}_y - m l_1^2 \sin(\theta_y)\cos(\theta_y)\dot{\theta}_x^2 - m g l_1 \cos(\theta_x)\sin(\theta_y) = 0, \end{cases} \tag{4}$$

where $q = (x, y, \theta_x, \theta_y)^\top$, F_x and F_y are the forces on the trolley toward x and y axes, respectively, f_{rx} and f_{ry} are the friction forces toward x and y axes, respectively, θ_x and θ_y are the sway angles with respect to the x and y axes, respectively. In case of varying link's length (but constant total mass), the single-pendulum 3D dynamics take the

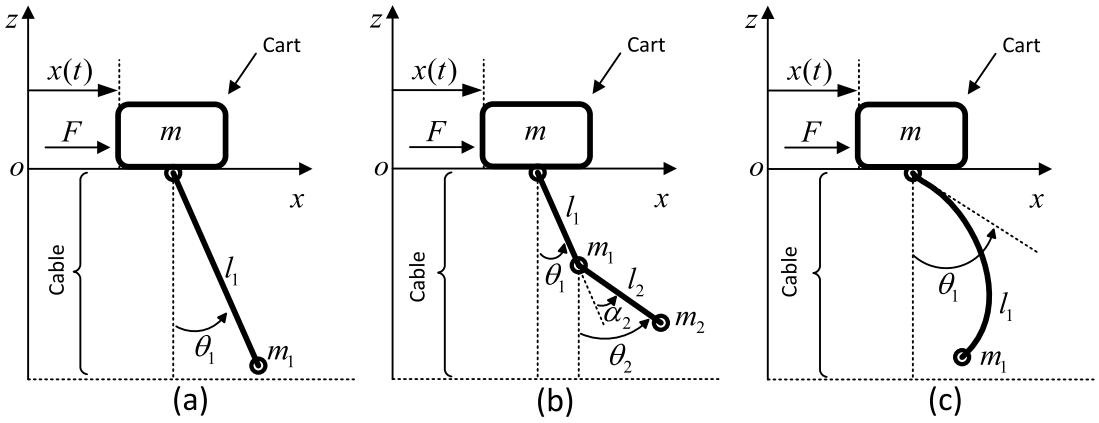

Fig. 2. 2D models used for OCs (a) single-pendulum (b) double-pendulum (c) flexible pendulum models.

form (Almutairi & Zribi, 2009; Brogliato, 2022; Lee, 1998) (see Fig. 3 (a) for an illustration of the notation):

$$\begin{cases}
(a)\ (m+m_1)\ddot{x} + m_1 l_1 \cos(\theta_x)\cos(\theta_y)\ddot{\theta}_x - m_1 l_1 \sin(\theta_x)\sin(\theta_y)\ddot{\theta}_y \\
+m_1 \sin(\theta_x)\cos(\theta_y)\ddot{l}_1 + \\
\quad +2m_1 \cos(\theta_x)\cos(\theta_y)\dot{l}_1\dot{\theta}_x - 2m_1 \sin(\theta_x)\sin(\theta_y)\dot{l}_1\dot{\theta}_y \\
-m_1 l_1 \sin(\theta_x)\cos(\theta_y)\dot{\theta}_x^2 - m_1 l_1 \sin(\theta_x)\cos(\theta_y)\dot{\theta}_y^2 \\
\quad -2m_1 l_1 \cos(\theta_x)\sin(\theta_y)\dot{\theta}_x\dot{\theta}_y = F_x - f_{rx} \\
(b)\ (m+m_1)\ddot{y} + m_1 l_1 \cos(\theta_y)\ddot{\theta}_y + m_1 \sin(\theta_y)\ddot{l}_1 + 2m_1 \cos(\theta_y)\dot{l}_1\dot{\theta}_y \\
-m_1 l_1 \sin(\theta_y)\dot{\theta}_y^2 = F_y - f_{ry} \\
(c)\ m_1 l_1 \cos(\theta_x)\cos(\theta_y)\ddot{x} + m_1 l_1^2 \cos^2(\theta_y)\ddot{\theta}_x + 2m_1 l_1 \cos^2(\theta_y)\dot{l}_1\dot{\theta}_x \\
-2m_1 l_1^2 \sin(\theta_y)\cos(\theta_y)\dot{\theta}_x\dot{\theta}_y \\
\quad +m_1 g l_1 \sin(\theta_x)\cos(\theta_y) = 0 \\
(d)\ -m_1 l_1 \sin(\theta_x)\sin(\theta_y)\ddot{x} + m_1 l_1 \cos(\theta_y)\ddot{y} + m_1 l_1^2 \ddot{\theta}_y \\
+m_1 l_1^2 \cos(\theta_y)\sin(\theta_y)\dot{\theta}_x^2 + 2m_1 l_1 \dot{l}_1\dot{\theta}_y \\
\quad +m_1 g l_1 \cos(\theta_x)\sin(\theta_y) = 0 \\
(e)\ m_1 \sin(\theta_x)\cos(\theta_y)\ddot{x} + m_1 \sin(\theta_y)\ddot{y} + m_1\ddot{l}_1 \\
-m_1 l_1 \cos^2(\theta_y)\dot{\theta}_x^2 - m_1 l_1 \dot{\theta}_y^2 + m_1 g \cos(\theta_x)\cos(\theta_y) = F_l
\end{cases} \tag{5}$$

where $q = (x, y, \theta_x, \theta_y, l_1)^\top$, F_x, F_y and F_l are as above. The kinetic energy and the specific form of the matrix $C(q,\dot{q})$ yielding the skew-symmetry property (useful for passivity-based control design) are given in Appendix C. The dynamics (5) are derived with a different pair of angles in Chwa (2009).

2.2. Double-pendulum models

This model is depicted in Fig. 2(b) in 2D operational space. Compared to (2), the effect of the tool can be considered. The dynamical equations corresponding to this model with constant links' lengths and constant masses are as follows with $q = (x, \theta_1, \theta_2)^\top$ (Sun, Fang, Chen, & Lu, 2017):

$$\begin{cases}
(a)\ (m+m_1+m_2)\ddot{x} + (m_1+m_2)l_1\left(\ddot{\theta}_1\cos(\theta_1) - \dot{\theta}_1^2\sin(\theta_1)\right) \\
\qquad + m_2 l_2\ddot{\theta}_2\cos(\theta_2) - m_2 l_2\dot{\theta}_2^2\sin(\theta_2) = F - f_r \\
(b)\ (m_1+m_2)l_1\cos(\theta_1)\ddot{x} + (m_1+m_2)l_1^2\ddot{\theta}_1 + m_2 l_1 l_2\cos(\theta_1-\theta_2)\ddot{\theta}_2 \\
\qquad + m_2 l_1 l_2\sin(\theta_1-\theta_2)\dot{\theta}_2^2 + (m_1+m_2)g l_1\sin(\theta_1) = 0 \\
(c)\ m_2 l_2\cos(\theta_2)\ddot{x} + m_2 l_1 l_2\ddot{\theta}_1\cos(\theta_1-\theta_2) + m_2 l_2^2\ddot{\theta}_2 \\
\qquad - m_2 l_1 l_2\sin(\theta_1-\theta_2)\dot{\theta}_1^2 + m_2 g l_2\sin(\theta_2) = 0,
\end{cases} \tag{6}$$

where m, m_1, m_2 are the cart, tool and payload masses, respectively, θ_1 and θ_2 are the primary and secondary sway angles, respectively, l_1 and l_2 are the (constant) lengths of the cable and (constant) distance between the tool and the payload, respectively. Eq. (6) has been considered by the references listed in Table 3. Such a model can be generalized to the case where the lengths of the links are variable as indicated by the letter l in the sixth column of Table 3. Moreover, the 3D form of this equation has been used by the references shown in Table 6. The mass matrix in 2D operational space and N links with varying lengths, is obtained in Appendix A. The mass matrix and the nonlinear inertial forces/torques are detailed for the double-pendulum in 2D operational space and with varying lengths l_1 and l_2 in Appendix B, for the 3D operational space with constant lengths in Appendix E, and for the 3D operational space with varying lengths in Appendix F. The next step is to consider the model for the 3D OC with varying links' lengths, and a 3D payload (a container) associated with three orientation angles. This yields an 11-degree-of-freedom system which would allow the designer to take payload rotational nonlinearities into account. This is not tackled in this article, however.

Remark 1. The pendulum-like models (2)–(6) may present extra dynamics. For instance, considering the payload as a liquid container, rather than a point mass payload, the system presents sloshing dynamics (Alshaya & Alghanim, 2020; Khorshid & Al-Fadhli, 2021; Li, Ma, Li, & Li, 2022). Various finite-dimensional, multibody models of sloshing are proposed in the literature (Di Leva, Carricato, Gattringer, & Müller, 2022; Ibrahim, 2005; Li, Ma, et al., 2022), and some of them have been validated experimentally (Di Leva et al., 2022). This adds degrees of freedom to the OC system and increases its underactuation.

Remark 2. In the models presented in Fig. 2, the dynamics of the supporting structure have been totally neglected. However, due to the weak materials, the supporting structures may not present infinite stiffness leading to deformation and vibration (Golovin, Maksakov, Shysh, & Palis, 2022). Modeling such flexible structures usually leads to coupled partial differential equation-ordinary differential equations (PDE-ODEs).

Remark 3. In this article the focus is on the design of F (or F_x and F_y) as feedback controllers. Another approach, usually employed in industrial contexts, consists of assuming that this control stage is designed such that any desired motion, possibly modified online by an operator, can be perfectly tracked. Then the control problem becomes that of designing a suitable desired motion. This is known in the literature as the operator-in-the-loop (Giacomelli et al., 2019, 2018a, 2018b; Khalid, Huey, Singhose, Lawrence, & Frakes, 2005; Parker, Robinett, Driessen, & Dohrmann, 1996; Ramli et al., 2017; Vaughan,

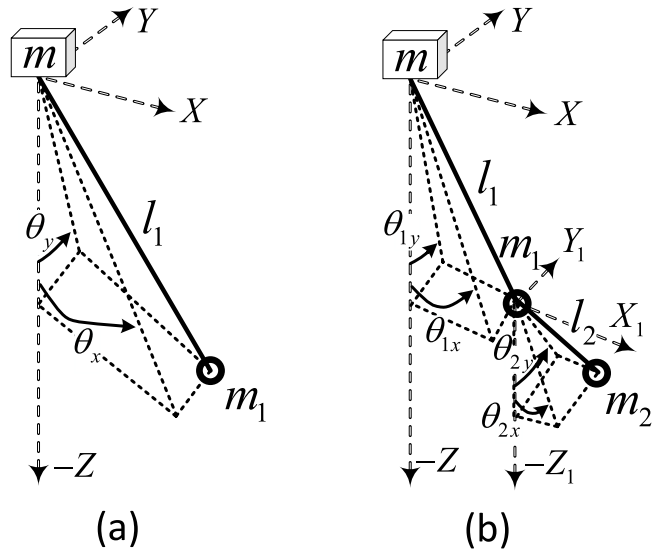

Fig. 3. 3D representation of the single-pendulum (a) and double-pendulum (b) models.

Karajgikar, & Singhose, 2011) method, with velocity commands. See Section 3.8 for more details and references.

The pendulum-like models, *e.g.*, (2)–(6), are presented in the fully nonlinear form that may be difficult to analyze, especially in closed-loop form. Hence, approximated models, such as the tangent linearized model as well as the cubic model have been developed in the literature (Nayfeh & Baumann, 2008). Compared to the linearized model, the cubic one contains cubic nonlinearities allowing the bifurcation analysis (see Remark 2 in Mojallizadeh, Brogliato, and Prieur (2022)).

2.3. Pendulum-like model with flexible link

Several kinds of flexibilities, *e.g.*, transversal deflection (see Fig. 2(c)) and length extension (Le et al., 2022; Pham et al., 2022) can be taken into account in this category, leading to several different equations depending on the flexibility types. The models in this category lead to PDE-ODEs, *e.g.*, linear wave equation (d'Andréa-Novel & Coron, 2000; Kim & Hong, 2009; d'Andréa Novel, Boustany, Conrad, & Rao, 1994; d'Andréa Novel & Coron, 2002) or semilinear wave equation (Lhachemi, Prieur, & Trélat, 2022), caused by the cart and cable dynamics, that need to be spatially discretized with finite-element methods (FEM) for simulation and for control application (for instance see Fatehi, Eghtesad, and Amjadifard (2014)) and yield finite-dimensional Lagrange systems based on FEM approximations of the wave equation (Egeland & Gravdahl, 2002), and Rayleigh–Ritz discretization (Damaren, 2000). According to the literature, the PDE-ODEs corresponding to such models follow several different conventions depending on the flexibility types, leading to different equations. The list of references dealing with the flexible cables in cranes is provided in Table 4 (see Table 1 for the notation). A modeling scheme in this category is briefly introduced below. Assuming that the coordinates are selected as in Fig. 2(c), the corresponding PDE-ODE model is as follows (d'Andréa-Novel & Coron, 2000):

$$\begin{cases} \bar{y}_{tt} - (a\bar{y}_z)_z = 0 \\ \bar{y}_z(-L,t) = 0 \\ \bar{y}(0,t) = x(t) \\ \ddot{x}(t) = \lambda(a\bar{y}_z)(0,t) + F/m \\ a(z) = g(z+L) + \frac{gm_1}{\rho}, \quad \lambda = \frac{(m_1+\rho L)g}{ma(0)} \end{cases} \tag{7}$$

where $\bar{y}(z,t)$ is the horizontal displacement at point z in $[-L,0]$ and time $t \geq 0$, x is the cart position, $\bar{y}_z(z,t)$ denotes the link's angular inclination, ρ is the mass per unit length of the link, and L is the length of the cable. Following d'Andréa-Novel and Coron (2000), (7) is only valid around the vertical posture when the cable is non-stretching, and the payload acceleration is negligible compared to g (another interpretation, as done in e.g., Wijnand, d´Andréa-Novel, and Rosier (2021), is that the mass of the payload is much larger than the mass of the cable). Another assumption is done in Chentouf and Mansouri (2022) where a coupled ODE-PDE-ODE model is considered, that is the same model as in (7), but with an ODE instead of the second line of (7). Furthermore Eq. (7) has been developed for the case when the length of the cable is variable (Kim & Hong, 2009; d'Andréa Novel & Coron, 2002). The letter *l* in the sixth column of Table 4 indicates the references dealing with flexible cables with variable lengths.

2.4. Paralleled multi-cable models

In a real crane, the payload is usually suspended through several parallel cables. To study the posture of the payload, kinematic models have been developed in 2D and 3D spaces. Compared to the pendulum-like models introduced in Sections 2.1–2.3, such models have not been yet used for the controller design and only the kinematic models have been developed without addressing the dynamics (to the best of authors' knowledge, Cartmell, Morrish, and Taylor (1998) is the only reference where a dynamic model has been developed for the multi-cable case. However, the obtained model has not been used for the controller design because of its complexity). The list of the references considering the kinematic of the cranes in 2D and 3D spaces are listed in Tables 7 and 8, respectively.

Remark 4. The introduced models are presented in their basic forms and several factors including cart friction (Antipov & Krasnova, 2022; Omar & Nayfeh, 2005), damping (Wen, Popa, Montemayor, & Liu, 2001; Zhang, Ma, Rong, Tian, & Li, 2016) and stiffness (Sun, Zhang, Xin, Yang, & Fang, 2019) in the joints, actuator dynamics (Park, Chwa, & Hong, 2008) and sensor noise (Karkoub & Zribi, 2001; Sano, Ohishi, Kaneko, & Mine, 2010), elasticity in the supporting structure (Golovin et al., 2022; Xing, Yang, & Liu, 2020), different uncertainties and disturbances (Park, Chwa, & Eom, 2014; Wu, Karkoub, Wang, Chen, & Chen, 2017; Xi & Hesketh, 2010; Zhang, 2019) can slightly modify the above-mentioned equations.

2.5. Properties of the models

OC systems have the following peculiar features:

1. **Large underactuation:** the degree of underactuation d_{unac} is equal to the number of degrees of freedoms, minus the number of independent torque inputs in Q. In N-pendulum multibody models of cranes, there are $1+2N$ (with N the number of joints) in the 2D case with varying lengths, or $1+N$ in the 2D case with fixed lengths, or $2+3N$ (3D case with varying lengths) or $2+2N$ in the 3D with fixed lengths, degrees of freedom. In a typical overhead crane, the number of independent inputs varies from 1 (trolley controller in 2D space) to 3 (trolley and length controllers with a winch in the 3D space). Thus d_{unac} is usually very large (if an infinite-dimensional cable's model is chosen, it is even infinity), which makes crane mechanisms occupy a particular place in the class of underactuated systems, which in fact contains a variety of systems (Liu & Yu, 2013).
2. **Dynamical couplings:** in view of large d_{unac}, the couplings between the actuated and the unactuated coordinates dynamics, and between the unactuated coordinates dynamics themselves, play a major role in the general dynamical behavior of cranes and more specifically in their control.

3. **Passivity:** passivity is one major property of Lagrange systems (Brogliato, Lozano, Maschke, & Egeland, 2020b). System (1), seen as an input/output operator $Q \mapsto \dot{q}$, and under a boundedness condition on the potential energy, is passive, *i.e.*, $V(q(t), \dot{q}(t)) - V(q(0), \dot{q}(0)) \leq \int_0^t Q^\top(s)\dot{q}(s)ds$ along the trajectories of the system, and where $V(q, \dot{q}) = T(q, \dot{q}) + U(q)$ is the total mechanical energy. However, the passive outputs usually do not correspond to the output to be controlled, mainly due to the noncollocation. A passive mapping can be recovered by defining another suitable output function (Damaren, 2000; Khalilpour et al., 2021).
4. **Output/input collocation or noncollocation:** a pair output/input is said collocated if the feedback is using only the part of the generalized coordinates on which the input torque performs work. For instance, the trolley is controlled with the force F which works on the displacement coordinate x, hence the pair (F, x) is collocated. If the actuator dynamics are considered and F is seen as the output of the actuator, then collocation is lost. If F uses the payload's coordinates it is lost also. Noncollocation is known to make the control problem much harder.
5. **High flexibility:** though cables are not the only flexible systems encountered in mechanics, they may be one of the most flexible ones. The high flexibility of cables also leads us to consider various different dynamical regimes:
    - Small amplitude-high frequency waves (vibrations) when the cable stays close to the vertical posture,
    - Large-amplitude motions during which the cable behaves like a pendulum that swings,
    - Large-amplitude waves with lower frequency, which travel through the cable.

    An important question for control design is: When do these regimes occur (*i.e.*, with which initial conditions and parameters)? Characterizing the modes of the cable seems mandatory. This may also imply splitting the overall control problem into subtasks relying on different models and controllers.
6. **Cables with variable length:** this may be a consequence of cable's longitudinal elasticity, or of winding mechanisms used to add a control input (see Section 3.5). This is considered in robotic systems involving cables (Khalilpour et al., 2021), in tethered systems with long hoisting ropes (marine or space applications (Kamman & Huston, 2001; Quan & Chang, 2020)). In case of winding, this implies considering varying cable's total mass (depending on the length in some way) in the derivation of the dynamical equations, and a variation of the trolley's mass as well (the total mass being kept constant). If the length variation is very small, or if the cables' total mass is small compared to the hook and payload masses, the cables' mass variation may be neglected, however (Quan & Chang, 2020). This is what is done to obtain (3) as well as its double-pendulum counterpart (Brogliato, 2022, section 5.4). See Appendix A.3 in Appendix A.
7. **Cables slackness mode:** cables can exert very large forces when in the tensile mode, however, they cannot exert any action when they are slack (Gueners, Bouzgarrou, & Chanal, 2021). Long cables undergoing large oscillations/deformations may undergo such phenomena. This yields models with complementarity constraints and impacts (Brogliato, 2016, Example 1.6).
8. **Large variations of the payload mass:** payloads can have very large mass (several tons), and typical tasks involve motions with and without payloads, hence huge variations of the system's inertial parameters. Should this be taken into account by designing robust inputs, adaptive inputs, or switching control strategies?

2.6. Main sources of disturbances and uncertainties

In addition to cable flexibilities, other effects considered as disturbances/uncertainties can be incorporated for control design or in the numerical benchmarks:

1. Disturbances: Coulomb-like friction between the trolley and the rails, mechanical play (static or dynamic backlash), measurement noise (sensors), uncertain parameters (inertial parameters), wind gust, collision and vessel movement for applications where the OC is mounted on a boat or a floating platform.
2. Large parameters variations (*e.g.*, switching between heavy-payload and payload-free subtasks),
3. Neglected dynamics: actuators dynamics, cable flexibilities (for pendulum-like models), multiple cables *vs.* single cable (kinematics at the payload attachment), 3D effects (for 2D designs), like payload rotations involving nonlinear inertial torques, and flexibility in the crane's structure.
4. Output definition: The cable flexibility hinders to define and measure specific sway angles, *e.g.*, θ_1 and θ_2, as shown in Fig. 2. Hence, sway measurement can be considered as a source of uncertainty and disturb the measurements.

2.7. Validity

The mentioned models have some limitations and cannot be used in any condition:

- Single-pendulum model: This is the simplest model, making the control design easier. However, the secondary sway caused by the presence of a tool is ignored in this model. Hence, such a model should be avoided when there are heavy tools.
- Double-pendulum model: This model is more accurate than the single-pendulum one since it takes into account the presence of the tool and can model the secondary sway. However, it still cannot take into account the cable dynamics other than the two sway angles θ_1 and θ_2. Hence, in the absence of payload, when the cable's flexibility is dominant, this model and the single-pendulum one should be avoided. Moreover, when there is a heavy payload, the cable may behave as a string and therefore high-frequency vibrations that exist in the cable cannot be shown with such models.
- Pendulum-like model with flexible link (string or wave equations): cables, in general, can present rich dynamical behaviors *e.g.*, transversal deflection, length extension, torsion. As can be seen in Table 4 this topic has not yet been considered deeply for the overhead cranes and it is not clear how these dynamics can affect the overall systems behavior of OCs. To the best of the authors' knowledge, and according to Table 4, such models are only valid around the vertical posture of the cable and, hence, they are quite local and are unable to show the global nonlinearities that can be modeled by the single and double-pendulum systems.
  It is noteworthy that the two main classes of models considered so far for control design belong to two "extreme" classes: (1) multibody model with few degrees of freedom, global nonlinearities, few vibrational modes, (2) infinite-dimensional (PDE) linear model, valid only very locally around the vertical posture.
- In the three above-mentioned modeling categories, it is always assumed that the payload is a point mass and therefore, it is not possible to model the orientation and 3D motions of the payload. Hence, in the presence of unbalanced payloads (payload eccentricity) more sophisticated models are required. However, controller design for such systems requires more elaborated kinematics and dynamical modeling which makes the controller design cumbersome. As can be seen in Tables 7 and 8, these kinds of models have not been used yet for the controller design.

Multibody models are limited in terms of flexibility and cable's vibration modeling. Nevertheless they can become quite complex and nonlinear when enough effects are taken into account (notwithstanding disturbances). This is witnessed by the dynamics reported in the Appendix, see also the multi-cable system's dynamics in Cartmell et al. (1998, Equations (28)–(30)).

A simulation-oriented model will be developed in Section 5 in order to provide a more accurate model for numerical simulations without some of the limitations mentioned above.

3. Review of the control strategies proposed for OCs

The main control objective in any industrial crane is payload positioning. However, due to the underactuation, the payload cannot be controlled directly, and the payload motions are controlled indirectly through the forces applied to the cart (F in Fig. 2). In this case, the payload sway introduced in Section 1 may result in poor positioning. The control strategies developed for OCs are classified into three categories in Sections 3.1 to 3.3.

3.1. Open-loop control

In this section, we introduced the open-loop controllers which have been used to control OCs.

3.1.1. Input shaping

In these schemes, the input $F(\cdot)$ of the system is calculated such that the natural frequencies of the system are not excited (Engelberg, 2021) (see for example Hazlerigg (1972) for the very first works in this topic). A common approach in this class is to obtain the dynamic equations and extract the tangent linearization around a nominal operating condition. The linear model is then used to derive the natural frequencies. This approach is usually used along with a human-operated crane system (Singhose, Porter, & Seering, 1997). In another approach, linearized equations are used to calculate the responses of the system. Subsequently, an acceleration profile is calculated such that the total response of the system satisfies constraints on the operation time, sway, and hoisting speed (Alghanim, Alhazza, & Masoud, 2015). Input shaping usually provides cost-effective solutions since the sensors and the feedback path are not required (Vaughan, Maleki, & Singhose, 2010). Following the literature, the application of open-loop input shaping is rare and it is usually integrated with sensors and control feedback to compensate for the wind rejection (Tang & Huang, 2016), systems initial sway (Wahrburg, Jurvanen, Niemelä, & Holmberg, 2022a, 2022b), uncertainties (Nguyen, Do, & Duong, 2022), or time-delay compensation (Vyhlídal, Kučera, & Hromčík, 2013).

Input shaping has also been developed for double-pendulum models to avoid excitation of the primary and secondary oscillatory modes (Nguyen et al., 2022; Singhose, Kim, & Kenison, 2008; Vaughan, Kim, & Singhose, 2010). Some references have considered input shaping design for specific applications such as a suspended liquid container with slosh effect (Alshaya & Alghanim, 2020; Khorshid & Al-Fadhli, 2021; Li, Ma, et al., 2022). Zero vibration (ZV) (Singhose, Seering, & Singer, 1990) and zero vibration derivative (ZVD) (Hong & Shah, 2019) are two well-known input shaping algorithms that achieve sway reduction by convolving the unshaped input (usually bang–bang time optimal input) with a sequence of impulses. These approaches have been utilized by taking into account some constraints on the sway angles during the transient (Hong, Huh, & Hong, 2003). While input shapers are usually designed based on tangent linearization of the nonlinear models, there are also some works that are dedicated to nonlinear input shaping design based on heuristic algorithms such as particle swarm optimization (PSO) (Maghsoudi et al., 2017). Another input shaping scheme has been proposed by Alhazza, Masoud, and Alotaibi (2016) based on the trigonometric manipulations of the responses, and it is shown that in the nominal case, the final sway can be eliminated. Moreover, this method may show a faster response compared to the ZV method. The effect of the hoisting during the motion in the presence of several input shapers has also been studied by Singhose, Porter, Kenison, and Kriikku (2000).

3.1.2. Flatness theory

Flatness theory is a known strategy in control theory to provide a mapping among inputs and outputs of the system, and hence, it can be used to handle the underactuated dynamics of OCs since the inputs and states of OCs can be expressed by flatness outputs. The aim of this method is to generate a reference trajectory for the cart in order to achieve the payload positioning without sway (Fliess, Lévine, Martin, & Rouchon, 1995). This is mainly an open-loop technique that can be combined with some closed-loop controllers (Diwold, Kolar, & Schöberl, 2022; Knierim, Krieger, & Sawodny, 2010; Zhang, Wu, & Huang, 2017). Before explaining this topic, it should be noted that the desired trajectory is normally defined for the payload and not for the cart. According to the literature, the flatness theory can help with the following items:

- Calculating a map between the desired cart and payload positions. This is especially useful for applications with the pre-installed speed driver where the input is the desired cart position (Bonnabel & Claeys, 2020; Fliess et al., 1995; Guo, Chai, & Liu, 2023; Yu & Niu, 2023).
- Flatness theory can be used to generate the desired trajectory based on the desired final position such that the total motion is robust against the perturbations (Zhang, Wu, & Huang, 2017).
- Calculating the control force required for tracking (Fliess et al., 1995; Zhang, Wu, & Huang, 2017).
- System linearization, different from the feedback linearization (FL) strategy (Zhang, Wu, & Huang, 2017).
- Taking the actuator dynamic into account for the controller design (Fliess et al., 1995; Knierim et al., 2010).

3.1.3. Path planning

In this method, the control law is calculated in an online (Sun & Fang, 2014a) or offline (Sun, Fang, Zhang, & Ma, 2012) manners based on the model to minimize an objective function for some sort of optimality such as energy (Sun, Wu, Chen, & Fang, 2018) or time (Zhang, Fang, & Sun, 2014). Some of the input shaping schemes can also be categorized in this section. For example, Zhang et al. (2014) has used dynamic programming to optimize the trajectory based on the input shaping strategy. However, the effect of the actuator dynamic on global optimality is usually neglected in such studies. Path planning strategies have been proposed in Sun and Fang (2014a), Sun, Fang, Zhang, and Ma (2012) to avoid payload sway.

3.2. Collocated control

Compared to the input shaping, this is a closed-loop strategy where a control algorithm computes the input signal according to the collocated feedback, *i.e.*, cart position, and/or velocity (x, $\dot{x}$) from the output. In other words, $F = F(x, \dot{x}, t)$ and $F_l = F_l(l_1, \dot{l}_1, t)$ in (3). PID (proportional integral derivative) control is the most used collocated control strategy. This kind of controller is implemented by default on many speed drivers used in OCs. PID controllers are designed based on the tangent linearized models using classic control tools like loop-shaping (Lee, Cho, & Cho, 1997). Its parameters can also be tuned using Ziegler–Nichols method (Shih, 2022). Ouyang, Hu, Zhang, Mei, and Deng (2019) has developed a trajectory velocity reference for the cart based on the S-curve technique to control the sway. Afterward, a PID controller has been used to track the mentioned velocity reference where the only required measurement to build the feedback is the cart position. A similar strategy has been presented in Garrido, Abderrahim, Gimenez, Diez, and Balaguer (2008) where many details like parameter tuning, filter design, and practical implementations have

been addressed. It is shown in Fang, Zergeroglu, Dixon, and Dawson (2001) that a single PD controller with just a measure of the cart position can make the whole system asymptotically stable, including the underactuated dynamics even in a 3D operating space (Ouyang, Zhao, & Zhang, 2021). However, as reported in Ouyang et al. (2021), such a collocated control may lead to poor sway reduction. Hence, noncollocated feedback, *e.g.*, sway angles are included in the control law by Ouyang et al. (2021) to increase the damping. A Lyapunov function allowing the calculation of control laws without having feedback from the sway angle has been developed in Sun, Fang, Chen, and He (2015). Furthermore, some adaptation rules are also developed in this study based on the Lyapunov function for uncertainties in the payload's weight, friction, etc. The collocated PID controller has been integrated with a neural network in Isa, Hamza, Adamu, and Adamu (2022), and it is shown that it provides a better payload positioning compared to the classic PID. Feed-forward terms can be added to the collocated PID controller for the tracking applications (Shi, Yao, Yuan, Hu, et al., 2022).

Remark 5. Some of the references have neglected the speed drivers and the feedback inside, and considered the collocated control strategy as an open-loop scheme. The main contribution of such works is to calculate or modify the reference trajectory, *e.g.*, using notch filters (R. L. Kress & Noakes, 1994), smoothing the reference trajectory (Bonnabel & Claeys, 2020), and flatness theory in order to avoid the payload sway (Bonnabel & Claeys, 2020). Because of the fast and accurate operation of modern speed drives, such methods can lead to appropriate solutions for industrial applications as reported in Bonnabel and Claeys (2020). It should be noted that while the modification of the reference trajectory can significantly help to reduce the payload sway, it has not been deeply taken into account in this work. The trajectory design or modification can be integrated with the majority of the controllers developed in this work.

3.3. Noncollocated control

Compared to the collocated control, the noncollocated one needs the payload coordinates as well, *e.g.*, payload sway, *i.e.*, $F = F(x, \dot{x}, \theta_1, \theta_2, \dot{\theta}_1, \dot{\theta}_1)$. The noncollocated control strategies introduced in the literature are as follows.

3.3.1. Gain-scheduling

Gain-scheduling refers to a method where the gains of the controllers are calculated offline to build a lookup table based on the operating condition. Such a strategy has been developed in Omar (2003), Omar and Nayfeh (2005) where the gains of a feedback controller are selected based on the linearized model such that the response is critically damped to avoid sway oscillations.

3.3.2. Noncollocated PID (quasi-PID) control

In addition to the collocated PID (see Section 3.2), the PID controller may use noncollocated feedback (Mohamed, Abdel-razak, Haraz, & Ata, 2022). Noncollocated quasi-PID control laws have been designed for single and double-pendulum systems in Zhang, He, Zhu, Li, and Liu (2022), Sun, Yang, Fang, Wu, and Chen (2019), respectively, based on the Lyapunov theorem to avoid control saturation. The PID controller may also be integrated with neural networks to compensate for the steady-state error as introduced in Toxqui, Yu, and Li (2006). It should be noted that the application of PID controllers in human-in-the-loop applications has also been considered by Peng, Singhose, and Bhaumik (2012). Furthermore, several configurations of PID control families have been studied for OCs in Omar (2003) and compared with a fuzzy controller. It is concluded that tuning the parameters of the fuzzy controller could be cumbersome. However, with proper tuning, the fuzzy controller shows a better transient time than the PID controller. But, in the case of sway control, the PID controller shows better performance than the fuzzy one. Another reference in this subject is (Shih, 2022) where the parameters of a PID controller are tuned based on a reinforcement learning scheme and it is concluded that such a scheme can supersede the classic PID controller in terms of performance.

3.3.3. Linear state-feedback control

In this method, a linear model is developed based on a linearized model (tangent linearization) and then a state-feedback law is developed based on classical methods (Ackermann, 2012; Jaulin & Walter, 1996; Moustafa, 1994; Piazzi & Marro, 1996). Such a strategy is used by Orsini (2022), Piazzi and Visioli (2002) along with state-observers.

3.3.4. Passivity-based control

Passivity-based control (PBC) is a well-known control strategy to analyze or guarantee stability by studying energy dissipation (Brogliato et al., 2020b). This method can be used to design a control signal such that the energy of the system remains bounded, leading to bounded-input bounded-output (BIBO) stability. Considering the system shown in (2), and assuming that the energy (Lyapunov function) can be defined as $E = 1/2m\dot{x}^2 + m_1 g l_1(1-\cos\theta_1)$, the rate of the system's energy is $\dot{E} = \dot{x}F$. Any control signal F leading to $\dot{E} \leq 0$ ensures the BIBO stability of the system (See Remark 6). It can be shown that a collocated PD control $F = -\dot{x}$ can lead to such stability. While a collocated control strategy, *e.g.*, $F = -\dot{x}$, can make the whole closed-loop control system asymptotically stable (as reported by several references such as Collado, Lozano, and Fantoni (2000), Fang, Dixon, Dawson, and Zergeroglu (2003)), it may not be able to control the payload sway efficiently since the noncollocated dynamics are controlled only because of the natural dynamical coupling between the cart dynamic and the payload one (Fang et al., 2003) (see (2) and (6)). This issue has been further addressed by Sun and Fang (2012) and supported by analytical results, where horizontal displacements of the payload have been considered as a new output (see (8) in Sun and Fang (2012) as well as Chen, Xuan, Yang, and Chen (2019)) and it is shown that the map between the input force and the horizontal payload velocity can also be passive and dissipative (see (11) in Sun and Fang (2012)). This can be done by defining a new storage function for the OC which includes the payload horizontal displacement. Subsequently, a new passivity-based control law has been proposed which includes both actuated (cart position) and underactuated (payload position) variables and the asymptotic stability has been ensured based on the Lyapunov and LaSalle's invariance theorems. Since the new control law contains the underactuated dynamics, it may lead to a more efficient sway control strategy as reported by Sun and Fang (2012).

Remark 6. Assuming again single-pendulum model (2), and the mentioned energy function $E = 1/2m\dot{x}^2 + m_1 g l_1(1-\cos\theta_1)$, leading to $\dot{E} = \dot{x}F$, the control $F = -\dot{x}$ just leads to $\dot{E} = -\dot{x}^2 \leq 0$ which is semi-negative (θ_1 is absent in $\dot{E}$). Hence, Lyapunov stability usually cannot ensure the asymptotic stability of the system (convergence of θ_1, θ_2 to the origin), and LaSalle's invariance principle should be further used to ensure the asymptotic stability.

Another passivity-based design is the interconnection and damping assignment (IDA) where the sum of the physical potential and kinetic energies are considered and the controller is designed such that the amount of this function is minimized for the desired equilibrium point. The IDA-PBC provides a systematic way to obtain stabilization through two steps. The first step is the so-called *energy shaping* where the desired storage function is designed (Zhang, He, Chen, & Feng, 2020). Subsequently, the *damping injection* technique is utilized to provide asymptotic stability. However, IDA-PBC law usually requires solving PDEs which might be difficult to handle. Such a strategy has been developed for underactuated systems by Aschemann (2009) and implemented on an OC based on some simplifying assumptions, *e.g.*, $\sin(\theta) \simeq$

θ and $\cos(\theta) \simeq 1$. In Alli and Singh (1998), two LTI models have been developed for OCs. The first one is based on the tangent linearization of the single-pendulum model. To obtain the other LTI model, the flexibility of the cable corresponding to the single-pendulum model has been taken into account which led to a PDE. This passivity approach has been successively used for infinite-dimensional crane models in particular in Chentouf and Mansouri (2022), d'Andréa-Novel and Coron (2000), d'Andrea Novel, Boustany, and Rao (1991), d'Andréa Novel and Coron (2002), exploiting the energy function that may differ from the considered model. Subsequently, the PDE has been solved based on the Laplace transformation to form the transfer functions in the Laplace domain. It is shown that these two transfer functions are positive real (PR) (Brogliato et al., 2020b). Hence, any strictly positive real (SPR) block can be placed in the feedback path to form a passive closed-loop control system. The coefficients of such SPR controllers are designed based on an optimization technique. The same strategy has been employed by Shen et al. (2021) with the difference that the torque applied to the winch (F_l in (3)) has been also taken into account for position tracking of the load. PBC has also been developed for the 3D operating space with initial control saturation avoidance (Zhang, Zhu, He, Feng, & Pang, 2022). This method has been extended in Zhang, He, and Chen (2020) without partial feedback linearization to improve the robustness. An energy shaping method has been introduced by Sun et al. (2013), Wu and He (2017) for 3D problems where the differentiations of the variable do not appear in the control law to form an output feedback control (see also Zhang, He, Zhu, Chen, and Feng (2020) which employs both the angle displacement and its derivative). The method is different from the IDA-PBC and another storage function has been defined based on the concept of virtual payload. Another PBC design has been introduced by Wu and He (2017) where the main contribution is to define a new output function that contains both cart and payload coordinates. Subsequently, a storage function is defined based on this output. Note that partial feedback linearization (PFL) is used in the beginning to obtain the appropriate dynamic equations for the control design. Since the position has been taken into account in the error signal, the damping characteristic is not constant and changes according to the distance to the desired position which can reduce both load sway and operation time. Lyapunov and LaSalle's theorems are employed to show the asymptotic stability.

In Zhang, He, Chen, and Zhu (2019), the PBC adopts barrier functions on the coupled-dissipation signal, so that the payload position is guaranteed in a predefined scope during the whole transportation. In the mentioned work, a new storage function containing both actuated and underactuated dynamics has been proposed to form a noncollocated control strategy (see also Chen and Sun (2020) where the barrier function-based antisway control of overhead crane is proposed). For infinite-dimensional systems, LaSalle's invariance principle could be also applied, but it requires proving a precompactness property for the solutions (Slemrod, 1989), that could be proven by studying an injection (as done in e.g. Prieur, Tarbouriech, and Gomes da Silva (2016)) that could be difficult to establish and that is not needed when using, e.g., backstepping control design (as described in Section 3.3.7 below). In the context of OC, this approach has been successively applied in d'Andréa-Novel and Coron (2000), d'Andréa Novel et al. (1994), d'Andrea Novel et al. (1991).

3.3.5. Feedback linearization (FL)

The aim of FL is to provide a linear input–output map by canceling the nonlinearities and hence enabling to use the design and analysis methods developed for the linear systems. As it is reported by Wu and He (2017), the FL cannot be implemented for the underactuated systems directly and it is necessary to use Spong's transformation (Spong, 1994) for the actuated and unactuated coordinates (Tuan, Lee, Ko, & Nho, 2014). In (2), one computes $\ddot{\theta}_1(\ddot{x})$ from (b), and inserts it in (a) to get the $(x, \dot{x})$ controlled dynamics. In (3), one computes $\ddot{\theta}_1(\ddot{x})$ (c), and insert it into (a) and (b) to get the $(x, \dot{x}, l_1, \dot{l}_1)$ controlled dynamics. Similar manipulations are performed with (4) (c) (d) and (a) (b), with (5) (c) (d) and (a) (b) (e), and (6) (a), (b) and (c) (see Appendix G for more details and developments). Using this transformation, it is possible to study the underactuated Euler–Lagrange systems in terms of controllability and the possibility of linearization by state feedback (Reyhanoglu, van der Schaft, McClamroch, & Kolmanovsky, 1999). However, as reported by Reyhanoglu et al. (1999), unactuated dynamics as in (G.5) are usually nonintegrable and thus can be interpreted as second-order nonholonomic constraints, which do not reduce the state-space dimension. Such studies seem to be absent in the literature for OCs control.

In Park, Chwa, and Hong (2007), firstly, the dynamic model of an OC with variable-length link has been obtained and it is shown that there is coupling between the cable's length and the sway dynamic (see Appendix A for more details). Subsequently, a control law has been proposed which can be divided into two parts, to control the actuated and underactuated dynamics. Asymptotic stability is also shown using the Lyapunov theorem. Le, Lee, and Moon (2014) has proposed a PFL controller to control the sway angle. Subsequently, a sliding-mode control (SMC) is designed for the hoisting mechanism. The combination of these two controllers is also addressed. A control scheme based on the FL has been developed in Chwa (2009) and its asymptotic stability has been studied. This scheme has also been compared with the PD (Fang et al., 2003) and a Lyapunov-based control called E^2 coupling control law (Fang et al., 2001). PFL has also been developed for 3D case (Sun, Fang, & Zhang, 2012; Wu & He, 2016). In Lee et al. (2013), firstly, a single-pendulum 3D model has been obtained which includes three inputs and five outputs and then the actuated and underactuated dynamics have been separated. Subsequently, a map between actuated and underactuated systems has been achieved. After that, the FL technique is used to obtain the required control forces for the actuated and unactuated dynamics, and finally, the linear combination of these control laws is applied to the system. This strategy has also been integrated with the SMC by Tuan et al. (2014). Furthermore, FL control for the 3D motion of an OC is introduced in Tuan, Kim, and Lee (2012) where the controller is mainly designed for the actuated parts and the sway angle is considered an unactuated dynamics. Subsequently, it is shown that the unactuated dynamics are locally stable by analyzing the zero dynamics using Lyapunov's linearization theorem. An FL control has been studied in Boustany and d'Andrea Novel (1992). Since this method can be sensitive to the payload mass, a mass estimator has been developed, and exponential stability has been assured using the Lyapunov theorem. While FL can lead to a lack of robustness (since it relies on the system's parameters) it can stabilize the internal dynamics (Hamdy, Shalaby, & Sallam, 2018). A deadbeat control scheme is then used by Hamdy et al. (2018) after FL to improve the time-optimality. According to Yu, Lewis, and Huang (1995), in FL, a singularity may occur around the equilibrium point which makes the control design complicated. This problem has been resolved by separating the whole dynamics into fast and slow parts, corresponding to the average and oscillatory movements, and designing two different controllers for these parts.

3.3.6. Sliding-mode control (SMC)

SMC is another widely used approach in this topic because of its robustness to matched and unmatched disturbances (Chen, Cheng, Liu, & Du, 2022; Gu & Xu, 2022; Hu & Xu, 2022; Wang, Wu, & Lei, 2022). It can also handle the elasticity exists in the supporting structure as reported by Cuong and Tuan (2023). In the simplest case, SMC has been designed for the single-pendulum model with a constant length link, and a linear sliding surface is defined containing the cart position (x) and sway angle (θ_1), as well as their time derivations (Chen, Yang, Ni, & Yan, 2020). Subsequently, an equivalent-based control law is proposed, and the asymptotic stability of the closed-loop system is ensured based on the Lyapunov stability theorem. This classic approach has been employed in Kuo-Kai Shyu, Cheng-Lung Jen, and Li-Jen Shang (2005).

A similar procedure with a variable length link has also been developed where the sliding surface also contains error variables corresponding to the length of the link (Lee, Liang, & Segura, 2006). Note that the SMCs in this topic usually need full-state feedback. SMC with a nonlinear sliding surface has also been introduced for the single-pendulum (Lee, 2004) with variable length cable and double-pendulum (Chen et al., 2022; Ouyang, Hu, Zhang, Mei, & Deng, 2019; Shehu, Li, & Zeng, 2022) systems. The SMC designed for the double pendulum system in Chen et al. (2022) does not require the payload feedback, *i.e.*, secondary sway (θ_2), length of the second link (l_2), and the payload mass (m_2). In addition, SMC has also been designed based on the tangent linearized model of the double-pendulum system integrated with the state observer.

SMC is integrated with disturbance observers to compensate for disturbances based on the single-pendulum model (Lu, Fang, & Sun, 2017b). Similarly, Park et al. (2014, 2008) have developed fuzzy observers for this purpose to estimate the dead-zone characteristic of the actuator as an uncertainty when the SMC is used. Furthermore, Moon et al. (2013) has proposed an SMC for cart position, hoisting, and sway control. Since this control law depends on the payload mass and friction factors, adaptation laws are developed to estimate these parameters (Moon et al., 2013) or to tune the control gains (Hu & Xu, 2022; Wang, Liu, He, et al., 2022). In addition to the first-order SMCs, other variants of the SMCs have also been developed for the OCs such as super-twisting SMC (Vázquez, Collado, & Fridman, 2014; Wang, Wu, & Lei, 2022) leading to continuous structures. Second-order SMC in 3D space without considering the hoisting mechanism has been addressed in Bartolini, Orani, Pisano, and Usai (2000). This strategy has been further developed by Bartolini, Pisano, and Usai (2002) to include the hoisting mechanism as in (3). The sliding surface depends on the load sway for sway reduction. As a result, a kind of virtual damping is added to the closed-loop equations which stabilizes the zero dynamics corresponding to the unactuated dynamics. Such a control strategy has been compared with the μ-synthesis controller (Karkoub & Zribi, 2001) and it is concluded that the SMC provides a better sway reduction, but it suffers from the chattering and higher energy consumption. An adaptive fuzzy SMC has been developed by Lee, Huang, Ku, Yang, and Chang (2014) for cart position and sway control in 3D space where two linear sliding surfaces have been defined for the position and sway angle. The value of the sliding surfaces is fed into a fuzzy system through two gains to generate the control signal. The gain of the sway angle is calculated adaptively to achieve both tracking and sway reduction simultaneously. The design of the SMC for the 3D operating space has been studied in other works (Ngo & Hong, 2012). For instance, SMC design for the single-pendulum model in 3D space with a variable-length link has been addressed in Almutairi and Zribi (2009) where a Luenberger observer is used to estimate the velocities.

It should also be noted that SMC has been used along with FL scheme because of its robustness. For instance, Le et al. (2014) has designed a PFL controller for the cart motion to control the sway angle. Subsequently, an SMC is designed for the hoisting mechanism. Furthermore, a hybrid control strategy has been proposed by Tuan et al. (2014) where SMC and PFL have been used together. The PFL is for sway control and the SMC is used for payload lifting. An adaptive tracking SMC has been developed in Ouyang, Wang, Zhang, Mei, and Deng (2019) for a double-pendulum model where one of the parameters of the sliding surface, *i.e.*, the pole of the linear sliding surface, is calculated based on an adaptation law. Asymptotic stability has been guaranteed based on the Lyapunov theorem. Practical experiments show that the adaptive method can improve the tracking performance, compared to a few non-adaptive schemes. A discrete-time integral SMC has been developed in Xi and Hesketh (2010) for a general class of discrete-time linear systems, and robustness in the presence of matched and mismatched uncertainties (which cannot be handled in typical SMCs) has been addressed. Application of this controller to an OC in 3D space is also considered. Another integral SMC has been designed for the negative imaginary systems in Abdullahi et al. (2016) and the application of this control method on the OCs has been studied.

Some studies have also been dedicated to the numerical chattering reduction of SMCs implemented with explicit Euler methods using alternative methods, *e.g*, Park et al. (2008) where the control gain of an SMC is calculated using a fuzzy system to determine the width of the boundary layer of the saturation function to reduce the numerical chattering. Two SMCs, *i.e.*, first and second orders strategies, along with the sliding-mode-based differentiators are developed in Bartolini, Pisano, and Usai (2003) and compared with the PI controller and a time-varying feedback strategy. Experimental results indicate that the SMC schemes are more robust than the other considered models. An SMC named "global-equivalent" has been introduced by Wang, Tan, Qiu, et al. (2021) and compared with conventional SMC and the PID controller. The control is designed for the single-pendulum model with varying length links. The simulations show smaller chattering compared to the conventional SMC. The reaching phase of the system has been ensured. However, the sliding phase, as well as the stability of the sliding surface, has to be further addressed. Additionally, the chattering reduction mechanism, *i.e.*, replacing the signum function with the saturation one to have a boundary layer, imposes extra design parameters to the system, where there is not any straightforward tuning procedure. This strategy has been further modified by Wang, Tan, Zhang, et al. (2021) to form a time-variant sliding surface.

3.3.7. Backstepping control design

According to the literature, backstepping control has been used for overhead cranes when the model has a triangular form. Such a model usually appears when dealing with pendulum-like systems with a flexible link (7). In d'Andréa Novel and Coron (2002), considering the flexibility of the cable with variable length, a PDE-ODE model is obtained. Subsequently, a boundary feedback law is proposed to stabilize the system. Such a control law has been integrated with the neural networks to handle the uncertainties (Ma, Lou, Wu, & Huang, 2022). Since the cascade structure directly appears in the PDE-ODEs model, the backstepping control scheme can be utilized for the system (d'Andréa Novel & Coron, 2002). See also d'Andréa-Novel and Coron (2000), where the backstepping design is used to prove the exponential stability of the closed-loop system. Moreover, finite-time stability can be ensured using the same approach as done in Liu, Li, and Ding (2012), d'Andréa Novel et al. (2019), Wen, Lou, Wu, and Cui (2022), Wijnand et al. (2021) for a fixed-length cable. To do that, a non-Lipschitz condition has been employed and nonlinear semigroup has been used to prove the global wellposedness of the closed-loop systems. Note that such property usually is not observed in the ODEs developed for the single and double pendulum systems (2) and (6), and a state transformation may be used to realize a triangular system. Such a model has been obtained in Chen and Saif (2008) for an experimental OC. Subsequently, a backstepping controller has been designed and combined with the sliding-mode observer to form an output feedback control law.

3.3.8. Fuzzy control

Fuzzy control can be considered a model-free control scheme since it is designed based on the behavior of the system rather than the mathematical models. These kinds of control strategies are usually provided without solid stability proof. One of the earliest works on this subject has been done in Liang and Koh (1997). In Zhao and Gao (2012), a Takagi–Sugeno fuzzy model has been developed for an OC based on obtaining the dynamical equations, and linearization over three different points using three fuzzy rules. Then, the control rules are developed based on these rules. Input delay and actuator saturation are also considered in the control design. A terminal SMC has been designed in Lin, Chou, Chen, and Lin (2012) where the uncertainties are estimated using a type-2 fuzzy system. The parameters of the fuzzy

system are also tuned online based on adaptation laws developed in the work using the Lyapunov theorem. In Chunshien Li, Chun-Yi Lee, and Kuo-Hsiang Cheng (2004), a self-organizing neuro-fuzzy system has been proposed based on the pseudo error concept. It seems that pseudo error is used as a kind of input shaping. As usual, there is no stability proof for such a model-free control strategy. An adaptive fuzzy control scheme coupled with H_∞ control is designed in Wu et al. (2017) for a class of nonlinear multi-input multi-output underactuated systems with a combination of dead-zone, hysteresis non-linearity in the input, external disturbance, and time-delays. The application of the control scheme for the cranes is then considered. Another fuzzy controller for a single-pendulum model has been developed in Yi, Yubazaki, and Hirota (2003) which requires full-state feedback. In Yi et al. (2003), a fuzzy inference system has been used for trajectory planning of the cart to reduce the payload sway based on the single-pendulum model and full-state feedback. Moreover, a fuzzy controller has been developed by Li, Chen, and Zhang (2022) for the double-pendulum system in 2D space with variable length cable to address input uncertainties, *e.g.*, dead-zone. The parameters of the fuzzy system are updated adaptively, and the effect of the adaptation has been taken into account for the stability proof using the Lyapunov theorem (see also Pham et al. (2022) for fuzzy gain tuning of SMC in 3D operating space and cable length extension due to cable's flexibility).

3.3.9. Model predictive control

Model predictive control (MPC) calculates the control sequences based on the model to minimize some objective functions (*e.g.*, corresponding to energy consumption Wu, Xia, & Zhu, 2015) over a horizon while satisfying some constraints like input saturation or collision avoidance. MPC can directly calculate the force (Chen, Fang, & Sun, 2016), or on the other hand, it may just calculate the optimal trajectory integrated with other controllers (Vu et al., 2022). MPC can be designed based on the tangent linearized (Chen et al., 2016; Vu et al., 2022) or nonlinear models (Schindele & Aschemann, 2011) of a single-pendulum. MPC has also been combined with offline trajectory planners to increase the calculation speed and realize a real-time implementation (Vu et al., 2022). In Smoczek and Szpytko (2017), it is assumed that the dynamics of the cart and the sway angle are decoupled which is obviously unrealistic, see (2)–(4) and (6). Then two discrete-time transfer functions are obtained for input force to cart velocity and cart velocity to the sway angle. These transfer functions have fixed orders (first and two-order models), and the coefficients of these models are obtained using PSO. Subsequently, MPC is used based on these models. Inspired by d'Andréa-Novel and Coron (2000), d'Andréa Novel et al. (1994), d'Andréa Novel and Coron (2002) (see also (Crépeau & Prieur, 2006; Le Gall, Prieur, & Rosier, 2007)), the paper Artola, Wynn, and Palacios (2021) developed a control design method for Euler–Bernoulli and Timoshenko beam models, using linear abstract theory and nonlinear model predictive approach. The performance of the closed-loop systems is checked on numerical simulations on a high-resolution scheme for the underlying PDE model. As explained in Krupa, Nemcik, Ozana, and Slanina (2022), MPC based on the nonlinear model may show a heavy calculation burden and special attention has to be made to its implementation, *e.g.*, the multi-threaded implementation may be necessary.

3.3.10. Optimal control

Optimal control refers to any control method where the aim to minimize an objective (cost) function. The LQR is probably the most well-known one in the control community. An LQR controller has been developed by Yoshida and Kawabe (1992) for the linearized model of a single-pendulum system while satisfying some constraints on the control input to avoid control saturation. This approach was further developed for 3D operating space by Al-Garni, Moustafa, and Javeed Nizami (1995). However, the LQR controller can ensure optimality just for linear systems (or locally for nonlinear systems). To solve this drawback, soft computing-based algorithms like PSO have also been developed for optimal control of nonlinear systems. PSO algorithm has been employed by Maghsoudi, Mohamed, Husain, and Tokhi (2016) to tune the parameters of a PID controller such that an objective function indicating the payload tracking error and sway are minimized. This scheme has been integrated with an input shaping scheme and compared with classic PID controllers. However, these approaches usually lead to offline optimizations which may lead to a lack of robustness to perturbations. Optimal controllers can be designed to satisfy some constraints on the state variables and the control input as well. Considering the constraints, the optimization usually leads to a boundary value problem (Auernig & Troger, 1987), which can be solved by Pontryagin maximum principle. However, Manson (1982) has reported that optimal controllers can be sensitive to parameters, and they just provide a kind of sub-optimality for real online applications. Optimal controllers have also been designed considering the presence of winding and input torque (Sakawa & Shindo, 1982) where the controller is designed based on five different operating conditions. Note that flatness theory is widely used in optimal control to provide a map among inputs and the desired outputs while respecting various constraints, *e.g.*, collision avoidance (Chen, Fang, & Sun, 2016).

3.3.11. Lyapunov-based control design

The Lyapunov method has been employed by almost all references either for control design or stability analysis. Methods that do not belong to other control classifications are reviewed here. This strategy may lead to full-state feedback for 2D (Shi, Li, Ma, & Sun, 2019; Sun, Wu, Fang, & Chen, 2018) and 3D problems (Fang et al., 2001). The Lyapunov-based design has been compared with the linear quadratic regulator (LQR) and PD controllers for single-pendulum (Zhang, Ma, Rong, Tian, & Li, 2017) and double-pendulum (Zhao, Ouyang, & Iwasaki, 2021) models. Note that there is a very strong link between the Lyapunov-based control and passivity-based control when the Lyapunov function is the physical energy of the system. In this case, passivity-based theory can be used to investigate the stability and behavior of the system (Fang et al., 2001; Sun & Fang, 2012). Some studies have also been conducted to develop output feedback strategies based on Lyapunov design (Sun et al., 2017) or to avoid control saturation (Sun et al., 2017). See also (Wu & He, 2015), where two Lyapunov functions have been proposed. The first one only includes the sway angle. By calculating their time derivatives, the desired velocity trajectory has been obtained to reduce the sway. The other Lyapunov function includes both the sway angle and the cart position and is used to obtain the control law.

The integration of the Lyapunov-based control with input shaping has been proposed in Antipov and Krasnova (2022), Zhang et al. (2016) to reduce the payload sway. The Lyapunov-based design can be used to handle the unknown system's parameters, *e.g.*, length of the cable, weights, and external forces (Antipov & Krasnova, 2022; Lu, Fang, & Sun, 2017a; Zhang et al., 2016). In Fang, Ma, Wang, and Zhang (2012), an input shaping is developed for the cart to reduce the sway. Afterward, an adaptive controller is designed based on the Lyapunov method. This is a full-state feedback control, and the adaptation laws are derived for friction, external forces, cable length, and weights. Lyapunov-based control design has also been considered for a multi-cable OC based on the equivalent single-pendulum model in Lu, Fang, and Sun (2018). A simple linear state-feedback controller is obtained, which contains the first derivatives of the state variables. The effect of the distributed parameter modeling in the state-feedback design when considering PDE models corresponding to flexible cables has been studied by Chentouf and Han (2020) and it is shown that the system can remain exponentially stable. A Lyapunov-based feedback controller has been introduced by d'Andréa Novel et al. (1994) where the model of the OC given by a PDE-ODE model and the flexibility of the cable has been taken into account (see also Cuong and Tuan (2023), Golovin et al. (2022), Oguamanam, Hansen, and Heppler (1998, 2001) for the

case where flexibility exists in the supporting structures). This control law only needs the absolute position of the cart and the angle between the cable and the vertical axis at the attached end. Asymptotic stability of the closed-loop system is ensured, and by studying the *decay of the energy*, it is concluded that the provided feedback cannot ensure uniform convergence (see also Chentouf and Han (2020) for similar results with an input delay, He and Ge (2016) for the use of cooperative control in the presence of parameter uncertainties, and Sun et al. (2019) with stiffness in the joints). A tracking controller has been developed in Zhang et al. (2018) for the 3D space, and it is concluded that this controller supersedes the collocated PD and the energy coupling output feedback (Sun et al., 2013) in terms of transient response. Another Lyapunov-based control strategy has been introduced for the double-pendulum system where the length of the first link is variable (Shi, Yao, Yuan, Tong, et al., 2022). Subsequently, a Lyapunov function has been defined containing the error variables of both cart position and the cable's length to obtain the coupled control forces applied to the cart as well as the cable's winch for the tracking case (see also Lu et al. (2017a) for the double-pendulum model where the length of the first link is variable). The Lyapunov design has also been employed for the double-pendulum system in 3D space integrated with a fuzzy gain tuner (Miao, Zhao, Wang, & Ouyang, 2022).

3.4. Control in 3D operational space

The control of OCs in 3D space has been studied from a different point of view. The studies considering the control of lumped mass multibody models in 3D space are as follows:

- **Decentralized control**: In this method, the linearized model around a stable equilibrium point (vertical position) is used to design the controller. Under such conditions, the coupling among the axes is eliminated and controllers can be designed for each axis independently, without taking the couplings into account. In this case, the controllers that are designed for the 2D space can be used to control each channel, separately (the studies in this category are Ebeid, Moustafa, and Emara-Shabaik (1992), Garrido et al. (2008), Toxqui et al. (2006), Yoshida and Tabata (2008)). Maghsoudi et al. (2016) has designed a PID controller to control one axis of a crane modeled in 3D space. The PID controller is tuned using the PSO algorithm to show the best possible payload positioning. Moreover, Maghsoudi et al. (2017) has designed an input shaping control for one axis of a crane. Similarly, the PSO algorithm is used to tune the parameters of the shaper. To handle the coupling effect, in at least one study, each controller has been designed independently for each channel and the coupling is considered a disturbance. For instance, Vázquez et al. (2014) developed a super-twisting controller while the coupling is considered a disturbance (though this is not an a priori bounded disturbance).
- **Control design considering the coupling**: In this category, the controllers are designed based on the nonlinear model of the system and the couplings among the axes have been taken into account in the control design. In this method, the controllers are usually designed based on a Lyapunov function containing the variables corresponding to all axes in order to derive a centralized control rule (Wu & He, 2017). PFL has been also employed in this category to take the coupling into account (Chwa, 2009; Lee et al., 2013; Sun, Fang, & Zhang, 2012; Sun et al., 2013; Tuan et al., 2012, 2014; Wu & He, 2016). While a centralized control law can be obtained based on these procedures to handle the coupling, the stability is usually ensured locally (Lee et al., 2013; Tuan et al., 2012, 2014). SMC is another approach in this category to handle the coupling (Chwa, 2017). Flatness control leads also to a centralized control law (Knierim et al., 2010) in 3D space.

3.5. Sway control using cable length manipulation

All the above-mentioned studies try to control the payload sway by manipulating the force applied to the cart as the only control input. However, there are still other studies (Abdel-Rahman & Nayfeh, 2002; Abdel-Rahman et al., 2003; Bockstedte & Kreuzer, 2005; Hayajneh, Radaideh, AL-Oqla, & Nejdawi, 2008; Moustafa, 1994; Wei, Limin, & Zhengnan, 2017) where the sway is controlled by manipulating the cable length l_1. In other words, the cable length is considered as a control input rather than a control output, and the dynamics corresponding to the winding mechanism are neglected. Couplings exist between the winding mechanism and the sway (Abdel-Rahman & Nayfeh, 2002; Abdel-Rahman et al., 2003; Moustafa, 1994) (and between the $l, \dot{l}$-dynamics and the rest of the dynamics, see Section 2, Appendices A–C and E for more details). Hence, cable length manipulation can be used to control the sway.

3.6. Sway control using passive mechanical elements

The above-mentioned references are considered as active control, *i.e.*, the required damping for the stability is injected virtually using the force applied to the cart. On the other hand, some of the control objectives can be achieved by the implementation of passive dampers as introduced in Balachandran, Li, and Fang (1999), which is out of the scope of this paper. In this strategy, the cart is attached to the frame through mechanical dampers. This approach can modify the bifurcation point of the mechanical system leading to the payload sway reduction, as done in Balachandran et al. (1999).

3.7. Summary of all methods

A summary of all studies presented for modeling and control of OCs is made in Tables 2–8. The nomenclature corresponding to these tables is provided in Table 1. These tables allow to review the literature at a glance and help in finding the most appropriate reference corresponding to each application.

3.8. Operator-in-the-loop methods

The foregoing sections deal with autonomous systems where no human intervenes in the loop. Another approach consists of considering the actions of the operator inside the control loop. A survey of this family of control methods is made in Bonnabel and Claeys (2020), see also Giacomelli et al. (2019, 2018a, 2018b). Trajectory tracking controllers combined with suitable desired trajectories (for the so-called velocity-command strategy) are very important in this context, see Section 7.2.2 and Remark 10. However, the basic assumption in the operator-in-the-loop control systems is that the low-level controller (usually a collocated feedback F) allows to perfectly track cart velocity profiles. In other words, it is assumed that the system's output is the cart's velocity (*i.e.*, $y = \dot{x}$) and $y(t) \to y_d(t)$ should be achieved by the collocated input $F(t)$. If the convergence is fast enough, the cart's velocity can be used to control the payload using suitable cart's motion designed with flatness (*i.e.*, the cart's desired velocity is a suitable function of the payload's desired motion, designed from a suitable inversion method, like flatness).

Remark 7. This paper follows the standard convention in the control community where the open-loop control strategy refers to any control method where there is no feedback. As explained in Section 3.1, in the open-loop strategies, the controller directly generates the force applied to the cart based on the reference trajectory without using feedback. However, the feedback that exists in the motor speed driver is usually neglected in the operator-in-the-loop literature and any collocated feedback where there is no feedback from the sway angle is called

Table 1
Symbols used in the tables.

Feedback (feed)	O: open-loop, C: collocated, N: noncollocated
Scenario (sce.)	R: regulation, T: tracking
Stability (stab.)	GE: global exponential, LE: local exponential GA: global asymptotic, LA: local asymptotic GF: global finite-time, LF: local finite-time, N/A: not available
Validation (val.)	S: simulation, E: experiment, SE: simulation and experiment
Control (cont.)	x: control cart in one direction, θ: just sway control x, y: control cart in two direction, l: control the cable's length
Number of cables (NC)	The indicated number is the number of parallel cables. Moreover, R and F stand for rigid and flexible links, respectively

the open-loop method in some of the resources (Bonnabel & Claeys, 2020). Because of the fast dynamics (compared to the dynamics of the crane), the dynamics of the speed drive are usually neglected in this approach and it is assumed that the payload exactly tracks the reference trajectory.

Following Bonnabel and Claeys (2020), the operator-in-the-loop application refers to a condition where the velocity trajectory is generated by an operator (a human who drives the crane). This case imposes the following two extra challenges to the controller design:

- The reference velocity is generated by the driver and therefore is not totally known for the future time steps. Hence, the application of the control method where the reference trajectory for the next time steps is required, *e.g.*, MPC and flatness (see the example in Bonnabel and Claeys (2020) where the second derivative of the reference trajectory has to be available for the flatness control) is limited.
- The driver may generate several impulses in order to drive the payload to the destination as fast as possible. Such discontinuous impulses can hinder the application of the controllers where the derivatives of the reference signal are required to synthesize the control signal, for instance, the flatness control where the second order derivative of the reference signal is necessary (Bonnabel & Claeys, 2020). To solve this issue, Bonnabel and Claeys (2020) has proposed to use a low-pass filter to make the reference trajectory continuous and differentiable. The cutoff frequency of this filter should be tuned accurately to avoid a large delay and a poor transient response (a detailed filter design procedure is available in Bonnabel and Claeys (2020)).

4. Review of the experimental systems considered in the literature

According to Tables 2–7, many references have considered experimental validation of the control systems on different kinds of experimental setups. Hence, it is of interest to review such references based on the methodology and employed laboratory setup. The experimental implementations made in the literature can be classified based on the size of the crane, the computer used to implement the control algorithms, the types of actuators, and sensors as explained in Sections 4.1 to 4.4, respectively.

4.1. Scale of the experimental setups

The cranes used in the literature can be classified into three categories, *i.e.*, full-scale setups, scaled laboratory setups adopted from the real industrial one, and small laboratory setups. The full-scale cranes are barely employed for the experiments because of clear reasons. A full-scale 15 tons crane with 25 m of hoisting cable is used by Singhose et al. (2000). A tower crane with 1650 kg lifting capacity and 45 m hoisting height is considered in Rauscher and Sawodny (2021). Another full-scale 3.2 tons crane has been employed by Arena et al. (2015). A tower crane with 40 m hoisting cable is used in Bonnabel and Claeys (2020). A 5-ton overhead crane is considered in Aschemann (2009) for the experiments. In addition to the mentioned full-scale cranes, scaled setups have also been used for the experiments. For instance, Kim et al. (2004), Sano et al. (2010) have considered the 1/4 and 1/50 scales of some specific industrial cranes. See also Ma, Lou, and Jia (2023) for the illustration on experiments of a Lyapunov and Neural Network approach for the control design. Moreover, most of the references have built or used small laboratory setups for the experiments. In this context, two commercially available laboratory setups with a few kilograms capacity made by INTECO (Alhazza et al., 2016; Chen & Saif, 2008; Cuong & Tuan, 2023; Hong & Ngo, 2012; Kim & Hong, 2009; Ngo & Hong, 2012; Park et al., 2007; Toxqui et al., 2006; Vázquez et al., 2014) and QUANSER (Khorshid & Al-Fadhli, 2021; Park et al., 2008; Shen et al., 2021) have been used in the literature. All other references have developed their own laboratory setups with small payloads (typically the cart mass is between 5 to 20 kgs and the payload is less than one kg with less than one meter of hoisting height) (Chen et al., 2019; Chwa, 2017; Lu et al., 2018; Ouyang et al., 2019, 2019; Peng et al., 2012; Sun & Fang, 2012; Sun et al., 2017; Sun et al., 2013, 2018; Sun et al., 2018, 2019; Sun et al., 2019; Wu & He, 2015, 2016; Wu & He, 2017; Yoon et al., 2014; Zhang, 2019; Zhang, Ma, et al., 2017). As it can be seen, most of the references have considered light payloads for the experiments. Under such conditions, the high-frequency vibrations caused by the hoisting cable may not be observed. Hence, future works with heavier payloads seem to be necessary to study the string behavior of the cable.

4.2. Computers employed to implement the control algorithms

Different kinds of computer architectures have been employed to implement control algorithms on OCs. In most cases, the hardware-in-the-loop (HIL) simulation strategy is used to do the experiments, where the controllers are implemented on a personal computer in the MATLAB environment, and data acquisition (DAQ) interfacing devices are connected to the computer to receive the measurements and send the control signals to the actuators (Alhazza et al., 2016; Chen et al., 2019; Diwold et al., 2022; Khorshid & Al-Fadhli, 2021; Le, Kim, Kim, & Lee, 2012; Le et al., 2014; Lee et al., 2014; Li, Ma, et al., 2022; Lu et al., 2017b; Miao et al., 2022; Moon et al., 2013; Ouyang et al., 2019, 2021; Sun & Fang, 2012; Sun et al., 2015; Sun et al., 2013; Sun et al., 2018, 2019; Sun et al., 2019; Tuan et al., 2012; Vázquez et al., 2014; Wu & He, 2016; Zhang, He, Chen, & Feng, 2020; Zhang, Ma, et al., 2017) are used. In this context, different kinds of DAQ systems, *e.g.*, dSPACE cards (Diwold et al., 2022; Rauscher & Sawodny, 2021), National Instrument (NI) boards (Le et al., 2012, 2014; Moon et al., 2013; Ouyang et al., 2021; Tang & Huang, 2016; Tuan et al., 2012, 2014), Advantech boards (Lee et al., 2014), Quanser data-acquisition terminal (Khorshid & Al-Fadhli, 2021), Googol boards (Li, Chen, & Zhang, 2022; Lu et al., 2017b, 2018; Ouyang et al., 2019; Sun & Fang, 2012; Sun et al., 2018, 2019), ARTISAN Technology boards (Bartolini et al., 2000; Bartolini et al., 2003) and INTECO DAQ boards (Alhazza et al., 2016; Chen & Saif, 2008; Hong & Ngo, 2012; Kim & Hong, 2009; Park et al., 2007; Toxqui et al., 2006; Vázquez et al., 2014) are used. Furthermore, customized digital signal processor (DSP) or microprocessor-based systems have been designed (Lin et al., 2012), especially for the industrial-scale cranes (Arena et al., 2015). For the

Table 2
Summary of the control methods in 2D space for the lumped single-pendulum.

Ref.	Feed.	Sce.	Stab.	Val.	Cont.	Control method
Park et al. (2007)	N	T	GE	SE	x	SMC
Chen et al. (2020)	N	T	GA	S	x	SMC
Kuo-Kai Shyu et al. (2005)	N	T	GA	S	x	SMC
Hamdy et al. (2018)	N	T	LA	S	x	Partial feed. lin. + deadbeat
Fang et al. (2012)	N	T	GA	S	x	Lyapunov der. + adap. frict. comp.
Lee et al. (1997)	C	R	LA	E	x	PID
Lee (2004)	N	T	GA	S	x, l	SMC
Fliess, Levine, and Rouchon (1991)	N	T	N/A	S	x, l	Flatness
Lee et al. (2006)	N	T	GA	E	x, l	SMC
Alhazza et al. (2016)	O	–	N/A	SE	x	Input shaping
Chen et al. (2016)	N	R	N/A	SE	x	MPC
He, Zhang, and Ge (2014)	N	T	LA	S	x	Feedback lin. + adaptive law
Sun et al. (2015)	C	R	GA	SE	x, l	Lyapunov derived adaptive law
Abdullahi et al. (2018)	O	–	N/A	E	x	Input shaping
Ngo and Hong (2012)	N	T	GA	SE	x	SMC
Moon et al. (2013)	N	T	GA	SE	x, l	SMC with parameter estimation
Park et al. (2014)	N	T	GA	S	x	SMC + fuzzy uncertainty estimation
Sano et al. (2010)	C	T	N/A	SE	x	Obs.-based time-delay tolerant PI
Yi et al. (2003)	N	R	LE	S	x	State-feedback + fuzzy traj. generator
Park et al. (2008)	N	T	GA	SE	x	SMC + fuzzy compensator
Ohnishi, Tsuboi, Egusa, and Uesugi (1981)	N	R	N/A	S	x	Linear state feedback
Collado et al. (2000)	C	R	GA	S	x	PD control
Omar (2003)	N	T	LA	SE	x	PD - fuzzy - time-delayed
Zhang, Wu, and Huang (2017)	N	R	Lya.	S	x, l	Flatness control
Diwold et al. (2022)	N	T	LE	E	x, l	Discrete-time flatness control
Hong et al. (2003)	O	–	N/A	S	x	Input shaping
Singhose et al. (2000)	O	–	N/A	SE	x	Input shaping with hoisting
Wu and He (2015)	N	R	LA	S	x	Lyapunov derived
Zhang, Ma, et al. (2017)	N	R	GA	SE	x	Lyapunov derived
Moustafa (1994)	N	T	LA	S	θ	Linear feedback (x, l are inputs)
Zhang (2019)	N	T	GF	SE	x	Terminal SMC
Fliess et al. (1995)	O	–	N/A	S	x	Flatness control
Kimiaghalam, Homaifar, Bikdash, and Dozier (1999)	N	T	N/A	S	x, l	Linear feedforward + GA generated traj.
Antipov and Krasnova (2022)	N	T	GA	S	x	State-feedback with trajectory modification
Wahrburg et al. (2022a)	N	R	N/A	SE	x	Input shaping robust to initial sway
Wahrburg et al. (2022b)	N	R	N/A	SE	x	Input shaping robust to initial sway
Wang, Liu, He, et al. (2022)	N	R	GA	E	x	Terminal SMC with adaptive parameters
Hu and Xu (2022)	N	R	GA	S	x, l	Adaptive SMC
Wang, Tan, Qiu, et al. (2021)	N	Sce.	GA	S	x, l	SMC
Qian and Yi (2016)	N	R	GA	S	x	SMC
Zhang, He, Chen, and Feng (2020)	N	R	GA	E	x	Lyapunov derived
Singhose et al. (1997)	O	–	N/A	S	x	Input shaping
Zhang et al. (2014)	O	–	N/A	SE	x	Dynamic programming
Shao, Zhang, Zhang, Zhao, and Chen (2020)	N	R	LA	S	x	LMI design based on fuzzy model
Fatehi et al. (2014)	N	T	LA	S	x	Linear state feedback
Wu et al. (2015)	N	R	N/A	S	x	MPC
Sun and Fang (2012)	N	R	GA	SE	x	Lyapunov derived
Fang, Dixon, Dawson, and Zergeroglu (2001)	N	R	GA	S	x	Lyapunov derived
Yu et al. (1995)	N	T	LA	S	x	Approx. FL + LQR
Sun and Fang (2014b)	N	T	GA	SE	x, l	Lyapunov derived
Piazzi and Visioli (2002)	C	T	N/A	S	x	Observer-based linear state-feedback
Wu and Xia (2014)	O	–	N/A	S	x	Offline trajectory design
Chen et al. (2016)	N	T	GE	SE	x	FL + flatness
Bartolini et al. (2003)	C	T	N/A	SE	x, l	SMC
Le et al. (2014)	N	T	GA	SE	x, l	PFL + SMC
Smoczek and Szpytko (2017)	N	T	N/A	E	x	PSO model identification + MPC
Aschemann (2009)	N	T	N/A	E	x, l	Observer-based IDA-PBC
Chunshien Li et al. (2004)	C	T	N/A	S	x	Neuro-fuzzy system
Karkoub and Zribi (2001)	N	R	N/A	S	x, l	SMC, μ synthesis, state-feedback
Hičár and Ritók (2006)	C	R	LA	SE	x, l	State-observer based classic linear
Bartolini et al. (2002)	N	T	GA	S	x, l	SMC
Singhose et al. (1990)	O	–	N/A	S	x	Input shaping
Vyhlídal et al. (2013)	O	–	N/A	S	x	Input shaping
Lu et al. (2017b)	N	T	GA	SE	x	Disturbance observer based SMC
Kolonic, Poljugan, and Petrovic (2006)	N	R	LA	SE	x	Convex combination of LTI systems
Auernig and Troger (1987)	O	–	N/A	S	x, l	Optimal control (Pontryagin's principle)
Manson (1982)	O	–	N/A	S	x	Optimal control
Peng et al. (2012)	C	R	N/A	SE	x	PD control
Golovin et al. (2022)	C	R	LA	SE	x	Lyapunov control considering structural deformations
Mohamed et al. (2022)	N	–	N/A	S	x	PID with multi-objective genetic gain optimization
Orsini (2022)	N	T	LA	S	x	Observer-based state feedback
Gu and Xu (2022)	N	R	GA	S	x, l	SMC robustness to matched and unmatched disturbances
Zhang, He, et al. (2022)	N	R	GA	E	x	Quasi-PID with control saturation avoidance
Krupa et al. (2022)	C	R	N/A	E	x	Nonlinear MPC
Wang, Wu, and Lei (2022)	N	R	GA	SE	x	SMC with disturbance observer

(*continued on next page*)

Table 2 (*continued*).

Ref.	Feed.	Sce.	Stab.	Val.	Cont.	Control method
Alghanim et al. (2015)	O	–	N/A	SE	x	Input shaping
Wu, Xu, and He (2020)	N	R	GA	SE	x	Lyapunov-based design

Table 3
Summary of the control methods in 2D space for the lumped-mass double-pendulum.

Ref.	Feed.	Sce.	Stab.	Val.	Cont.	Control method
Ouyang et al. (2019)	N	T	GF	SE	x	SMC
Chen et al. (2019)	N	R	GA	E	x	Lyapunov derived
Wang, Tan, Zhang, et al. (2021)	N	R	GA	S	x	SMC
Zhang et al. (2016)	N	T	GA	E	x	Lyapunov der. + adap. param. estim.
Vaughan et al. (2010)	O	–	N/A	SE	x	Input shaping
Sun et al. (2017)	N	R	GA	E	x	Lyapunov der. output feedback
Sun et al. (2018)	O	–	N/A	SE	x	Dynamic programming
Vaughan et al. (2010)	O	–	N/A	SE	x	Input shaping
Ouyang et al. (2019)	C	T	LA	SE	x	PID control + S-shaped trajectory
Li, Chen, and Zhang (2022)	N	R	GA	E	x, l	SMC with Adaptive fuzzy law
Hong et al. (2003)	O	–	N/A	S	x	Input shaping
Tang and Huang (2016)	O	–	N/A	SE	x	Input shaping for distributed mass
Zhao and Gao (2012)	N	R	N/A	SE	x	Input shaping for distributed mass
Qian and Yi (2016)	N	R	Asymptotic	S	x	SMC
Singhose et al. (2008)	O	–	N/A	SE	x	Input shaping
Sun et al. (2018)	N	R	GA	E	x	Adaptive Lyapunov derived
Ouyang et al. (2019)	N	T	GA	E	x	SMC with adaptive pole surface
Khorshid and Al-Fadhli (2021)	O	–	N/A	SE	x	Input shaping for sloshing payload
Li, Ma, et al. (2022)	O	–	N/A	SE	x	Trajectory planning with sloshing payload
Khorshid and Al-Fadhli (2021)	O	–	N/A	SE	x	Input shaping for sloshing payload
Weiping, Diantong, Jianqiang, and Dongbin (2004)	C	R	GA	S	x	PD control
Shi, Yao, Yuan, Tong, et al. (2022)	C	R	GA	SE	x, l	PBC
Tuan and Lee (2013)	N	R	GA	S	x	SMC
Sun et al. (2019)	N	R	GA	E	x	Quasi-PID
Nguyen et al. (2022)	C	R	LA	S	x	Robust input shaping with state-observer
Shehu et al. (2022)	N	R	GA	S	x	SMC
Chen et al. (2022)	N	R	GE	S	x	SMC
Shi, Yao, Yuan, Hu, et al. (2022)	C	T	GA	SE	x	Tracking PID with feedforward terms

Table 4
Summary of the control methods for flexible single-pendulum model.

Ref.	Feed.	Sce.	Stab.	Val.	Cont.	Control method
d'Andréa-Novel and Coron (2000)	N	R	LE	S	x	Lyapunov derived
Wen, Lou, et al. (2022)	N	R	LE	S	x	Lyapunov derived
d'Andréa Novel et al. (1994)	N	R	LA	S	x	Lyapunov derived
d'Andréa Novel et al. (2019)	N	R	LF	S	x	Lyapunov derived
Shen and Caverly (2020)	N	R	LA	E	x, l	PBC with Ritz discretization
Sun et al. (2019)	C	R	GA	E	x	Joint stiffness + Lyapunov derived
Chentouf and Han (2020)	N	R	LA	S	x	Lyapunov derived with extra actuators
Alli and Singh (1998)	C	T	LA	S	x	PBC
Shen et al. (2021)	C	R	LA	SE	x, l	Adaptive PBC
d'Andréa Novel and Coron (2002)	N	R	LA	S	x, l	Boundary Lyapunov derived controller
Cui and Zheng (2019)	N	R	LA	S	x	Lyapunov derived
Pham et al. (2022)	N	R	GA	S	x, y, l	Fuzzy SMC in 3D space
Le et al. (2022)	N	R	GA	S	x, y, l	Control of sway because of cable's length extension in 3d
Ma et al. (2022)	N	R	LA	SE	x	Boundary Lyapunov derived controller

older implementations, the use of the VMEbus computer has been reported by Lee (1998), Lee and Cho (2001), Lee et al. (1997, 2006). Note that to connect the computers to the actuators and sensors, RS-232 communication protocol is usually employed according to the literature (Tuan et al., 2014).

4.3. Actuators employed for the experiments

Electric motors are installed on the cranes as actuators to drive the cart and the winding mechanism. The nominal powers of these actuators are calculated based on the weights of the cart and payload. The motors used for the cart movements are employed with different powers, *e.g.*, 100 W (Sun et al., 2019), 200 W (Li, Chen, & Zhang, 2022), 400 W (Chen et al., 2019; Li, Ma, et al., 2022). On the other hand, electric machines with different powers, *e.g.*, 100 W (Chen et al., 2019; Li, Chen, & Zhang, 2022) are employed to actuate the winding mechanism for the payload hoisting.

4.4. Sensors used in the experiments

Sensors have been used in the experiments to measure the position of the cart, the length of the hoisting cable, as well as the sway angles. The cart's position and the length of the hoisting cables are usually measured through the optical encoders installed on the shaft of the motor driving the cart and the hoisting mechanism. Shaft encoders are identified by their resolutions in the pulse per rotation (PPR) unit, *e.g.*, 100 (Khorshid & Al-Fadhli, 2021), 360 (Bartolini et al., 2000; Bartolini et al., 2003), 550 (Miao et al., 2022), 2000 (Lee et al., 2014), 2500 (Sun et al., 2015, 2019), 4096 (Chang & Chiang, 2008), 131072 (Li, Ma, et al., 2022), 1048576 (Ouyang et al., 2019; Ouyang et al., 2019) PPR. Note that considering rigid links, some references have measured the sway angles using the shaft encoders installed at the attached point of the link to the cart with different resolutions, *e.g.*, 2500 (Lee et al., 2014; Li, Ma, et al., 2022), 6000 (Sun et al., 2015), 16384 (Miao et al., 2022) PPR. In addition, the inertial measurement units (Arena et al.,

Table 5
Summary of the control methods in 3D space for the lumped single-pendulum with rigid link.

Ref.	Feed.	Sce.	Stab.	Val.	Cont.	Control method
Wu and He (2017)	N	R	GA	SE	x, y	Lyapunov derived
Tuan et al. (2014)	N	R	GA	SE	x, y, l	PFL
Tuan et al. (2012)	N	R	LA	SE	x, y, l	PFL
Lee et al. (2013)	N	R	LA	S	x, y, l	PFL
Sun et al. (2013)	N	R	GA	E	x, y	Lyapunov derived
Chwa (2009)	N	T	GA	S	x, y	Lyapunov derived
Wu and He (2016)	N	T	GA	SE	x, y	PFL
Chwa (2017)	N	R	GA	S	x, y	SMC
Knierim et al. (2010)	N	T	GA	E	x, y, l	Flatness
Lee and Cho (2001)	C	T	N/A	E	x, y, l	Fuzzy
Yang and Yang (2006)	C	R	GA	E	x, y	Lyapunov derived adap. param. est.
Zhang et al. (2018)	N	T	GA	SE	x, y	Lyapunov derived.
Maghsoudi et al. (2017)	O	–	N/A	SE	x, y	PSO optimized input shaping
Maghsoudi et al. (2016)	C	R	N/A	SE	x, y	optimized PID with PSO
Toxqui et al. (2006)	N	R	LA	E	x, y	PID + neural compensator
Garrido et al. (2008)	C	R	N/A	E	x, y	PID + input shaping
Xi and Hesketh (2010)	C	R	LA	SE	x, y	Discrete-time integral SMC
Chen, Gao, and Zhang (2005)	N	T	GA	S	x, y, l	PFL
Hong and Ngo (2012)	–	–	N/A	SE	–	Kinematic of ship mounted cranes
Lee et al. (2014)	N	T	N/A	E	x, y	adaptive fuzzy SMC + visual feedback
Ebeid et al. (1992)	N	T	LE	S	x, y, l	Classic linear control + motor dynamics
Schindele and Aschemann (2011)	N	T	N/A	E	x, y	MPC
Bartolini et al. (2000)	N	T	LA	E	x, y	SMC
Lee (1998)	C	T	LA	E	x, y, l	Classic linear control
Fang et al. (2003)	N	R	GA	S	x, y	Lyapunov derived
Fang et al. (2001)	N	R	GA	SE	x, y	Lyapunov derived
Al-Garni et al. (1995)	N	T	N/A	S	x, y, l	Linear state feedback
Chen and Saif (2008)	N	T	GA	E	x, y, l	backstepping + exact differentiators
Vázquez et al. (2014)	N	T	GA	SE	x, y, l	SMC (coupling as disturbance)
Chang and Chiang (2008)	N	R	N/A	E	x, y	Fuzzy control
Lin et al. (2012)	N	T	GA	E	x, y	TSMC + adaptive fuzzy tuning
Yoshida and Tabata (2008)	N	R	N/A	E	x, y	Optimal control
Vu et al. (2022)	N	–	N/A	SE	x, y	Trajectory optimization + MPC
Yoshida and Tabata (2008)	N	R	N/A	E	x, y	Optimal control
Zhang, Zhu, et al. (2022)	N	R	GA	S	x, y	PBC
Almutairi and Zribi (2009)	N	R	GE	S	x, y, l	SMC + Luenberger observer

Table 6
Summary of the control methods in 3D space for the lumped double-pendulum with rigid link.

Ref.	Feed.	Sce.	Stab.	Val.	Cont.	Control method
Zhao et al. (2021)	N	T	GA	E	x, y	Adaptive Lyapunov derived
Ouyang et al. (2021)	N	R	GA	SE	x, y	Lyapunov derived
Miao et al. (2022)	N	R	GA	E	x, y	Adaptive Lyapunov derived with fuzzy gain tuner
Guo et al. (2023)	N	T	LA	SE	x, y	Flatness SMC neglecting nonlinearities and couplings

Table 7
Summary of the control methods in 2D space for multi-cable models.

Ref.	Feed.	Sce.	Stab.	Val.	NC	Cont.	Control method
Kim, Hong, and Sul (2004)	N	R	LE	E	4R	x	Linear state-feedback
Yoon, Nation, Singhose, and Vaughan (2014)	O	–	N/A	SE	2F	x	Input shaping
Yoon et al. (2010)	O	–	N/A	SE	2F	x	Input shaping
Nayfeh, Masoud, and Baumann (2005)	C	T	N/A	S	2R	x	LQR time-delayed and classic linear
Nayfeh and Baumann (2008)	N	R	LE	S	2R	θ	Control θ when x is input
Lu et al. (2018)	N	R	GA	E	2R	x	Lyapunov derived

Table 8
Summary of the control methods in 3D space for multi-cable models.

Ref.	Feed.	Sce.	Stab.	Val.	NC	Cont.	Control method
Klaassens, Honderd, El Azzouzi, Cheok, and Smid (1999)	C	R	N/A	S	4R	x, l	classic linear
Arena et al. (2015)	–	–	N/A	SE	4RF	–	kinematic modeling
Morrish, Cartmell, and Taylor (1997)	–	–	N/A	S	4R	–	kinematic modeling
Ngo, Hong, Kim, Shin, and Choi (2008)	C	R	N/A	S	4R	x	Kinematic + skew control
Ngo and Hong (2012)	N	T	GA	S	6R	x	SMC
Arena, Casalotti, Lacarbonara, and Cartmell (2013)	–	–	N/A	S	4RF	–	kinematic modeling

2015) as well as cameras have been used to measure the sway angles or payload position (Lee et al., 2014; Peng et al., 2012; Schindele & Aschemann, 2011). Moreover ultrasonic sensors are used in Li, Ma, et al. (2022) to measure the sloshing level of the liquid container cranes.

5. Modeling for numerical simulations

As it was seen in Section 2, different types of models have been developed for OCs allowing to design and study the controllers in the closed-loop, analytically, *e.g.*, the single and double-pendulum models.

Table 9
A list of the review papers in the literature.

Ramli et al. (2017)	Review of several control methods for single and double-pendulum systems in 2D space
Hong and Shah (2019)	Review of control methods for several models in 2D and 3D spaces
Bonnabel and Claeys (2020)	Survey on flatness control
Nayfeh et al. (2005)	Comparison of three different feedback controllers

This is also the case for the PDE-ODE models developed to capture the cable's flexibility since, in the end, spatial discretization is used to obtain a model with a small number of degrees of freedom suitable for the controller implementation. While such models are convenient for the controller design, they suffer from some drawbacks as explained in Section 2.7. Another model has been developed in this work, allowing the implementation and evaluation of all the controllers, regardless of the model used to design them. The proposed model is a multibody, pendulum-like system with a large number N of links. Lumped-mass models consist of a multibody system's approach to model cables (Huston & Kamman, 1981, 1982; Huston, Passerello, & Harlow, 1978; Kamman & Huston, 1985, 2001; Winget & Huston, 1981). As such, they can easily handle large deformations and associated nonlinearities. Sometimes they can also be seen as a set of particles linked by suitable potentials. Then they become closer to finite-element spatial (inconsistent) discretization of PDEs (Egeland & Gravdahl, 2002). They can also be seen as an extension of linear oscillators: if the cable is in the vertical posture, and a torsional spring is associated with each flexible link, the system is equivalent to a linear chain of oscillators, the control of which is tackled in Ovseevich and Ananievski (2021), Ovseevich and Fedorov (2015). Such models are known to be less accurate than those stemming from continuum mechanics (Lv et al., 2020), but they have the advantage of being more tractable for control and thus are abundantly used in Robotics and in Automatic Control. *Hence, it is expected that the simulations based on the proposed model lead to more realistic results compared to the case where the simulations are conducted based on the low-degrees-of-freedom control-oriented models*. The dynamics is studied in Appendix A. The MATLAB MULTIBODY TOOLBOX has been used in this study to realize such a model without writing down the equations.

The scheme of the 20-link model is depicted in Fig. 4, where two sets of joint angles are indicated since both can be useful for the analysis. The model is composed of 18 links with damping and stiffness in the joints to model cables' dynamics. Moreover, two other links are considered to take into account the presence of the tool and the payload as seen in the double-pendulum model Fig. 2(b). Note that the first 18 links can be considered as a simplified finite element model of the cable yielding a non-consistent mass matrix in a spatial set of coordinates (Brogliato, 2022). While increasing the number of links can improve the model's accuracy, it increases the required time for the numerical simulations. Hence, the number of 18 links is considered by trial and error to provide the best trade-off between the simulation time and the accuracy of the model. In addition, the damping and stiffness considered in the joints are selected empirically. One can change all these parameters in the toolbox and redo the simulations to have customized results corresponding to each specific application (see Section 7).

6. State, parameter and disturbance estimation

As it was seen, the reviewed controllers need different types/numbers of sensors depending on the feedback structure. Sensor selection was the topic of some references. For instance, the implementation of vision-based sensors for sway detection has been addressed in Huang, Xu, Zhao, and Yuan (2022), Lee et al. (2014), Sano et al. (2010). Moreover, feedback based on inclinometers and IMUs have been considered in Kim and Hong (2019), Kim et al. (2004), respectively, and it is reported in Kim et al. (2004) that a simple inclinometer sensor can provide the same performance as sophisticated vision-based

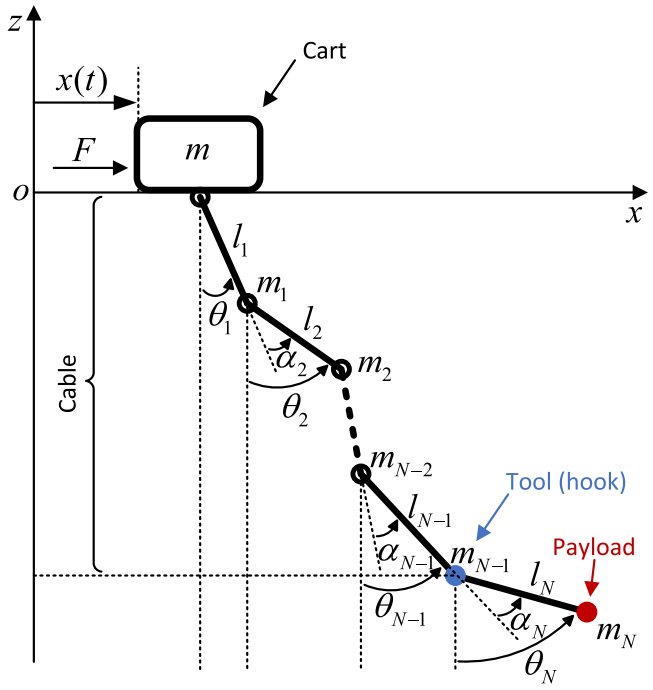

Fig. 4. Schematic diagram of the simulation-oriented model in 2D operating space with 20 links used for the simulations.

feedback. However, there are still cases where it is not possible to use sensors for measurements. In addition, some of the system's parameters contributing to the control law synthesis may be unknown in general. All these issues motivate the design of the estimation and observation methods for the overhead cranes as explained below.

6.1. State-observation

The state variables required to synthesize the control signal cannot be always measured because of the cost, and technical constraints. In such cases, it is necessary to develop state-observation algorithms. The state-observer design based on the tangent linearized models of the cranes, *e.g.*, Luenberger observer (Guo et al., 2023; Hičár & Ritók, 2006; Kim et al., 2004; Piazzi & Visioli, 2002), or its discrete-time form (Sano et al., 2010) has already been addressed in the literature. A Kalman–Bucy filter is developed in Rauscher and Sawodny (2021) to improve the accuracy of the measurements by removing the sensors' offset error. Since these observers are designed based on the linearized model, their stability is only valid locally, when the sway angle is small. The parameters of such linear observers can be designed using Ackermann's formula as used by Hičár and Ritók (2006). In order to estimate the velocities, *e.g.*, $\dot{x}, \dot{\theta}_1, \dot{\theta}_2$, from the position and angles x, θ_1, θ_2, time-differentiation methods, *e.g.*, pure differentiator integrated with low-pass filters (Zhang, He, Chen, & Feng, 2020), sliding-mode based differentiators (Chen & Saif, 2008) (see also Mojallizadeh, Brogliato, and Acary (2021) for a general introduction to the differentiators) are employed.

6.2. Disturbance and uncertainty observer

In Lu et al. (2017b), Ren, Chen, and Wu (2019), Wu et al. (2020), nonlinear adaption laws based on the Lyapunov theorem are obtained in order to estimate the matched disturbance when it is bounded and differentiable which relaxes more conservative assumptions considered in the previous works, *e.g.*, Sawodny, Aschemann, and Lahres (2002). It is shown, in Wu et al. (2020), that the control, integrated with the observer, eliminates the disturbance effect in finite time. The matched disturbance observer design based on the algebraic manipulations on the dynamic equations is studied by Ouyang et al. (2019). In addition to the external disturbance, more general types of uncertainties, *e.g.*, system parameter variations, unknown actuator nonlinearities (dead-zone), and unmodeled dynamics have been estimated based on fuzzy inference systems (Li, Chen, & Zhang, 2022; Park et al., 2014, 2008). Note that apart from estimation algorithms, the adaptation laws have been designed along with the control design using the Lyapunov method (Zhao et al., 2021) for the uncertain parameters. In addition, static laws in algebraic forms (Omar, 2003; Omar & Nayfeh, 2005) as well as neural networks (Ma et al., 2023) have been developed to estimate or compensate the friction.

7. Numerical experiments

As it was seen in Section 3, a very large number of controllers have been developed for OCs. For the sake of briefness, and since our goal in this article is to pave the way toward more general studies, a few typical controllers have been selected from each category to extract their key properties. An overview of these controllers as well as their structures are presented in Tables 10 and 11, respectively. They are briefly introduced below.

- **Unshaped input**: In this method, the whole system is considered as a point mass and the required force is calculated using the Newton formula as shown in Table 11, where m_t is the total system's mass and a_d is the provided acceleration trajectory. The application of this method is rare because of too much payload sway and is considered in the literature only for comparisons. Hence, this controller is usually integrated with input shapers, *e.g.*, ZV and ZVD.
- **ZV**: In this method, the unshaped input is convoluted with two impulses included in P_1 (see Table 11) to avoid payload sway.
- **ZVD**: Compared to ZV, in this method, the unshaped input is convoluted with three impulses included in P_2 (see Table 11) in order to reduce the payload sway more effectively.
- **Collocated PD**: This controller has a proportional gain k_p and a derivative gain k_d. Moreover, $e_x = x - x_d$ and $e_v = \dot{x} - \dot{x}_d$ with x_d as the reference position.
- **Quasi-PID**: This controller has five gains k_p, k_d, $k_{\phi 1}$, $k_{\phi 2}$, λ. Since this controller has been designed based on the double-pendulum system, it needs two feedbacks from the first (θ_1) and the second (θ_2) sway angles.
- **Noncollocated PD regulation**: This controller has been designed for the single-pendulum system and needs the corresponding sway angle θ_1. The three gains are k_p, k_d and k_a.
- **Collocated PD tracking**: The stability of this controller has been ensured for the tracking case. This controller has five gains k_p, k_d, λ, ξ, ϕ.
- **PD-PD**: This controller has been designed based on PDEs with the four gains $\alpha_i, i = 1, 2, 3, 4$.
- **SMC single and double-pendulum**: The control law in these methods is based on the nonlinear combination of several parameters. For the sake of space, the formula of these controllers are neglected in this article. The single-pendulum SMC has six parameters c_1, c_2, c_3, c_4, k, η and the SMC designed based on the double-pendulum system has five tuning parameters λ, α, β, K, c.
- **PD energy**: The parameters of this controller are $k_p, k_d, k_q, \lambda, \zeta$. Moreover, $\chi = e_x + \lambda \sin(\theta_1)$ and $\varepsilon = x + \lambda \sin(\theta_1)$.
- **Coupling tracking**: Compared to the previous 2D controllers, in this scheme, two control signals, *e.g.*, F_x and F_y (see (4)) are calculated in order to control the payload in 3D space. This controller has five tuning parameters $k_{px}, k_{dx}, k_{py}, k_{dy}, \lambda$. Note that if this controller is used for the 2D case, one can simply ignore one of the axis, *e.g.*, $k_{px} = k_p, k_{dx} = k_d, k_{py} = 0, k_{dy} = 0, \lambda = 0$. Moreover, θ_x and θ_y are the projection of θ_1 on the x and y axes, respectively.

Remark 8. According to Table 11, it can be seen that, apart from the classifications, most controllers are composed of the linear combination of feedforward, proportional, derivative, and integration terms.

7.1. Hoisting toolbox

A computer software named Hoisting Toolbox has been developed in this work in order to compare all the considered controllers using numerical simulations for an OC with parameters listed in Table 12. The toolbox is briefly introduced in Appendix H. Two main functionalities of this toolbox, *i.e.*, parameter tuning and evaluation are introduced in Sections 7.1.1 and 7.1.2, respectively. Before that, three remarks are presented as follows:

1. Sway angle, in the pendulum-like models, *e.g.*, single and double-pendulum models shown in Fig. 2 (a, b), refers to the angle of the links with respect to the vertical axis. For the single pendulum model Fig. 2(a), the only sway angle is θ_1 while for the double-pendulum model Fig. 2(b), two sway angles θ_1 and θ_2 can be defined. Note that, with such a definition, the sway angle cannot be clearly defined for the pendulum-like model with flexible links Fig. 2(c).
2. The controllers have been tuned based on a double-pendulum model. The implementation of the controllers designed for the double-pendulum system is straightforward on such a model. However, some of the control methods are originally designed for the single-pendulum system and only a single angle can contribute to the control law. This issue has not been addressed in the literature and it is not clear how to manage it. In this study, two independent implementations have been considered for such methods with the first and last sway angles feedback. These implementations are indicated by (first) and (last) in Table 13.
3. The SMCs are mainly composed of discontinuous (set-valued) signum functions. It is well-known that the time-discretization of such controllers is a crucial step in their implementation, and that the implicit (or semi-implicit) algorithms drastically supersede explicit ones (Acary, Brogliato, & Orlov, 2012; Brogliato & Polyakov, 2021; Brogliato, Polyakov, & Efimov, 2020; Huber, Acary, & Brogliato, 2016; Mojallizadeh et al., 2021). Therefore these set-valued inputs have been implemented based on two different discretization schemes, *i.e.*, Euler explicit and implicit methods, indicated by "exp" and "imp", respectively.

7.1.1. Parameter tuning

Parameter tuning is one of the most important topics that has to be addressed clearly for providing a fair comparison among all control methods. As it can be seen in Table 11, each controller has some parameters that need to be tuned. The appropriate intervals of some parameters have been obtained in the literature in order to ensure stability, *etc*. However, a systematic and comprehensive method has not been yet introduced in the literature to tune the parameters corresponding to all controllers. In fact, because of the complexity of the tuning raised by the nonlinearity and perturbation, parameter tuning is still an

Table 10
Overview of the controllers.

Controller	Feedback	Model	Space	Scenario
Unshaped input (Hong & Shah, 2019)	open-loop	point mass	2D	–
ZV (Hong & Shah, 2019)	open-loop	1,2-pendulum	2D	–
ZVD (Hong & Shah, 2019)	open-loop	1,2-pendulum	2D	–
Collocated PD (Chen et al., 2019; Sun & Fang, 2012)	collocated	1,2-pendulum	2D	regulation
Noncollocated Quasi-PID (Sun et al., 2019)	noncollocated	2-pendulum	2D	regulation
Noncollocated PD (Sun & Fang, 2012)	noncollocated	1-pendulum	2D	regulation
Collocated PD tracking (Sun & Fang, 2014b)	collocated	2-pendulum	2D	tracking
PD-PD (d'Andréa Novel et al., 2019)	noncollocated	PDE	2D	regulation
SMC single-pendulum (Qian & Yi, 2016)	noncollocated	1-pendulum	2D	regulation
SMC double-pendulum (Tuan & Lee, 2013)	noncollocated	2-pendulum	2D	regulation
PD energy (Zhang, He, Chen, & Feng, 2020)	noncollocated	1-pendulum	2D	regulation
Coupling tracking (Zhang et al., 2018)	noncollocated	1-pendulum	3D	tracking

Table 11
Structure of the selected controllers for the simulations.

Controller	Feed-forward terms	Proportional terms	Derivative terms	Integration terms
Unshaped input	$+m_t a_d$	–	–	–
ZV	$+\text{conv}(m_t a_d, P_1)$	–	–	–
ZVD	$+\text{conv}(m_t a_d, P_2)$	–	–	–
Collocated PD	–	$+k_p e_x$	$+k_d e_v$	–
Quasi-PID	–	$-k_p \tanh(e_x)$	$-k_d \tanh(e_v)\ -k_i \tanh\left(\lambda^2 e_x\right.$ $-k_{\phi 1} \tanh^2(\theta_1)\tanh(e_v)$ $-k_{\phi 2} \tanh^2(\theta_2)\tanh(e_v)$	$\left. +\ \lambda \int_0^t \tanh(e_x)dt\right)$
Noncollocated PD	–	$-k_p\left(e_x - k_a \sin(\theta_1)\right)$	$-k_d\left(e_v - k_a\dot{\theta}_1 \cos(\theta_1)\right)$	–
Collocated PD tracking	$+m_t a_d$	$-k_p e_x$ $-\frac{2\lambda\xi^2}{\xi^2 - e_x^2} e_x$	$-k_d e_v$ $-\phi\ \text{sgn}(e_v)$	—
PD-PD	–	$-\alpha_1 e_x$ $-\alpha_3\theta_1$	$-\alpha_2 e_v$ $-\alpha_4\dot{\theta}_1$	–
SMC single-pendulum	discontinuous combination of			
SMC double-pendulum	–	proportional and derivative terms		
PD energy	–	$-k_p \tanh(\chi) - k_q\chi\times$ $\frac{(x_d+\zeta)^2 - \varepsilon^2 + \chi\varepsilon}{((x_d+\zeta)^2 - \varepsilon^2)^2}$	$-k_d\dot{\chi}$	–
Coupling track.				
F_x	$+m_t a_{dx}$	$-k_{px}\int_0^t \zeta_x dt$	$-k_{dx}\zeta + \lambda m_t \cos(\theta_x)\cos(\theta_y)\dot{\theta}_x$	–
F_y	$+m_t a_{dy}$	$-k_{py}\int_0^t \zeta_y dt$	$-k_{dy}\zeta_y + \lambda m_t\dot{\theta}_y$	–

open problem and there exist only embryonic solutions, *e.g.*, parameter optimization based on genetic algorithm (Mohamed et al., 2022). In this work, heuristic algorithms, *i.e.*, PSO, FMINUNC and PATTERNSEARCH,[1] available in MATLAB, are implemented in an iterative manner to tune the parameters in order to minimize the objective function:

$$J = \|e_p(t)\|_{2,t\in[0,100]s} + 60\|e_p(t)\|_{2,t\in[16,100]s} + 300\|e_p(t)\|_{2,t\in[33,100]s} + 600\|e_p(t)\|_{\infty} + 0.05\sum_{k=1}^{t_f/h} |F(kh) - F((k-1)h)| \tag{8}$$

where $e_p = x_p - x_d$, x_p is the payload position on x axis, t is the time, $t = kh$, and h is the sampling time. The term $\sum_{k=1}^{t_f/h} |F(kh) - F((k-1)h)|$ is added to J to decrease the chattering on the force since a real actuator may not be able to produce a force with large chattering. As can be seen in (8), $\|e_p(t)\|_2$ is calculated in different windows with different gains to decrease the steady-state error. As it was mentioned, the parameters are optimized for a double-pendulum system with the following condition:

- The system starts with initial sway angles $\theta_1(0) = 15°, \theta_2(0) = -15°$;
- A white noise with signal-to-noise ratio (SNR) = 90 dB is added to the feedback;
- A disturbance force is applied directly on the cart to simulate the external disturbances (a pulse force with period 20 s and amplitude ±19600 N);
- Damping is considered for the cart ($1000v(t)$ N) to simulate a kind of friction between the cart and the surface under the full payload.

The above-mentioned condition is selected in order to tune the controller gains for as realistic as possible conditions under the regulation trajectory defined in Section 7.1.3. The optimized parameters are provided in the report corresponding to this study which is available online (Mojallizadeh et al., 2022). In addition, one may use the HOISTING TOOLBOX to regenerate the parameters. Since heuristic algorithms used for the optimization are based on random initial guesses, the tuning results are not unique. In addition, these optimization algorithms do not necessarily lead to optimal solutions since different executions lead to different gains: only suboptimal gains are calculated.

It should be noted that the parameters of the only controller designed for the 3D case, *i.e.*, coupling tracking, have been calculated for two cases. In the first case, this controller has been tuned for the 2D case when the feedback is made of the first and the last sway angles separately. Compared to the previous controllers, this controller has also been tuned for the 3D case based on the single-pendulum system (tuning in 3D space using the double-pendulum model takes too much time on INTEL CORE I7-10850H) processor. Hence, the 3D implementation of this controller with the last angle as the feedback has been ignored. Moreover, the total calculation time required for

[1] See MATLAB manual for more information about these optimization methods.

Table 12
Parameters of the simulation.

cart mass	10 T
tool mass	13.6 T
maximum payload mass	40 T
distance between the tool and the payload	1 m
damping coefficient for the joints	1.6 (NM/(deg/s))
joint flexibility coefficient	0.8 NM/deg
cart damping coefficient	1000 N/(m/s)
distance between the cart and the payload	10 m
controller sampling time	50 ms
measurement delay	100 ms

the parameter tuning and the numerical simulations corresponding to 12 selected controllers, shown in Table 10, under different conditions, listed in Table 13, is around one week. The developed toolbox can do all the procedures automatically without user intervention. However, one may easily change all the parameters in the toolbox to achieve customized results. Also computation time may be reduced by choosing smaller N. Optimizing N is possible and worth doing, but it is outside the scope of this article.

7.1.2. Evaluation

Ideally increasing the number of links for the developed model (see Section 5) helps improving the accuracy which is not always possible because of the limited computational resources. In this study, a 20-link pendulum system is considered for this purpose, where the payload and the tool are connected to the last and the one before the last link, respectively. The implementations of the methods designed for the single and double-pendulum system on such a model follow the same rule mentioned in Section 7.1, where the first (θ_1) and the last (θ_{20}) angles are used for double-pendulum based design. Two separate implementations have been considered for single-pendulum-based controllers with the first and the last angles as the sway angles. Note that such a selection is not unique and one may use the provided toolbox to verify other feedback's configuration, depending on sensors which are mounted on the OC.

7.1.3. Trajectory profile

Two different trajectory profiles have been employed to evaluate the performances of the controllers under regulation and tracking conditions. The regulation trajectory is generated as follows (this trajectory has been employed by industrial crane developers):

$$\begin{cases} x_d(t) = 3.5t^2/8 + 1 & 0 \le t \le 4 \\ x_d(t) = 3.5t - 6 & 4 < t < 8 \\ x_d(t) = -3.5t^2/8 + 10.5t - 34 & 8 \le t \le 12 \\ x_d(t) = 29 & t > 12 \end{cases} \tag{9}$$

The regulation profile is composed of three constants values for the acceleration. Moreover, the target position is constant for $t > 12$ s (the duration of each simulation is 100 s as in (8)). On the other hand, the tracking trajectory is $x_d(t) = 5\sin(\omega t)$. Note that for the 3D case, the trajectory along the y axis is defined as follows:

$$\begin{cases} y_d(t) = \dfrac{x_d(t-2)}{2} & \text{for} \quad t \ge 2 \\ y_d(t) = 0 & \text{for} \quad t < 2 \end{cases} \tag{10}$$

7.2. Numerical simulation under different conditions

A set of comparative analyses have been performed for the regulation and the tracking profiles in Sections 7.2.1 and 7.2.2, respectively. Note that, in the tables, the colors blue, black, and red indicate the best, moderate and the worst performances in Table 13. Moreover, the results, *i.e.*, L_2 norm of the payload position error, corresponding to each case are listed in one column of Table 13.

7.2.1. Regulation in nominal condition

This simulation has been performed under six different conditions as follows and the results are shown in Table 13. The cable's parameters are shown in Table 12, they were chosen according to some industrial OC parameters. They can be customized for a specific industrial crane in the developed Hoisting Toolbox.

- **Unperturbed case**: This simulation has been conducted under an unperturbed condition, *i.e.*, no feedback noise and no cart damping with the piecewise-smooth trajectory (9). Since there is no perturbation, even the performances of the open-loop methods are comparable with the closed-loop ones. According to this simulation, the collocated PD tracking controller seems to be the best in minimizing the payload position error under this unperturbed condition. Another observation is that the SMC designed for the double-pendulum system shows the worst responses. The waveforms corresponding to the best and the worst results are shown in Fig. 5 (many other responses can be found in the report Mojallizadeh et al. (2022)).
- **Initial sway**: In this experiment, $\theta_1(0) = \pi/6$ rad while other initial sway angles are zero. Double-pendulum SMC is one of the worst. On the other hand, collocated PD tracking shows one of the best tracking performances.
- **Disturbance on the payload**: The aim of this simulation is to study the performances when a disturbance affects the payload. To this end, a pulse force with period 20 s and amplitude ±19600 N is applied directly to the payload toward the x-axis. According to Table 13, the open-loop methods show the worst responses since they cannot compensate for the perturbation because of the lack of feedback. In general, the best responses belong to the quasi-PID, noncollocated PD regulation, collocated PD tracking, PD-PD, and the single-pendulum SMCs. Note that, compared to the previous cases, the SMC designed for the single-pendulum model shows one of the best responses in this specific case since it is mainly designed to be robust against disturbances.
- **Measurement noise**: This simulation mainly evaluates the controllers in the presence of measurement noise where a white noise with SNR = 90 dB affects all measurements within the feedback path. The results, in this case, are not unexpected since the noise affects the closed-loop controllers more than the open-loop ones. Moreover, the tracking controllers are less affected by noise, since according to Table 11, the control law is synthesized based on the feedforward terms in addition to the feedback ones, which are not affected by noise.
- **No-load condition**: The aim of this simulation is to study the regulation performances under an unperturbed case where there is no load (the masses of the tool and the payload are equal to 20 kg to avoid singularity in the simulations). The double-pendulum SMC has achieved the worst results again. Unexpectedly, the PD-PD method does not achieve good results for this case. In fact, PD-PD is designed based on the PDEs enabling to capture the vibrations that appear when the payload is heavy. The lumped-mass model does not incorporate enough modes to show this controller's capabilities, especially with light loads.
- **3D space**: The spherical joints are used in the model along with the distributed mass payload in order to model the 3D payload rotations. Moreover, the objective functions in this simulation are different. The L_2 notation in Table 13 denotes the standard norm and the measurements are sampled with the same sampling rate as the controller, *i.e.*, 50 ms. This simulation is conducted for the nominal conditions with full payload and the regulation profile (9). It can be seen that the open-loop methods show the worst responses even for this unperturbed case which was not the case for the 2D case. This is probably caused by the coupling effects between x and y axis that each axis generates disturbances on the other axis. Hence, feedback is crucial for the 3D case, even

Table 13
L_2 norms of the payload position error.

Method	Nominal	Initial sway	Disturbance	Noise	No-load	3D
Unshaped input	1.08	3.55	34.69	1.08	2.24	223.84
ZV	2.14	5.23	36.70	2.14	2.17	144.75
ZVD	3.13	5.32	36.66	3.13	3.16	209.58
Collocated PD	2.12	2.03	1.95	2.12	1.82	142.18
quasi-PID	1.38	2.81	1.29	1.38	1.94	87.58
Non.CO.PD.Reg. (first)	2.14	2.04	1.97	2.14	1.81	143.40
Non.CO.PD.Reg. (last)	1.37	1.68	1.44	1.37	1.86	92.05
Col.PD.Track	0.55	0.90	1.42	0.55	1.78	36.70
PD-PD	1.40	1.71	1.47	1.40	6.86	93.60
SMC-single-first (explicit)	1.39	1.70	1.47	1.39	6.34	93.36
SMC-single-first (implicit)	1.39	1.70	1.47	1.39	6.32	93.30
SMC-single-last (explicit)	1.37	1.68	1.44	1.37	1.86	92.04
SMC-single-last (implicit)	1.37	1.68	1.44	1.37	1.86	91.85
SMC-double (explicit)	21.65	35.33	18.32	13.08	123.33	178.71
SMC-double (implicit)	1.86	17.18	2.04	3.81	4.52	76.20
PD energy (first)	2.00	4.44	1.79	2.00	3.78	131.31
PD energy (last)	2.14	2.04	1.91	2.14	1.81	141.57
Coupling tracking (first)	1.17	1.74	3.43	1.17	1.36	78.73
Coupling tracking (last)	1.11	1.44	2.44	1.11	1.94	74.28
Coupling tracking (3D)	-	-	-	-	-	69.68

The data provided in this table are presented to show the abilities of the developed toolbox and have been obtained under specific conditions and may change depending on several factors *e.g.*, gain optimization algorithm and the corresponding cost function. One may modify such parameters in the toolbox to obtain the customized results corresponding to different conditions.

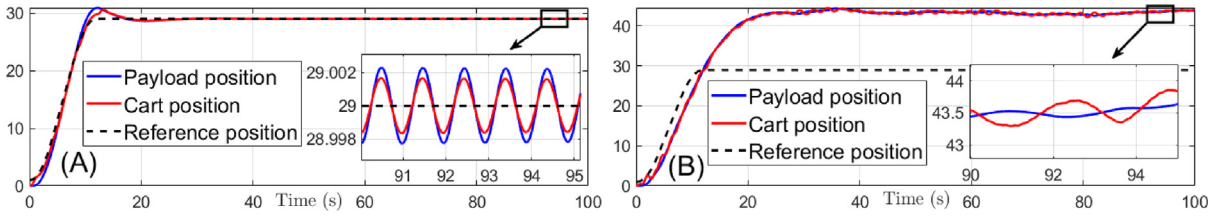

Fig. 5. Waveforms corresponding to the best and the worst performances under the unperturbed condition (a) collocated PD tracking controller (b) SMC-double-pendulum (explicit).

for the unperturbed condition. Another observation is that the collocated PD tracking control shows one of the best responses. As before, the SMC designed for the double-pendulum system shows the worst responses. Comparing the coupling tracking controller implemented in a decentralized way (with two separate implementations with the first and the last angles as sway) with the centralized form (see the last row of the last column, where the coupling in 3D space has been taken into account) one can see that while it can slightly improve the results, there is no significant difference between these implementations.

Remark 9. As alluded to above, the results reported in Table 13 are preliminary and are to be considered as an illustration of the proposed toolbox capabilities for parameter tuning. More results can be found in the report Mojallizadeh et al. (2022). Clearly controllers gains have to be tuned according to the considered applications. Nevertheless, globally the obtained results seem logical: explicit SMC performs worse than its implicit counterpart, open-loop controllers are not robust, and collocated controllers perform better. From Fig. 5, trajectory tracking controllers show the best performance when the sinusoidal desired trajectory frequency increases.

7.2.2. Tracking under nominal condition

In this case, the sinusoidal tracking trajectory is considered, instead of the regulation one, to evaluate the trajectory tracking performances under an unperturbed case and the results are shown in Fig. 6. The first observation is that the tracking controllers, *i.e.*, collocated PD tracking, and the coupling tracking achieve the best results. Moreover, for the coupling tracking controller, it is better *to measure the last sway angle rather than the first one*. Also, non-collocation feedback may not provide any advantages for this scenario since the best results have been achieved for the collocated PD tracking controller. It can be seen that the open-loop methods are the worst in the case of tracking. Similar to the previous case, the SMC designed for the double-pendulum with the first angle sensing has achieved the worst results among the closed-loop controllers. Moreover, the tracking controllers show the smallest position tracking errors and are almost insensitive to ω.

Remark 10. Trajectory tracking controllers F may be very important in the context of operator-in-the-loop systems. Indeed such trajectory tracking controllers could be used in such control systems, where the operator would assign online desired trajectories to be tracked by the overall system (cart+ payload). Apparently, this is not yet considered in operator-in-the-loop control strategies with velocity control inputs.

7.2.3. Summarized results

According to the preliminary comparative analyses made in this section, the following conclusions can be drawn:

- The open-loop control strategies could provide good performances in unperturbed cases for the regulation scenario in 2D space. Moreover, they are easy to implement since they do not need feedback measures. However, in the presence of perturbation or for the tracking problem, they show one of the worst responses, as expected.
- It is clear that noncollocated feedback can lead to a more complex implementation since the sway angles or payload's coordinate have to be measured for control law synthesis. However, the results show that in some specific cases, the collocated controllers show better responses than the noncollocated ones. Such a conclusion may not be true for all cases. For instance, quasi-PID

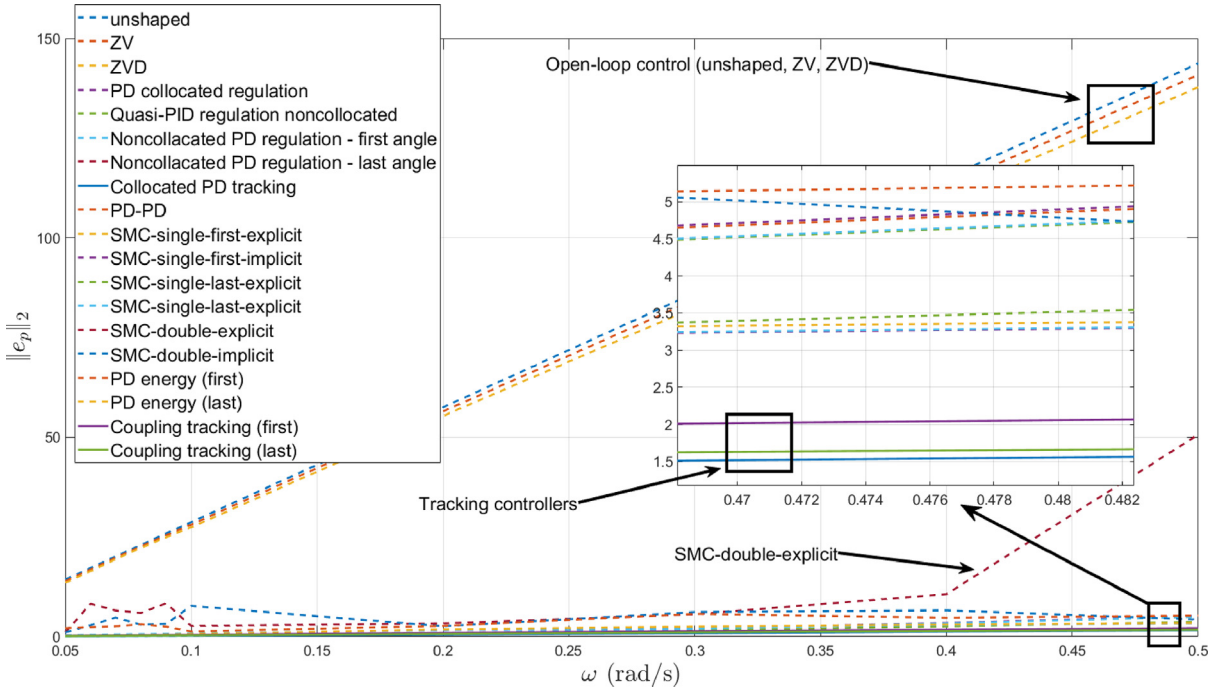

Fig. 6. L_2 norms of the payload position tracking error for the trajectory $x_d(t) = 5\sin(\omega t)$ under nominal condition.

sometimes leads to a better result compared to the collocated PD controller, meaning that this noncollocated feedback strategy behaves better than some collocated strategies.

- For the tracking problem, the tracking controllers show better results compared to the regulation ones, and their performances are almost independent of the trajectory's frequency (see Fig. 6). This is an expected feature since they are designed to achieve this preference. Moreover, the tracking controllers are more robust to the measurement noise because according to Table 11, their control laws also depend on the feedforward terms in addition to the feedback which decreases their sensitivity.
- Some of the controllers are designed based on the PDE models, *e.g.*, PD-PD controller. One of the key assumptions in their design is that the payload mass is much larger than the mass of the cable (see Section 2.3). As a result, as it was seen in Table 13, this controller presents one of the worst responses for the no-load case.
- The PDE-based models enabling one to take into account the cable's flexibility are unable to model large nonlinearities and lose their accuracy in the presence of large sway angles. As a result, the controllers designed based on such models (PD-PD for example) cannot guarantee global stability. This issue should be addressed in the future by either calculating the domain of attraction of such controllers or extending them to take into account general nonlinearities. The characterization of the domain of attraction may also bring an answer to the previous idea.
- The controllers designed for the 3D space can handle the coupling between the axes and are expected to show advantages for such conditions. The only 3D controller shows almost the best result after the collocated PD tracking controller (which is in fact designed for the 2D case). Based on these results, it can be seen that the 3D design of the coupling tracking controller shows slightly better responses than the 2D counterpart (the same controller when the coupling exists in the 3D space is neglected, see the last row of Table 13).

The full report corresponding to this work can be found in Mojallizadeh et al. (2022), where one may find the extended results as follows:

- The complete mass matrix of the Euler–Lagrange dynamics of the proposed simulation-oriented model with an arbitrary number of links has been developed in Mojallizadeh et al. (2022, Section 3) and Brogliato (2022). Moreover, the key characteristics of the model under different conditions, *e.g.*, presence of elasticity in the links, heavy and light payloads, have been extracted.
- A more comprehensive comparative study under different operating conditions has been made in Mojallizadeh et al. (2022, Section 7) for 2D operating space, where several different objective functions such as control energy, cart and payload tracking performances, and the required time to satisfy the control objectives have been calculated. Note that, in this survey, only the payload tracking position has been selected for the comparisons of the controllers as shown in Table 13. However, considering other objective functions for the comparisons may lead to different results as explained in Mojallizadeh et al. (2022, Section 7). For instance, while the open-loop methods present one of the worst responses in the presence of disturbances, they always need the smallest amount of control energy which makes them energy optimal among all the considered controllers.
- The extended results for the 3D case when the payload eccentricity can cause undesired 3D motions are presented in Mojallizadeh et al. (2022, Section 8), where the general results are in accordance with the 2D case except that the controllers taking into account the dynamic coupling between x and y axes, *e.g.*, the coupling tracking controller, may be more efficient in payload positioning.

Remark 11. It should be again asserted that the results presented in this survey are drawn under specific conditions and controller parameters which are obtained in Mojallizadeh et al. (2022) and may not be valid under all scenarios and applications. Hence, the toolbox developed in this work has to be used for each specific application to achieve customized results.

8. Conclusion

A complete review of the modeling schemes developed for overhead cranes has been presented in this review article, with their key properties. Subsequently, a comprehensive review has been made for the control methods based on their characteristics, *e.g*, the feedback (open-loop, collocated, and noncollocated feedback), scenario (regulation and tracking), operating space (2D and 3D), stability (local, global, *etc*.), and the model used to design the controller. Moreover, a compact tabular presentation allows one to select the appropriate controller at a glance. Some controller candidates have been selected from each class and preliminary comparative analysis has been made based on numerical experiments under different conditions to extract the main properties of each classification. The results obtained from such a comparison and the available toolbox for gains calculation provided a user's guideline to select the most appropriate method for each specific condition. The following research gaps have been identified in this study which potentially can be addressed in future research, as far a modeling issues are concerned:

- In the literature, the forces applied to the cart toward the x and y axes as well as the force on the hoisting mechanism are the only accessible control inputs. While these inputs might be sufficient for the payload positioning toward the x and y axes, they cannot be used to control the 3D payload's orientation. The reason is that the lengths of the cables are always equal and there is not any freedom to change the cables' lengths independently (note that in a real crane, the tool is suspended to the cart through several cables). For the equal cables' lengths, in this context, the literature just addressed the kinematic problem without taking the control design into account (Arena et al., 2013, 2015; Cartmell, Morrish, Alberts, & Taylor, 1996; Cartmell et al., 1996; Morrish, Cartmell, & Taylor, 1996; Morrish et al., 1997). The authors believe that the methods developed for the cable-driven robotic systems (Wei et al., 2017) may be useful to control the payload rotation in 3D space based on the kinematic developed in Arena et al. (2013, 2015), Cartmell et al. (1996, 1996), Klaassens et al. (1999), Morrish et al. (1996, 1997) if each cable's length can be controlled independently. Such a scenario has been addressed in Klaassens et al. (1999), Ngo et al. (2008) where the payload is suspended by four cables which can be adjusted separately by four actuators. Note that in Carricato (2013), Carricato and Merlet (2013), Merlet (2017), it can be seen that the considered system is quite similar to an OC. Apparently, such references do not consider dynamics but just static analysis with inextensible cables that are in two modes: taut or slack. Another relative issue is the definition of the payload in 3D space usually defined by industrial terms such as trim, list, and skew motions in the literature which are unable to describe the motions when they occur simultaneously. Hence, a more accurate convention should be proposed for the 3D motions of the payload, *e.g.*, based on the Euler or Bryan angles used in the mechanics community.
- There are many different ways to model a cable (Lv et al., 2020), which is a complex mechanical deformable system to characterize (many cables are made of braided wires, and their behavior depends not only on materials but on the braiding structure (Gueners et al., 2021) and internal interactions). A simplified pendulum-like 20-link model has been implemented in the toolbox developed in this work to capture the global inertial nonlinearities and cable flexibility simultaneously (this type of modeling approach is often used for virtual environment simulation (Choe, Choi, & Ko, 2005; Servin & Lacoursière, 2008)). It has the advantage that several parameters can be changed and tuned easily (like longitudinal, joint stiffnesses, total mass, number N of links), and it is the natural extension of the single and double-pendulum models widely used in the Automatic Control literature. However, as said above this is a preliminary multibody system model which oversimplifies some cable's dynamics. While cables' models based on finite element method (FEM) have been thoroughly studied, it has not yet been considered for OC control, except for very few works. Hence, FEM models of cables should be implemented in the toolbox in future works, leading to a more accurate and customizable cable model for simulation (this is especially true for multiple-cable systems). The FEM approaches proposed in Bertrand, Acary, Lamarque, and Svadkoohi (2020), Sonneville and Brüls (2014) look promising because they incorporate large-deformation nonlinear dynamics, hence bridging the gap between global, multibody models, and local FEM discretizations of the string equation. The ALE-ANCF method yields cable's dynamics which can be recast in a multibody framework, familiar to Automatic Control and Robotics researchers. It takes the form of quasi-Lagrange equations with equality holonomic constraints (Fotland & Haugen, 2022, Equ. (12)) (Hong, Tang, & Ren, 2011, Equ. (26)). It is well-suited for cables with varying lengths (Hong et al., 2011), and applies to slender geometries with large deformations, and circular cross-sections. It models axial and bending stiffnesses. The inertial nonlinearities stem from the varying length (which implies some mass flows between the elements), and the mass matrix is constant. Concerning control: advanced control methods have been applied to FEM cables models in Faravelli, Fuggini, and Ubertini (2010), Faravelli and Ubertini (2009), Gattulli (2007), Gattulli, Martinelli, Perotti, and Vestroni (2004), Ubertini (2008), however, they seem to apply primarily to cables with important sag, in a static framework. *The main obstacle with FEM models is that stability and feedback control may not be obvious using these models, in particular with respect to the available measured outputs.* For the moment they are expected to be useful mainly for numerical simulation. Computational time may be an issue the designer has to take into account when performing the FEM spatial discretization (see Section 7.1.1).
- As alluded to above, some industrial multiple-cable gantry cranes possess a rotational degree-of-freedom along the vertical axis. When limited to small deviations from the vertical axis, such systems possess dynamics of the form (see also Bauer, Schaper, Schneider, and Sawodny (2014) for slightly different equations):

$$\begin{cases} I_1\ddot{\beta}_1 = K(\beta_1,\beta_2) \\ I_2\ddot{\beta}_2 = -K(\beta_1,\beta_2) + \tau, \end{cases} \tag{11}$$

  where τ is the control torque (applied by a motor mounted on the trolley), β_1 is the payload rotation angle, β_2 is the motor angle, $K(\beta_1,\beta_2)$ is the elastic torque due to the cables deformation, I_1 and I_2 are some equivalent moments of inertia. The dynamics in (11) possesses the required triangular form for backstepping (Brogliato, Ortega, & Lozano, 1995; Lozano & Brogliato, 1992). In an industrial context, the difficulties may be: a good estimation of the mapping $K(\cdot,\cdot)$ from experimental data, where $K(\cdot,\cdot)$ represents a kind of equivalent rotational stiffness which depends on the multiple cables kinematics and mechanical properties, the payload angle β_1 measurement or observation according to available sensors (in an industrial context, this may be a crucial issue). This should be extended to the 3D operational space, where the payload orientation plays a crucial role.
- In the same vein, sloshing dynamics inside payloads carrying liquids, involve a hard control problem. Multibody finite-dimensional models exist for sloshing effects dynamics. A fine

analysis of the couplings introduced by sloshing and payload rotations may be mandatory if the application involves liquid transport.

- From a general control perspective (not restricted to OC carrying very large payloads), one has to take into account the fact that cables can pull but not push. This yields models incorporating slack modes, hence complementarity constraints and possible impacts inside the cables (Brogliato, 2016). The multibody lumped masses dynamics is unable to model such effects (Mojallizadeh et al., 2022). Thus when light cables are considered, which are likely to reach such slack modes, another model has to be chosen. See Appendix A.5.
- Negative-imaginary (NI) systems are well suited to the study of lightweight mechanical structures (Brogliato et al., 2020b, Chapter 2). This has not been exploited much in OC control (we could find only one reference using it (Abdullahi et al., 2016)), but it has been studied for quadrotors with cable-suspended payloads (Tran, Santoso, Garrat, & Anavatti, 2021a; Tran, Santoso, Garratt, & Anavatti, 2021b; Tran, Santoso, Garratt, & Petersen, 2020). NI theory mainly applies to linear time-invariant systems, hence may yield an alternative solution for local stabilization only.
- In some applications (Sawodny et al., 2002), the connection point of the last link is not located at the payload's center of mass. Hence a kind of triple-pendulum effect may appear in the system. However, mathematical modeling and control of triple-pendulum systems have never been addressed in the literature corresponding to cranes. A systematic modeling procedure has been presented in Appendix A to address the modeling of a pendulum-like system with an arbitrary number of links, which may help addressing this research gap.
- This study is only dedicated to OCs in their very basic form illustrated in Fig. 1. However, there are still other kinds of overhead cranes with different structures. For instance, according to the field investigations, the overhead cranes implemented in steel production companies usually have an extra degree of freedom, *e.g.*, cart skew rotation. More clearly, in such applications, the trolley can rotate around the vertical axis to handle the steel bars in the warehouse. Moreover, the overhead cranes with two independently controlled carts have also been studied in the literature (Wen, Fang, & Lu, 2022). Another specific structure is the spider crane where the cart can also move vertically (Romero, Gandarilla, Santibáñez, & Yi, 2022). Moreover, several hoisting mechanisms may be implemented on the large-scale carts that modify the dynamic equations (Zhu & Xu, 2023). Such specific structures and their control have not yet received much attention in the Automatic Control literature.

A fundamental question which involves both modeling and control, is how detailed the model should be for control design. Clearly adding more degrees of freedom in a multibody lumped-mass model, quickly yields complex dynamics (see the appendix for examples) which may not be easily tractable for control design. As far as open questions on control design are concerned, some possible future research lines follow:

- As it was seen, the controllers are only designed based on the single or double-pendulum systems, and their stability is ensured only based on such models. For instance, LaSalle's invariance principle along with the Lyapunov stability theorem (see Remark 6) has been used to show the stability of the control systems on the single and double-pendulum systems. However, it is still not clear whether the stability will remain valid for a larger number of links (like the used 20-link simulation-oriented model) or not, in spite of the fact that the global structure for partial feedback linearization (à la Spong) can still be applied for the N-link pendulum OC, see Appendix G. Hence, the stability analysis for pendulum-like systems with an arbitrary number of links should be considered in the future. The developments presented in Appendix A may be useful (starting with $N = 3$, for instance).
- In a real crane, several cables are usually used to suspend the payload and manipulate it in 3D space. According to Table 8, while the kinematics has been addressed for such a scenario, the control design based on the derived kinematics remains largely unaddressed (as pointed out above, the only reference we could find where a dynamic model has been developed for the multi-cable case is Cartmell et al. (1998). However, the obtained model is very complex and has not yet been used for control design purpose). Designing a feedback controller based on the derived kinematics would allow the manipulation of the payload more effectively by controlling the 3D payload motions. To this end, the control methods developed for cable-driven robotic systems can be potentially extended to this topic, see, *e.g.*, Picard, Caro, Claveau, and Plestan (2018), Picard, Caro, Plestan, and Claveau (2018), Zake, Chaumette, Pedemonte, and Caro (2019, 2021) and references therein. Usually, massless rods with varying length are used for such manipulation tasks (Gueners et al., 2021).
- In this study, the so-called intelligent control schemes, *e.g.*, data-driven machine learning (Shih, 2022), fuzzy control (Smoczek, Szpytko, & Hyla, 2012; Sun & Xie, 2020; Zhang, Zhao, & Ding, 2022), are excluded from the comparisons because of the lack of solid stability analysis (that do exist in classical control methods analyses). However, such methods can potentially provide advantages over the classic ones and are worth considering in future research. Indeed, as an alternative solution to the physics-based modeling approach, *e.g.*, the Euler–Lagrange framework used in this study to obtain the dynamic equations, data-driven modeling schemes can also be employed. Since such methods are obtained based on real system measurements, they can potentially lead to more realistic models (though, limited to the subspace spanned by the measurements) and are worth considering in future studies. For instance, an adaptive neuro-fuzzy inference system has been trained by a genetic algorithm in Zhu and Wang (2022) to realize such a data-driven model. Alternatively, a neural network with online parameter tuning has been developed in Kim, Yoon, Jeon, and Hong (2022) for this purpose. Estimating cable's dynamics (even multi-cable systems) using data-driven machine learning, seems to be largely open in the OC literature.
- The design or modification of the reference velocity and its effect on the sway reduction has not been considered in this work. Such methods, *e.g.*, using notch filters, smoothing the reference trajectory, delayed feedback (Vazquez & Collado, 2009), path planning (Sun & Fang, 2014a; Sun, Fang, Zhang, & Ma, 2012), and flatness theory can be integrated with the majority of the controllers developed in this work to achieve a better sway reduction. Such integration remains for future works.
- In a real crane, a kind of path planning has to be considered in order to avoid collisions. In Section 3, we identified two control methods, *i.e.*, MPC and optimal control, that can be used directly to avoid the collision. For the other methods, a dedicated path-planning algorithm should be designed to generate a collision-free trajectory. This issue has not been deeply considered in this work and the study of the controllers for collision avoidance is necessary in future works.
- The conclusions drawn in this review, are mainly based on the simulation-oriented model developed in this work. Hence, experimental validations of the results are mandatory doing in future works. In particular, the results compiled in Fig. 6 should be validated on laboratory setups (since it may be difficult to lead such experiments in an industrial context).

Declaration of competing interest

The authors declare that they have no known competing financial interests or personal relationships that could have appeared to influence the work reported in this paper.

Data availability

Data will be made available on request.

Acknowledgments

This work has been developed within the scope of an "Institut de Recherche Technologique NanoElec" project, founded by the french program "Investissement d'Avenirs" ANR-10- AIRT-05.

Appendix A. Ingredients of the N-link Lagrange multibody model with lumped masses

The well-known single-pendulum and double-pendulum multibody models in 2D and 3D operational spaces are recalled in Sections 2.1 and 2.2. Though this may be sufficient in many industrial cases, some tasks may require cables' models with more degrees of freedom (think also of tasks involving payload-free OC, so that cables can hardly be considered as being always tight). In view of Sections 5 and 7, it is of interest to provide some details on the N-pendulum Lagrange dynamics. In this work we consider an N-link pendulum as in Fig. 4, with massless links, all masses are lumped at the joints, in 2D operational space.

A.1. The mass matrix

In this appendix we make the choice of pendulum angles θ_i, such that $\theta_i = \sum_{j=1}^{i} \alpha_j$. The mass matrix of the system in Fig. 4 (2D operational space with variable length cable) is denoted as:

$$M(q) = \begin{pmatrix} M_{x\theta}(q) & M_{x\theta l}(q) \\ M_{lx\theta}(q) & M_{ll}(q) \end{pmatrix} \in \mathbb{R}^{(1+2N)\times(1+2N)}, \tag{A.1}$$

with $M_{x\theta}(q) \in \mathbb{R}^{(1+N)\times(1+N)}$, $M_{ll}(q) \in \mathbb{R}^{N\times N}$, and $M_{x\theta l}(q) = M_{lx\theta}^{\top}(q) \in \mathbb{R}^{(1+N)\times N}$. It is also possible to go a step further with:

$$M_{x\theta}(q) = \begin{pmatrix} M_{xx}(q) & \bar{M}_{x\theta}(q) \\ \bar{M}_{x\theta}^{\top}(q) & M_{\theta\theta}(q) \end{pmatrix} \tag{A.2}$$

with $M_{xx}(q) \in \mathbb{R}$, $\bar{M}_{x\theta}(q) \in \mathbb{R}^{1\times N}$, $M_{\theta\theta}(q) \in \mathbb{R}^{N\times N}$. This expression of the mass matrix corresponds to the choice of the generalized coordinates as $q = (x, \theta_1, \dots, \theta_N, l_1, \dots, l_N)^{\top} \in \mathbb{R}^{2N+1}$. Other choices can be made, like those splitting the coordinates into actuated q_a and nonactuated ones q_{na}, which is a classical way of doing in the Control literature (Reyhanoglu et al., 1999).

Proposition 1. *Let $q = (x, \theta_1, \dots, \theta_N, l_1, \dots, l_N)^{\top}$, and constant masses m and m_i, $1 \le i \le N$. The mass matrix entries are calculated as follows:*

- $M_{xx}(q) = m_{11}(q) = m + \sum_{i=1}^{N} m_i$
- *The components of* $M_{ll}(q)$ *are* $m_{(N+1+n)(N+j+1)}(q) = m_{(N+j+1)(N+1+n)}(q) = \left(\sum_{i=\max(j,n)}^{N} m_i\right)\cos(\theta_n - \theta_j)$, $1 \le j \le N$, $1 \le n \le N$.
- *The components of* $M_{\theta\theta}(q)$ *are* $m_{(n+1)(j+1)}(q) = \left(\sum_{i=\max(j,n)}^{N} m_i\right) l_n l_j \cos(\theta_n - \theta_j) = m_{(j+1)(n+1)}(q)$, $1 \le j \le N$, $1 \le n \le N$.
- *The components of* $\bar{M}_{x\theta}(q)$ *are: for all* $2 \le k \le N+1$ *(components which multiply* $\ddot{\theta}_k$*):* $m_{1k}(q) = m_{k1}(q) = \left(\sum_{i=k-1}^{N} m_i\right) l_{k-1}\cos(\theta_{k-1})$.
- *The components of* $M_{x\alpha l}$ *are: for all* $N+2 \le k \le 2N+1$, $m_{1k}(z) = m_{k1}(q) = \left(\sum_{i=k-3}^{N} m_i\right)\sin(\theta_{k-3})$*; and for* $1 \le n \le N$, $1 \le j \le N$: $m_{(n+1)(N+j+1)}(z) = \left(\sum_{i=\max(n,j)}^{N} m_i\right) l_n \sin(\theta_j - \theta_n)$.

Details of the calculation can be found in Brogliato (2022). Some properties of the mass matrix can be deduced.

Lemma 1. *Let $N \ge 1$ and $q = (x, \theta_1, \theta_2, \dots, \theta_N, l_1, l_2, \dots, l_N)^{\top}$. Consider the mass matrix in (A.1) and (A.2).*

1. *The diagonal components of $M(q)$ are always all constant positive.*
2. *The components of $M_{x\theta l}$ are small for small angles (neighborhood of the cable's vertical posture) with $\sin(\theta_k) \approx \theta_k$. Hence the mass matrix possesses an almost-diagonal structure for small angles, in the limit: $M(q) = \begin{pmatrix} M_{x\theta}(q) & 0 \\ 0 & M_{ll}(q) \end{pmatrix} \in \mathbb{R}^{(1+2N)\times(1+2N)}$. When the links are aligned (equal angles θ_i) the inertial couplings between the angles and the lengths vanish, with $\sin(\theta_j - \theta_n) \approx \theta_j - \theta_n$.*
3. *The components of $M_{\theta\theta}(q)$ and of $M_{ll}(q)$ are constant positive for small angles.*
4. *Assume that $M(q) = M(q)^{\top} \succ 0$ for all q. Then it follows that $M_{\theta\theta}(q) \succ 0$ and $M_{ll}(q) \succ 0$ for all q.*
5. *In case of large payload mass (i.e., $m_N \gg m_i$ for all $1 \le i \le N-1$), the mass matrix becomes ill-conditioned, since $M_{ll}(q)$ loses its rank around the vertical position when $m_i = 0$, $1 \le i \le N-1$, and has low rank when in addition the zero order approximation for small angles is made.*

Item 4 is a consequence of the Schur Complement Lemma (Brogliato et al., 2020a, Theorem A.65) (Bernstein, 2018, Proposition 10.2.5). The proof of item 5 is as follows. The components of $M_{ll}(q)$ are $m_{(N+1+n)(N+j+1)}(q) = \left(\sum_{i=\max(j,n)}^{N} m_i\right)\cos(\theta_n - \theta_j)$, $1 \le j \le N$, $1 \le n \le N$. The zero-order approximation implies $\cos(\theta_n - \theta_j) \approx 1$, hence $m_{(N+1+n)(N+j+1)}(q) = \sum_{i=\max(j,n)}^{N} m_i$. In the limit where $m_i = 0$ for all $1 \le i \le N-1$, then all components are equal to m_N and M_{ll} has rank 1.

Let us define $\theta = (\theta_1, \dots, \theta_N)^{\top}$ and $\alpha = (\alpha_1, \dots, \alpha_N)^{\top}$, and $z = (x, \alpha^{\top}, l^{\top})^{\top}$. Then $\theta = J\alpha$ where J is an invertible Toeplitz matrix. Thus $q = Lz$, with $L = \begin{pmatrix} 1 & 0_{1\times N} & 0_{1\times N} \\ 0_{N\times 1} & J & 0_{N\times N} \\ 0_{N\times 1} & 0_{N\times N} & I_N \end{pmatrix}$, I_N is the identity matrix of size N. In theory, using the kinetic energy invariance, it is systematic to calculate $M(z) = L^{\top}M(Lz)L$. It is obtained:

$$M(z) = \begin{pmatrix} \begin{pmatrix} M_{xx} & M_{x\theta}J \\ J^{\top}M_{x\theta}^{\top} & J^{\top}M_{\theta\theta}J \end{pmatrix} & \begin{pmatrix} 1 & 0 \\ 0 & J^{\top} \end{pmatrix} M_{x\theta l} \\ M_{x\theta l}^{\top}\begin{pmatrix} 1 & 0 \\ 0 & J \end{pmatrix} & M_{ll} \end{pmatrix} \tag{A.3}$$

Therefore the above conclusions still hold with the mass matrix $M(z)$ partitioned similarly as (A.1) and (A.2).

A.2. Nonlinear inertial forces

The Coriolis/centrifugal forces $C(q,\dot{q})\dot{q}$ in (1) can be deduced from it using the classical Christoffel's symbols as $C(q,\dot{q}) = \left(\sum_{k=1}^{n} \Gamma_{ijk}\dot{q}_k\right)_{ij}$, where $\Gamma_{ijk} = \frac{1}{2}\left(\frac{\partial m_{ij}}{\partial q_k} + \frac{\partial m_{ik}}{\partial q_j} - \frac{\partial m_{kj}}{\partial q_i}\right)$ (Brogliato et al., 2020a, Lemma 6.16), n being the generalized coordinate dimension. In spite of the fact that such calculations may not be straightforward in general using Proposition 1, they are doable, see Appendices B and C. Such developments are mandatory doing to extend passivity-based approaches to the N-link pendulum case.

A.3. Varying masses

If the links' lengths vary only because of longitudinal flexibility, the masses remain constant. In case of a winding mechanism mounted at the attachment point, the cable's total mass varies with its length, *i.e.*, $m_1 = m_1(l_1)$. In all rigor, this has to be taken into account when deriving the Lagrange dynamics. If l_1 varies little then this may be neglected (Quan & Chang, 2020). In some applications cables' lengths vary a lot and this dependence becomes mandatory modeling (Kamman & Huston, 2001; Khalilpour et al., 2021; Quan & Chang, 2020). The Lagrange dynamics as in (1) cannot be applied directly in this case: it is

necessary to add a corrective term in the dynamics (Pesce, 2003; Pesce, Tannuri, & Casetta, 2006), see also Pesce and Casetta (2007) for a short historical summary. It is noteworthy that the mass may vary because of the payload's mass variations: $m_N = m_N(t)$, with constant lengths. Time-varying masses should be treated differently from position-dependent ones (Pesce, 2003): the generalized nonconservative forces have to incorporate a corrective term involving the rate $\dot{m}_N(t)$ times the gained or expelled mass' velocity (in a Galilean frame of reference). See Appendix D for computations in case of the 2D single-pendulum with position-dependent mass.

A more general multibody model of rigid links modeled as rigid slender rods may be considered, instead of the lumped-mass model. Rotational kinetic energies $\frac{1}{2}J_i\dot{\alpha}_i^2$, $1 \le i \le N$, J_i the inertia momentum of body i, add terms $J_i\ddot{\alpha}_i$ in the Lagrange dynamics. They modify the matrix $M_{\alpha\alpha}(q)$ and the nonlinear terms. If this approach is chosen instead of the lumped-mass approach, and if lengths and masses are varying, then the bodies have to be considered as deformable: one can rely on continuum Mechanics or on the finite-element method. These approaches are briefly reviewed in this article. In general, if the moment of inertia can be calculated as $J_i(t)$ in a reference frame attached to the body i at its center of gravity, then the fundamental principle of dynamics applies which makes $\dot{J}_i(t)\dot{\alpha}_i(t)$ appear in the dynamics (Acary & Brogliato, 2008, section 3.2).

A.4. Potential energies

They may have several sources: gravity, longitudinal elastic energy of the links (modeling cables extension), rotational elasticity at the joints (modeling cables bending elastic energy). If no elastic torsional joint stiffness and no longitudinal deformation is modeled, this reduces to the gravity potential energy of each link, that of the trolley being constant chosen equal to zero:

$$U_g(\theta, l) = -\sum_{i=1}^{N} m_i g \sum_{k=1}^{i} l_k \cos(\sum_{j=1}^{k} \alpha_j) = -\sum_{i=1}^{N} m_i g \sum_{k=1}^{i} l_k \cos(\theta_k) \tag{A.4}$$

Thus for $1 \le n \le N$:

$$\frac{\partial U_g}{\partial \theta_n} = -g\frac{\partial}{\partial \theta_n}\sum_{k=1}^{N} l_k \cos(\theta_k) \sum_{i=k}^{N} m_i = g l_n \sin(\theta_n) \sum_{i=n}^{N} m_i \tag{A.5}$$

$$\frac{\partial U_g}{\partial l_n} = -g\frac{\partial}{\partial l_n}\sum_{k=1}^{N} l_k \cos(\theta_k) \sum_{i=k}^{N} m_i = -g \cos(\theta_n) \sum_{i=n}^{N} m_i \tag{A.6}$$

The corresponding generalized forces satisfy $F_g(q) = -\frac{\partial U_g}{\partial q}$. If joint flexibility is added at joints A_i, $1 \le i \le N$ (corresponding to the masses m_i in Fig. 4), in order to model some bending stiffness for the cable, then the additional potential energy is $U_{flex}(\alpha) = \frac{1}{2}\sum_{j=0}^{N-1} \kappa_j \alpha_{j+1}^2 = \frac{1}{2}\alpha^\top \mathcal{K}\alpha$, where $\kappa_j \ge 0$ is the angular stiffness at joint A_j and $\mathcal{K} = \text{diag}(\kappa_i)$, $0 \le i \le N-1$. Thus:

$$\frac{\partial U_{flex}(\alpha)}{\partial \alpha_i} = \kappa_{i-1}\alpha_i, \quad 1 \le i \le N. \tag{A.7}$$

This introduces no couplings between the coordinates, contrarily to what occurs in flexible joint manipulators (Brogliato et al., 1995; Lozano & Brogliato, 1992; Tomei, 1991). In the coordinate angles $\theta_i = \sum_{j=1}^{i} \alpha_j$, $1 \le i \le N$, $\theta = J\alpha$, $\alpha = J^{-1}\theta$, hence $U_{flex}(\theta) = \frac{1}{2}\alpha^\top \mathcal{K}\alpha = \frac{1}{2}\theta^\top J^{-\top}\mathcal{K}J^{-1}\theta$. Here J is full-rank Toeplitz (Bernstein, 2009, Definition 3.1.3), and its inverse is calculated using Bernstein (2009, Fact 3.18.11). This yields $J^{-1}\theta = \begin{pmatrix} \theta_1 \\ \theta_2 - \theta_1 \\ \vdots \\ \theta_N - \theta_{N-1} \end{pmatrix}$, hence $U_{flex}(\theta) = \frac{1}{2}\kappa_0\theta_1^2 + \sum_{i=1}^{N-1} \kappa_i(\theta_{i+1} - \theta_i)^2$. It is inferred that

$$\frac{\partial U_{flex}(\theta)}{\partial \theta_1} = \kappa_0\theta_1 - \kappa_1(\theta_2 - \theta_1) = (\kappa_0 + \kappa_1)\theta_1 - \kappa_1\theta_2, \tag{A.8}$$

for $2 \le j \le N-1$:

$$\frac{\partial U_{flex}(\theta)}{\partial \theta_j} = \kappa_{j-1}(\theta_j - \theta_{j-1}) - \kappa_j(\theta_{j+1} - \theta_j) = (\kappa_{j-1} + \kappa_j)\theta_j - \kappa_j\theta_{j+1} - \kappa_{j-1}\theta_{j-1}, \tag{A.9}$$

and

$$\frac{\partial U_{flex}(\theta)}{\partial \theta_N} = \kappa_{N-1}(\theta_N - \theta_{N-1}), \tag{A.10}$$

so that

$$\frac{\partial U_{flex}(\theta)}{\partial \theta} = \begin{pmatrix} \kappa_0 + \kappa_1 & -\kappa_1 & 0 & \dots & & & 0 \\ -\kappa_1 & \kappa_1 + \kappa_2 & -\kappa_2 & 0 & \dots & & 0 \\ 0 & -\kappa_2 & \kappa_2 + \kappa_3 & -\kappa_3 & 0 & \dots & 0 \\ \vdots & & & & & & \vdots \\ \vdots & & & & & & \vdots \\ 0 & \dots & & & 0 & -\kappa_{N-2} & \kappa_{N-2} + \kappa_{N-1} & -\kappa_{N-1} \\ 0 & \dots & & & & 0 & -\kappa_{N-1} & \kappa_{N-1} \end{pmatrix} \tag{A.11}$$

The joint flexibility introduces a triangular structure in the torques that derive from the elasticity potential, since the row $1 + n$ of the Lagrange dynamics, $1 \le n \le N$, corresponding to $M_{(1+n)\bullet}(q)$ and $\ddot{\theta}_n$, contains the flexibility torque $(-\kappa_{n-1}\theta_{n-1} + (\kappa_{n-1} + \kappa_n)\theta_n) - \kappa_n\theta_{n+1}$. One can think of using a backstepping-like control design using the fictitious input θ_{n+1}. However, as seen in Lemma 1, the *vis-à-vis* terms in the submatrix $M_{\theta\theta}(q)$ always contain strong inertial couplings between $\ddot{\theta}_n$ and the other angular accelerations. Therefore the global triangular structure of Spong's model for flexible-joint manipulators (Brogliato et al., 1995; Lozano & Brogliato, 1992) does not exist in such overhead crane systems.

The same system is considered with elastic links to approximate extensible cables. In this case the generalized coordinate is $q = (x, \theta_1, \dots, \theta_N, l_1, \dots, l_N)^\top$. Each link has a longitudinal linear elasticity with stiffness $k_i > 0$, $1 \le i \le N$. Damping can also be modeled, see Gueners et al. (2021) for details on Kelvin–Voigt model parameters estimation. The same framework as in the foregoing sections is adopted, but the potential energy is augmented with terms $\frac{1}{2}k_i(l_i - l_{i,r})^2$ (assuming that springs are at rest for $l_i = l_{i,r}$). This model is close in spirit to the lumped-mass models developed in Caverly, Forbes, and Mohammadshahi (2014), Khalilpour et al. (2021), but nonlinearities are considered here. It is also easy to add some viscous friction (linear spring–dashpot or Kelvin–Voigt model) $c_i\dot{l}_i$, which is some kind of Rayleigh dissipation (Brogliato et al., 2020a, Definition 6.12). Reminding that $l = (l_1, l_2, \dots, l_N)^\top$, we have:

$$\frac{\partial U_{elas}}{\partial l} = (k_1(l_1 - l_{1,r}), \dots, k_N(l_N - l_{N,r}))^\top \tag{A.12}$$

A.5. Cable's slack behavior

As alluded to above, cables can pull but cannot push (they work only in traction). This is translated into a set of complementarity constraints between the cable's internal tension $T_{cab}(q)$ at its edges, and its length $L_{cab}(q)$ as: $0 \le T_{cab}(q) \perp L_{\max} - L_{cab}(q) \ge 0$, where $L_{\max}$ is the cable's maximum length when it is stretched. If $L_{cab}(q) = L_{\max}$, then nonnegative tension is possible. If $L_{cab} < L_{\max}$, then the tension vanishes, this is the slack mode. If $T_{cab}(q) > 0$, then necessarily $L_{cab}(q) = L_{\max}$. Such a model implies that an impact can occur at times when the cable attains its maximum length (Brogliato, 2016, Example 1.6). The complementarity-slackness behavior remains true if longitudinal elasticity is modeled. The lumped-mass multibody model is unable to model such complementary-slackness behavior. In particular, no impact can be modeled this way, showing the limitation of the multibody modeling approach. A detailed analysis can be found in Mojallizadeh et al. (2022, Section 3.7).

A.6. Change of generalized coordinates

It is worth studying the dynamics using various sets of generalized coordinates, like $z = (x, \alpha^\top, l^\top)^\top$ or $q = (x, \theta^\top, l^\top)^\top$. As seen above, $\theta = J\alpha$ with J full-rank Toeplitz can be used. In the same vein $L = Jl$ can be chosen, where L_i represents an approximation of the curvilinear coordinate of node i (see Fig. 4). The nodes Cartesian coordinates can also be used (Lv, Liu, & Jia, 2021). As shown in Mojallizadeh et al. (2022, section 3.1.3) this yields Lagrange dynamics as:

$$M\ddot{q}(t) + K_{elas}(q(t))q(t) + K_{flex}(q(t))q(t) = Q(t). \tag{A.13}$$

This form of the Lagrange dynamics shares common features with the FEM dynamics studied in Bertrand et al. (2020) and Gattulli (2007) (constant matrix and nonlinear stiffness). Horizontal positions of the nodes $x_i = x + \sum_{j=1}^{i} l_j \sin(\sum_{k=1}^{j} \alpha_k)$ can also be chosen. With small angles assumption we obtain linear Lagrange dynamics $M\ddot{q}(t) + K_{flex}q(t) = Q(t)$. However, the mass matrix stemming from the lumped-mass model is diagonal and nonconsistent (while that obtained from FEM is tridiagonal and consistent (Egeland & Gravdahl, 2002)). We infer that if the objective is to control the OC in a neighborhood of the vertical position using a finite-degrees-of-freedom model, then the consistent FEM model should be chosen instead of the tangent linearization of the multibody model.

Appendix B. Lagrange dynamics of the 2D double-pendulum with varying lengths and constant masses

Let us first provide the 5×5 mass matrix $M(q)$ (the angles as in Fig. 4, with $q = (x, \theta_1, \theta_2, l_1, l_2)^\top$). Detailed calculations are in Brogliato (2022). The system's kinetic energy is given by the sum of the kinetic energies of the cart, mass m_1 and mass m_2:

$$\begin{aligned} T(q,\dot{q}) = \; & \tfrac{1}{2}m\dot{x}^2 + \tfrac{1}{2}m_1[\dot{x} + l_1\dot{\theta}_1\cos(\theta_1) + \dot{l}_1\sin(\theta_1)]^2 \\ & + \tfrac{1}{2}m_1[l_1\dot{\theta}_1\sin(\theta_1) - \dot{l}_1\cos(\theta_1)]^2 \\ & + \tfrac{1}{2}m_2[\dot{x} + l_1\dot{\theta}_1\cos(\theta_1) + \dot{l}_1\sin(\theta_1) + l_2\dot{\theta}_2\cos(\theta_2) \\ & + \dot{l}_2\sin(\theta_2)]^2 \\ & + \tfrac{1}{2}m_2[l_1\dot{\theta}_1\sin(\theta_1) - \dot{l}_1\cos(\theta_1) + l_2\dot{\theta}_2\sin(\theta_2) - \dot{l}_2\cos(\theta_2)]^2 \end{aligned} \tag{B.1}$$

The mass matrix' components are obtained from the expression of $\frac{d}{dt}\frac{\partial T}{\partial \dot{q}}$ and they are given by (from row 1 to row 5):

$$\begin{aligned} & m_{11}(q) = m + m_1 + m_2, \;\; m_{12}(q) = (m_1 + m_2)l_1\cos(\theta_1) \\ & m_{13}(q) = m_2 l_2\cos(\theta_2), \;\; m_{14}(q) = (m_1 + m_2)\sin(\theta_1), \;\; m_{15}(q) = m_2\sin(\theta_2) \\ & \\ & m_{21}(q) = (m_1 + m_2)l_1\cos(\theta_1) = m_{12}(q), \;\; m_{22}(q) = (m_1 + m_2)l_1^2 \\ & m_{23}(q) = m_2 l_1 l_2\cos(\theta_2 - \theta_1), \;\; m_{24}(q) = 0, \;\; m_{25}(q) = m_2 l_1\sin(\theta_2 - \theta_1) \\ & \\ & m_{31}(q) = m_2 l_2\cos(\theta_2) = m_{13}(q), \;\; m_{32}(q) = m_2 l_1 l_2\cos(\theta_2 - \theta_1) = m_{23}(q) \\ & m_{33}(q) = m_2 l_2^2, \;\; m_{34}(q) = -m_2 l_2\sin(\theta_2 - \theta_1), \;\; m_{35}(q) = 0 \\ & \\ & m_{41}(q) = (m_1 + m_2)\sin(\theta_1) = m_{14}(q), \;\; m_{42}(q) = 0 = m_{24}(q) \\ & m_{43}(q) = -m_2 l_2\sin(\theta_2 - \theta_1) = m_{34}(q), \;\; m_{44}(q) = m_1 + m_2, \\ & m_{45}(q) = m_2\cos(\theta_2 - \theta_1) \\ & \\ & m_{51}(q) = m_2\sin(\theta_2) = m_{15}(q), \;\; m_{52}(q) = m_2 l_1\sin(\theta_2 - \theta_1) = m_{25}(q) \\ & m_{53}(q) = 0 = m_{35}(q), \;\; m_{54}(q) = m_2\cos(\theta_2 - \theta_1) = m_{45}(q), \;\; m_{55}(q) = m_2 \end{aligned} \tag{B.2}$$

The mass matrix $M(z)$, with $z = (x, \alpha^\top, l^\top)^\top$, is also derived in Brogliato (2022). The potential energy in (A.4) is given by:

$$U_g(\theta_1, \theta_2, l_1, l_2) = -m_1 g l_1\cos(\theta_1) - m_2 g(l_1\cos(\theta_1) + l_2\cos(\theta_2)). \tag{B.3}$$

The Lagrange dynamics are given as: $\frac{d}{dt}\frac{\partial L}{\partial \dot{q}} - \frac{\partial L}{\partial q} = Q$, where $L(q,\dot{q})$ is the Lagrangian function, $L(q,\dot{q}) = T(q,\dot{q}) - U(q)$, $T(q,\dot{q}) = \frac{1}{2}\dot{q}^\top M(q)\dot{q}$ is the system's kinetic energy, $U(q)$ is its potential energy, Q is the vector of generalized forces. It is deduced that the inertial nonlinear forces/torques are given by $C(q,\dot{q})\dot{q} = (\frac{d}{dt}M(q))\dot{q} - \frac{1}{2}\frac{\partial}{\partial q}\dot{q}^\top M(q)\dot{q}$, while the forces that derive from the potential are $G(q) = \frac{\partial U}{\partial q}$. The first row of $C(q,\dot{q})$ is

$$\begin{aligned} C_1.(q,\dot{q}) \; = & (0, -(m_1 + m_2)l_1\sin(\theta_1)\dot{\theta}_1 + (m_1 + m_2)\cos(\theta_1)\dot{l}_1, \\ & -m_2 l_2\sin(\theta_2)\dot{\theta}_2 + m_2\cos(\theta_2)\dot{l}_2, \\ & (m_1 + m_2)\cos(\theta_1)\dot{\theta}_1, m_2\cos(\theta_2)\dot{\theta}_2), \end{aligned} \tag{B.4}$$

the second row of $C(q,\dot{q})$ can be chosen as

$$\begin{aligned} C_2.(q,\dot{q}) \; = & (0, (m_1 + m_2)l_1\dot{l}_1, \\ & m_2 l_1 l_2\sin(\theta_1 - \theta_2)\dot{\theta}_2 + m_2 l_1\cos(\theta_2 - \theta_1)\dot{l}_2, (m_1 + m_2)l_1\dot{\theta}_1, \\ & m_2 l_1\cos(\theta_2 - \theta_1)\dot{\theta}_2), \end{aligned} \tag{B.5}$$

the third row of $C(q,\dot{q})$ can be chosen as

$$\begin{aligned} C_3.(q,\dot{q}) \; = & (0, -m_2 l_1 l_2\sin(\theta_1 - \theta_2)\dot{\theta}_1 + m_2\dot{l}_1 l_2\cos(\theta_1 - \theta_2), m_2 l_2\dot{l}_2, \\ & + m_2\dot{\theta}_1 l_2\cos(\theta_1 - \theta_2), m_2 l_2\dot{\theta}_2), \end{aligned} \tag{B.6}$$

the fourth row of $C(q,\dot{q})$ can be chosen as

$$\begin{aligned} C_4.(q,\dot{q}) \; = & (0, -\dot{\theta}_1(m_1 + m_2)l_1, -m_2 l_2\cos(\theta_1 - \theta_2)\dot{\theta}_2 \\ & + m_2\dot{l}_2\sin(\theta_1 - \theta_2), 0, m_2\dot{\theta}_2\sin(\theta_1 - \theta_2)), \end{aligned} \tag{B.7}$$

so the fifth row of $C(q,\dot{q})$ can be chosen as

$$\begin{aligned} C_5.(q,\dot{q}) \; = & (0, -m_2 l_1\cos(\theta_2 - \theta_1)\dot{\theta}_1 + m_2\sin(\theta_2 - \theta_1)\dot{l}_1, -\dot{\theta}_2 m_2 l_2, \\ & -m_2\sin(\theta_1 - \theta_2)\dot{\theta}_1, 0). \end{aligned} \tag{B.8}$$

↝ *It is noteworthy that the above choice for $C(q,\dot{q})$ corresponds to the Christoffel's symbols with $\frac{d}{dt}(M(q)) = C(q,\dot{q}) + C^\top(q,\dot{q})$ (Brogliato et al., 2020a, Lemma 6.17). This choice is important because this form of the matrix $C(q,\dot{q})$ is useful in passivity-based controllers requiring the well-known skew-symmetry property (Brogliato et al., 2020a, Chapter 7).*

It remains to calculate the generalized forces which derive from the gravity potential energy. They are given by:

$$\begin{aligned} & \frac{\partial U_g}{\partial x} = 0, \qquad \frac{\partial U_g}{\partial \theta_1} = (m_1 + m_2)g l_1\sin(\theta_1), \\ & \frac{\partial U_g}{\partial \theta_2} = m_2 g\sin(\theta_2), \qquad \frac{\partial U_g}{\partial l_1} = -(m_1 + m_2)g\cos(\theta_1), \\ & \frac{\partial U_g}{\partial l_2} = -m_2 g\cos(\theta_2) \end{aligned} \tag{B.9}$$

The corresponding generalized forces satisfy $F_g(z) = -\frac{\partial U_g}{\partial q}$. Thus once the torque inputs have been defined, the Lagrange dynamics with varying lengths and constant masses is complete for $N = 2$.

Remark 12. When l_2 does not vary (the whole cable's length variation is modeled with varying l_1, which is realistic if a winch mechanism is mounted at the cable's attachment point and the cable is inextensible, while the total mass is assumed constant), then the dynamics take the following form (Lu et al., 2017a; Shi et al., 2019; Shi, Yao, Yuan, Tong,

et al., 2022), as a reduced form of the above:

$$
\begin{aligned}
&(a)\ (m+m_1+m_2)\ddot{x}+(m_1+m_2)\cos(\theta_1)l_1\ddot{\theta}_1+m_2l_2\cos(\theta_2)\ddot{\theta}_2\\
&\quad+(m_1+m_2)\sin(\theta_1)\dot{l}_1\\
&\quad-(m_1+m_2)l_1\sin(\theta_1)\dot{\theta}_1^2-m_2l_2\sin(\theta_2)\dot{\theta}_2^2+2(m_1+m_2)\cos(\theta_1)\dot{\theta}_1\dot{l}_1=F_x\\
&(b)\ (m_1+m_2)l_1\cos(\theta_1)\ddot{x}+(m_1+m_2)l_1^2\ddot{\theta}_1+m_2l_1l_2\cos(\theta_1-\theta_2)\ddot{\theta}_2\\
&\quad+m_2l_1l_2\sin(\theta_1-\theta_2)\dot{\theta}_2^2\\
&\quad+2(m_1+m_2)l_1\dot{\theta}_1\dot{l}_1+gl_1\sin(\theta_1)(m_1+m_2)=0\\
&(c)\ m_2l_2\cos(\theta_2)\ddot{x}+m_2l_2l_1\cos(\theta_1-\theta_2)\ddot{\theta}_1+m_2l_2^2\ddot{\theta}_2+m_2l_2\sin(\theta_1-\theta_2)\ddot{l}_1\\
&\quad-m_2l_2l_1\sin(\theta_1-\theta_2)\dot{\theta}_1^2+2m_2l_2\cos(\theta_1-\theta_2)\dot{\theta}_1\dot{l}_1+m_2l_2g\sin(\theta_2)=0\\
&(d)\ (m_1+m_2)\sin(\theta_1)\ddot{x}+m_2l_2\sin(\theta_1-\theta_2)\ddot{\theta}_2+(m_1+m_2)\ddot{l}_1\\
&\quad-(m_1+m_2)l_1\dot{\theta}_1^2\\
&\quad-m_2l_2\cos(\theta_1-\theta_2)\dot{\theta}_2^2-(m_1+m_2)g\cos(\theta_1)=F_l
\end{aligned}
\tag{B.10}
$$

where it is still assumed that the cable's total mass variation is negligible, and $q=(x,\theta_1,\theta_2,l_1)^\top$.

Appendix C. 3D single-pendulum with varying link's length: Coriolis/centrifugal matrix

Let us first provide the system's kinetic energy, from which $M(q)$ in (5) is derived (Brogliato, 2022):

$$
\begin{aligned}
T(q,\dot{q})=\ &\tfrac{1}{2}m\dot{x}^2+\tfrac{1}{2}m\dot{y}^2+\tfrac{1}{2}m_1[\dot{y}+\dot{l}_1\sin(\theta_y)+l_1\dot{\theta}_y\cos(\theta_y)]^2\\
&+\tfrac{1}{2}m_1[\dot{x}+\dot{l}_1\sin(\theta_x)\cos(\theta_y)+l_1\dot{\theta}_x\cos(\theta_x)\cos(\theta_y)\\
&-l_1\sin(\theta_x)\sin(\theta_y)\dot{\theta}_y]^2\\
&+\tfrac{1}{2}m_1[-\dot{l}_1\cos(\theta_x)\cos(\theta_y)+l_1\dot{\theta}_x\sin(\theta_x)\cos(\theta_y)\\
&+l_1\dot{\theta}_y\cos(\theta_x)\sin(\theta_y)]^2
\end{aligned}
\tag{C.1}
$$

The nonlinear inertial forces matrix in (5) which satisfies the skew-symmetry property $\frac{d}{dt}(M(q))=C(q,\dot{q})+C^\top(q,\dot{q})$ is given by (row by row):

$$
\begin{aligned}
C_{1\bullet}(q,\dot{q})=\ &(0,0,-m_1l_1\sin(\theta_x)\cos(\theta_y)\dot{\theta}_x-m_1l_1\cos(\theta_x)\sin(\theta_y)\dot{\theta}_y\\
&+m_1\cos(\theta_x)\cos(\theta_y)\dot{l}_1,\\
&-m_1l_1\sin(\theta_x)\cos(\theta_y)\dot{\theta}_y-m_1l_1\sin(\theta_x)\sin(\theta_y)\dot{l}_1\\
&-m_1l_1\cos(\theta_x)\sin(\theta_y)\dot{\theta}_x,\\
&-m_1\sin(\theta_x)\sin(\theta_y)\dot{\theta}_y+m_1\cos(\theta_x)\cos(\theta_y)\dot{\theta}_x)
\end{aligned}
\tag{C.2}
$$

$$
C_{2\bullet}(q,\dot{q})=(0,0,0,-m_1l_1\sin(\theta_y)\dot{\theta}_y+m_1\cos(\theta_y)\dot{l}_1,m_1\cos(\theta_y)\dot{\theta}_y)
\tag{C.3}
$$

$$
\begin{aligned}
C_{3\bullet}(q,\dot{q})=\ &(0,0,m_1l_1\cos^2(\theta_y)\dot{l}_1-m_1l_1^2\cos(\theta_y)\sin(\theta_y)\dot{\theta}_y,\\
&-m_1l_1^2\sin(\theta_y)\cos(\theta_y)\dot{\theta}_x,m_1l_1\cos^2(\theta_y)\dot{\theta}_x)
\end{aligned}
\tag{C.4}
$$

$$
C_{4\bullet}(q,\dot{q})=(0,0,m_1l_1^2\cos(\theta_y)\sin(\theta_y)\dot{\theta}_x,m_1l_1\dot{l}_1,m_1l_1\dot{\theta}_y)
\tag{C.5}
$$

$$
C_{5\bullet}(q,\dot{q})=(0,0,-m_1l_1\cos^2(\theta_y)\dot{\theta}_x,-m_1l_1\dot{\theta}_y,0)
\tag{C.6}
$$

As above the coefficients can be obtained from the Christoffel's symbols (see Appendix A.2) or by computing $C(q,\dot{q})\dot{q}=(\frac{d}{dt}M(q))\dot{q}-\frac{1}{2}\frac{\partial}{\partial q}\dot{q}^\top M(q)\dot{q}$ and rearranging the terms in a suitable way so that $\dot{m}_{ij}=c_{ij}+c_{ji}$ for all $1\le i,j\le 5$.

Appendix D. Dynamics of 2D single-pendulum with varying mass and link's length

Lagrangian dynamics for multibody systems with varying masses deserve special attention (Pesce, 2003; Pesce & Casetta, 2007; Pesce et al., 2006). As alluded to above, the mass variation can be neglected if the length variation remains small (or if the cable's mass is much smaller than the hook's and payload's masses). However in some applications it may happen that the cable mass' variation is no longer negligible (Kamman & Huston, 2001; d'Andréa Novel & Coron, 2002; Quan & Chang, 2020). In this case the 2D (or the 3D) single-pendulum or double-pendulum model should reflect this mass variation, by allowing for $m_1=m_1(l_1)$. In other words, the cable's mass is lumped at the first joint, and its variation implies a varying m_1. If a winding mechanism is mounted at the first joint, then $m_2=m_2(l_2)$. Let us provide now the extension of (3) with $m_1(l_1)$, relying on the theoretical results in Pesce (2003), Pesce and Casetta (2007), Pesce et al. (2006). Such a modeling approach belongs to a multibody system model and is obviously quite different from the one in d'Andréa Novel and Coron (2002) which is based on a coupled ODE-PDE (see Section 2.3).

Let us recall the modified Lagrange equations derived in Pesce (2003), Pesce and Casetta (2007), Pesce et al. (2006):

$$
\frac{d}{dt}\frac{\partial(T-U)}{\partial\dot{q}}-\frac{\partial(T-U)}{\partial q}=Q+\hat{Q},
\tag{D.1}
$$

where the corrective term is with varying masses $m_i(q,\dot{q},t)$:

$$
\hat{Q}_j=\sum_i\dot{m}_i\mathbf{v}_{0i}^\top\frac{\partial P_i}{\partial q_j}+\sum_i\left\{-\frac{1}{2}\frac{\partial m_i}{\partial q_j}\mathbf{v}_i^\top\mathbf{v}_i+\frac{1}{2}\frac{d}{dt}\left(\frac{\partial m_i}{\partial\dot{q}_j}\mathbf{v}_i^\top\mathbf{v}_i\right)\right\}
\tag{D.2}
$$

where the sum is made over the particles with varying mass, $\mathbf{v}_{0i}$ are the velocities of expelled or gained masses, P_i are their position in the Galilean frame of reference. In our case only particle with mass $m_1(l_1)$ varies, hence the corrective terms become ($1\le j\le 3$):

$$
\hat{Q}_j=-\frac{1}{2}\frac{\partial m_1}{\partial q_j}\mathbf{v}_1^\top\mathbf{v}_1
\tag{D.3}
$$

where $\mathbf{v}_1\in\mathbb{R}^2$ is the velocity of the mass m_1 in Fig. 2(a): $\mathbf{v}_1=\begin{pmatrix}\dot{x}+l_1\cos(\theta_1)\dot{\theta}_1+\dot{l}_1\sin(\theta_1)\\ l_1\sin(\theta_1)\dot{\theta}_1-\dot{l}_1\cos(\theta_1)\end{pmatrix}$. Therefore:

$$
\hat{Q}=\begin{pmatrix}0\\ -\frac{1}{2}\frac{\partial m_1}{\partial l_1}[\dot{x}^2+\dot{l}_1^2+l_1^2\dot{\theta}_1^2+2\dot{x}(l_1\dot{\theta}_1\cos(\theta_1)+\dot{l}_1\sin(\theta_1))]\\ 0\end{pmatrix}
\tag{D.4}
$$

This term has to be added in the right-hand side of (3). The above derivations assume that the system's total mass varies, which is untrue if the winch mechanism is mounted on the cart. In all rigor one also has to consider the dynamics of the reel from which the cable is deployed, augmenting the generalized position vector q, and the input F_l is the torque which acts on the reel (pulley). In fact several options and assumptions are possible, depending on the different masses distribution and on the control objective, and also on whether or not the winch mechanism is mounted on the cart or is fixed with respect to the Galilean reference frame (Hong & Shah, 2019, Figures 2.4 and 2.5). Similar modifications can be made in (B.10) for the double-pendulum with varying l_1 and $m_1(l_1)$.

Appendix E. Dynamics of 3D double-pendulum with constant links' lengths and masses

The system is depicted in Fig. 3(b). The dynamics of this OC have been derived in Ouyang et al. (2021, Equations (1)-(6)) and Guo et al. (2023, Equations(1)–(6)). The system's kinetic energy is given by:

$$
\begin{aligned}
T(q,\dot{q})=\ &\tfrac{1}{2}m\dot{x}^2+\tfrac{1}{2}m\dot{y}^2+\tfrac{1}{2}m_1[\dot{y}+l_1\dot{\theta}_{1y}\cos(\theta_{1y})]^2\\
&+\tfrac{1}{2}m_1[\dot{x}+l_1\dot{\theta}_{1x}\cos(\theta_{1x})\cos(\theta_{1y})-l_1\sin(\theta_{1x})\sin(\theta_{1y})\dot{\theta}_{1y}]^2\\
&+\tfrac{1}{2}m_1[l_1\dot{\theta}_{1x}\sin(\theta_{1x})\cos(\theta_{1y})+l_1\dot{\theta}_{1y}\cos(\theta_{1x})\sin(\theta_{1y})]^2\\
&+\tfrac{1}{2}m_2[\dot{x}+l_1\dot{\theta}_{1x}\cos(\theta_{1x})\cos(\theta_{1y})-l_1\dot{\theta}_{1y}\sin(\theta_{1x})\sin(\theta_{1y})\\
&+l_2\dot{\theta}_{2x}\cos(\theta_{2x})\cos(\theta_{2y})\\
&\quad-l_2\dot{\theta}_{2y}\sin(\theta_{2x})\sin(\theta_{2y})]^2\\
&+\tfrac{1}{2}m_2[\dot{y}+l_1\dot{\theta}_{1y}\cos(\theta_{1y})+l_2\dot{\theta}_{2y}\cos(\theta_{2y})]^2\\
&+\tfrac{1}{2}m_2[l_1\dot{\theta}_{1x}\sin(\theta_{1x})\cos(\theta_{1y})+l_1\dot{\theta}_{1y}\cos(\theta_{1x})\sin(\theta_{1y})\\
&+l_2\dot{\theta}_{2x}\sin(\theta_{2x})\cos(\theta_{2y})\\
&\quad+l_2\dot{\theta}_{2y}\cos(\theta_{2x})\sin(\theta_{2y})]^2
\end{aligned}
\tag{E.1}
$$

From the expression of $\frac{d}{dt}\frac{\partial T}{\partial \dot{q}}$, it is deduced the mass matrix $M(q) \in \mathbb{R}^{6\times 6}$, $q = (x, y, \theta_{1x}, \theta_{1y}, \theta_{2x}, \theta_{2y})^\top$, given row by row:

$$\begin{aligned}&m_{11}(q) = m + m_1 + m_2, m_{12}(q) = 0, m_{13}(q) = (m_1 + m_2)l_1\cos(\theta_{1x})\cos(\theta_{1y}),\\&m_{14}(q) = -(m_1 + m_2)l_1\sin(\theta_{1x})\sin(\theta_{1y}), m_{15}(q) = m_2 l_2\cos(\theta_{1x})\cos(\theta_{2y}),\\&m_{16}(q) = -m_2 l_2\sin(\theta_{2x})\sin(\theta_{2y})\end{aligned} \tag{E.2}$$

$$\begin{aligned}&m_{21}(q) = m_{12}(q), m_{22}(q) = m + m_1 + m_2, m_{23}(q) = 0, m_{24}(q)\\&= (m_1 + m_2)l_1\cos(\theta_{1y}),\\&m_{25}(q) = 0, m_{26}(q) = m_2 l_2\cos(\theta_{2y})\end{aligned} \tag{E.3}$$

$$\begin{aligned}&m_{31}(q) = m_{13}(q), m_{32}(q) = m_{23}(q), m_{33}(q) = (m_1 + m_2)l_1^2\cos^2(\theta_{1y}),\\&m_{34}(q) = 0, m_{35}(q) = m_2 l_1 l_2\cos(\theta_{2y})\cos(\theta_{1y})\cos(\theta_{2x} - \theta_{1x}),\\&m_{36}(q) = m_2 l_1 l_2\sin(\theta_{2y})\cos(\theta_{2x})\sin(\theta_{1x} - \theta_{2x})\end{aligned} \tag{E.4}$$

$$\begin{aligned}&m_{41}(q) = m_{14}(q), m_{42}(q) = m_{24}(q), m_{43}(q) = m_{34}(q), m_{44}(q) = (m_1 + m_2)l_1^2\\&m_{45}(q) = m_2 l_1 l_2\cos(\theta_{2y})\sin(\theta_{2x})\sin(\theta_{1y} - \theta_{1x}),\\&m_{46}(q) = m_2 l_1 l_2(\sin(\theta_{1y})\sin(\theta_{2y})\cos(\theta_{1x} - \theta_{2x}) + \cos(\theta_{2y})\cos(\theta_{1y}))\end{aligned} \tag{E.5}$$

$$\begin{aligned}&m_{51}(q) = m_{15}(q), m_{52}(q) = m_{25}(q), m_{53}(q) = m_{35}(q), m_{54}(q) = m_{45}(q)\\&m_{55}(q) = m_2 l_2^2\cos^2(\theta_{2y}),\\&m_{56}(q) = 0\end{aligned} \tag{E.6}$$

$$\begin{aligned}&m_{61}(q) = m_{16}(q), m_{62}(q) = m_{26}(q),\\&m_{63}(q) = m_{36}(q), m_{64}(q) = m_{46}(q), m_{65}(q) = m_{56}(q),\\&m_{66}(q) = m_2 l_2^2\end{aligned} \tag{E.7}$$

Using the Christoffel's symbols (see Appendix A.2) allows us to calculate the matrix $C(q, \dot{q})$ possessing the useful property that $\dot{m}_{ij}(q, \dot{q}) = c_{ij}(q, \dot{q}) + c_{ji}(q, \dot{q})$, $1 \le i, j \le 6$ (the argument $(q, \dot{q})$ is dropped):

$$\begin{aligned}C_{1\bullet} = (0,\ 0,\ &-(m_1 + m_2)l_1(\sin(\theta_{1x})\cos(\theta_{1y})\dot{\theta}_{1x} + \cos(\theta_{1x})\sin(\theta_{1y})\dot{\theta}_{1y}),\\&-(m_1 + m_2)l_1(\cos(\theta_{1x})\sin(\theta_{1y})\dot{\theta}_{1x} + \sin(\theta_{1x})\cos(\theta_{1y})\dot{\theta}_{1y}),\\&-m_2 l_2(\sin(\theta_{2x})\cos(\theta_{2y})\dot{\theta}_{2x} + \cos(\theta_{2x})\sin(\theta_{2y})\dot{\theta}_{2y}),\\&-m_2 l_2(\cos(\theta_{2x})\sin(\theta_{2y})\dot{\theta}_{2x} + \sin(\theta_{2x})\cos(\theta_{2y})\dot{\theta}_{2y}))\end{aligned} \tag{E.8}$$

$$C_{2\bullet} = (0,\ 0,\ 0,\ -(m_1 + m_2)l_1\sin(\theta_{1y})\dot{\theta}_{1y},\ 0,\ -m_2 l_2\sin(\theta_{2y})\dot{\theta}_{2y}) \tag{E.9}$$

$$\begin{aligned}C_{3\bullet} = (0,\ 0,\ &-(m_1 + m_2)l_1^2\sin(\theta_{1y})\cos(\theta_{1y})\dot{\theta}_{1y},\\&-(m_1 + m_2)l_1^2\sin(\theta_{1y})\cos(\theta_{1y})\dot{\theta}_{1x},\\&m_2 l_1 l_2\sin(\theta_{1x} - \theta_{2x})[\cos(\theta_{1y})\cos(\theta_{2y})\dot{\theta}_{2x} + \sin(\theta_{1y})\sin(\theta_{2y})\dot{\theta}_{2y}],\\&-m_2 l_1 l_2\cos(\theta_{1y})[\cos(\theta_{1x})\cos(\theta_{2x})\sin(\theta_{2y})\dot{\theta}_{2x} +\\&\sin(\theta_{1x})\sin(\theta_{2x})\sin(\theta_{2y})\dot{\theta}_{2x}\\&+\cos(\theta_{1x})\cos(\theta_{2y})\sin(\theta_{1x})\dot{\theta}_{2y} - \sin(\theta_{1x})\cos(\theta_{2x})\cos(\theta_{2y})\dot{\theta}_{2y}])\end{aligned} \tag{E.10}$$

$$\begin{aligned}C_{4\bullet} = (0,\ 0,\ &(m_1 + m_2)l_1^2\sin(\theta_{1y})\cos(\theta_{1y})\dot{\theta}_{1x},\ 0,\\&m_2 l_1 l_2\sin(\theta_{1y})[\cos(\theta_{1x})\cos(\theta_{2x})\cos(\theta_{2y})\dot{\theta}_{2x}\\&+\sin(\theta_{1x})\sin(\theta_{2x})\cos(\theta_{2y})\dot{\theta}_{2x} - \cos(\theta_{1x})\sin(\theta_{2x})\sin(\theta_{2y})\dot{\theta}_{2y}\\&+\sin(\theta_{1x})\sin(\theta_{2y})\cos(\theta_{2x})\dot{\theta}_{2y}],\\&m_2 l_1 l_2[\cos(\theta_{1x})\cos(\theta_{2x})\cos(\theta_{2y})\sin(\theta_{1y})\dot{\theta}_{2y}\\&+\sin(\theta_{1x})\sin(\theta_{1y})\sin(\theta_{2x})\cos(\theta_{2y})\dot{\theta}_{2y}\\&-\cos(\theta_{1y})\sin(\theta_{2y})\dot{\theta}_{2y} - \cos(\theta_{1x})\sin(\theta_{1y})\sin(\theta_{2x})\sin(\theta_{2y})\dot{\theta}_{2x}\\&+\sin(\theta_{1x})\sin(\theta_{1y})\sin(\theta_{2y})\cos(\theta_{2x})\dot{\theta}_{2x}])\end{aligned} \tag{E.11}$$

$$\begin{aligned}C_{5\bullet} = (0,\ 0,\ &-m_2 l_2\cos(\theta_{2y})[\cos(\theta_{1y})\cos(\theta_{2x})\sin(\theta_{1x})\dot{\theta}_{1x}\\&-\cos(\theta_{1x})\cos(\theta_{1y})\sin(\theta_{2x})\dot{\theta}_{1x}\\&+\cos(\theta_{1x})\cos(\theta_{1y})\sin(\theta_{1y})\dot{\theta}_{1y} + \sin(\theta_{1x})\sin(\theta_{1y})\sin(\theta_{2x})\dot{\theta}_{1y}],\\&-m_2 l_1 l_2\cos(\theta_{2y})[\cos(\theta_{1x})\cos(\theta_{2x})\sin(\theta_{1y})\dot{\theta}_{1x}\\&+\sin(\theta_{1x})\sin(\theta_{1y})\sin(\theta_{2x})\dot{\theta}_{1x}\\&-\cos(\theta_{1x})\cos(\theta_{1y})\sin(\theta_{2x})\dot{\theta}_{1y} + \cos(\theta_{1y})\cos(\theta_{2x})\sin(\theta_{1x})\dot{\theta}_{1y}],\\&-m_2 l_2^2\sin(\theta_{2y})\cos(\theta_{2y})\dot{\theta}_{2y},\\&-m_2 l_2^2\sin(\theta_{2y})\cos(\theta_{2y})\dot{\theta}_{2x})\end{aligned} \tag{E.12}$$

$$\begin{aligned}C_{6\bullet} = (0,\ 0,\ &m_2 l_1 l_2\sin(\theta_{2y})[\cos(\theta_{1x})\cos(\theta_{1y})\cos(\theta_{2x})\dot{\theta}_{1x}\\&+\sin(\theta_{1x})\sin(\theta_{2x})\sin(\theta_{2y})\dot{\theta}_{2x}\\&+\cos(\theta_{1x})\cos(\theta_{1y})\sin(\theta_{2x})\dot{\theta}_{1y} - \sin(\theta_{1x})\sin(\theta_{1y})\cos(\theta_{2x})\dot{\theta}_{1y})],\\&m_2 l_1 l_2[\cos(\theta_{1x})\cos(\theta_{1y})\cos(\theta_{2x})\sin(\theta_{2y})\dot{\theta}_{1y}\\&+\sin(\theta_{1x})\sin(\theta_{2x})\sin(\theta_{2y})\cos(\theta_{1y})\dot{\theta}_{1y}\\&-\cos(\theta_{2y})\sin(\theta_{1y})\dot{\theta}_{1y} + \cos(\theta_{1x})\sin(\theta_{1y})\sin(\theta_{2x})\sin(\theta_{2y})\dot{\theta}_{1x}\\&-\sin(\theta_{1x})\sin(\theta_{1y})\sin(\theta_{2y})\cos(\theta_{2x})\dot{\theta}_{1x}],\ m_2 l_2^2\sin(\theta_{2y})\cos(\theta_{2y})\dot{\theta}_{2x},\ 0\end{aligned} \tag{E.13}$$

Notice that the expressions given in Ouyang et al. (2021, Appendix A) also use the Christoffel's symbols. The gravity potential energy is given by:

$$\begin{aligned}&U_g(q) = -m_1 g l_1\cos(\theta_{1x})\cos(\theta_{1y}) - m_2 g[l_1\cos(\theta_{1x})\cos(\theta_{1y})\\&+ l_2\cos(\theta_{2x})\cos(\theta_{2y})],\end{aligned} \tag{E.14}$$

so that the gravity generalized force is equal to:

$$-\frac{\partial U_g}{\partial q} = \begin{pmatrix}0\\0\\-(m_1 + m_2)g l_1\sin(\theta_{1x})\cos(\theta_{1y})\\-(m_1 + m_2)g l_1\cos(\theta_{1x})\sin(\theta_{1y})\\m_2 g l_2\sin(\theta_{2x})\cos(\theta_{2y})\\m_2 g l_2\cos(\theta_{2x})\sin(\theta_{2y})\end{pmatrix} \tag{E.15}$$

Appendix F. Dynamics of 3D double-pendulum with varying links' lengths and constant masses

The system is depicted in Fig. 3(b). The system's kinetic energy is given by:

$$\begin{aligned}T(q, \dot{q}) = \ &\tfrac{1}{2}m\dot{x}^2 + \tfrac{1}{2}m\dot{y}^2 + \tfrac{1}{2}m_1[\dot{y} + \dot{l}_1\sin(\theta_{1y}) + l_1\dot{\theta}_{1y}\cos(\theta_{1y})]^2\\&+\tfrac{1}{2}m_1[\dot{x} + \dot{l}_1\sin(\theta_{1x})\cos(\theta_{1y}) + l_1\dot{\theta}_{1x}\cos(\theta_{1x})\cos(\theta_{1y})\\&-l_1\sin(\theta_{1x})\sin(\theta_{1y})\dot{\theta}_{1y}]^2\\&+\tfrac{1}{2}m_1[-\dot{l}_1\cos(\theta_{1x})\cos(\theta_{1y}) + l_1\dot{\theta}_{1x}\sin(\theta_{1x})\cos(\theta_{1y})\\&+l_1\dot{\theta}_{1y}\cos(\theta_{1x})\sin(\theta_{1y})]^2\\&+\tfrac{1}{2}m_2[\dot{x} + \dot{l}_1\sin(\theta_{1x})\cos(\theta_{1y}) + l_1\dot{\theta}_{1x}\cos(\theta_{1x})\cos(\theta_{1y})\\&-l_1\dot{\theta}_{1y}\sin(\theta_{1x})\sin(\theta_{1y}) + \dot{l}_2\sin(\theta_{2x})\cos(\theta_{2y})\\&\quad+l_2\dot{\theta}_{2x}\cos(\theta_{2x})\cos(\theta_{2y}) - l_2\dot{\theta}_{2y}\sin(\theta_{2x})\sin(\theta_{2y})]^2\\&+\tfrac{1}{2}m_2[\dot{y} + \dot{l}_1\sin(\theta_{1y}) + l_1\dot{\theta}_{1y}\cos(\theta_{1y}) + \dot{l}_2\sin(\theta_{2y})\\&+l_2\dot{\theta}_{2y}\cos(\theta_{2y})]^2\\&+\tfrac{1}{2}m_2[-\dot{l}_1\cos(\theta_{1x})\cos(\theta_{1y}) + l_1\dot{\theta}_{1x}\sin(\theta_{1x})\cos(\theta_{1y})\\&+l_1\dot{\theta}_{1y}\cos(\theta_{1x})\sin(\theta_{1y})\\&\quad-\dot{l}_2\cos(\theta_{2x})\cos(\theta_{2y}) + l_2\dot{\theta}_{2x}\sin(\theta_{2x})\cos(\theta_{2y})\\&+l_2\dot{\theta}_{2y}\cos(\theta_{2x})\sin(\theta_{2y})]^2\end{aligned} \tag{F.1}$$

The mass matrix $M(q) \in \mathbb{R}^{8\times 8}$ is given as follows, with $q = (x, y, \theta_{1x}, \theta_{1y}, \theta_{2x}, \theta_{2y}, l_1, l_2)^\top$, row by row:

$$\begin{aligned}
&m_{11}(q) = m + m_1 + m_2,\ m_{12}(q) = 0,\ \ m_{13}(q) = (m_1 + m_2) l_1 \cos(\theta_{1x}) \cos(\theta_{1y}),\\
&m_{14}(q) = -(m_1 + m_2) l_1 \sin(\theta_{1x}) \sin(\theta_{1y}),\ m_{15}(q) = m_2 l_2 \cos(\theta_{2x}) \cos(\theta_{2y}),\\
&m_{16}(q) = -m_2 l_2 \sin(\theta_{2x}) \sin(\theta_{2y}),\ m_{17}(q) = (m_1 + m_2) \sin(\theta_{1x}) \cos(\theta_{1y}),\\
&m_{18}(q) = m_2 \sin(\theta_{2x}) \cos(\theta_{2y})
\end{aligned} \tag{F.2}$$

$$\begin{aligned}
&m_{21}(q) = 0,\ m_{22}(q) = m + m_1 + m_2,\ m_{23}(q) = 0,\\
&m_{24}(q) = (m_1 + m_2) l_1 \cos(\theta_{1y}),\\
&m_{25}(q) = 0,\ m_{26}(q) = m_2 l_2 \cos(\theta_{2y}),\ m_{27}(q) = (m_1 + m_2) \sin(\theta_{1y}),\\
&m_{28}(q) = m_2 \sin(\theta_{2y})
\end{aligned} \tag{F.3}$$

$$\begin{aligned}
&m_{31}(q) = m_{13}(q),\ m_{32}(q) = m_{23}(q) = 0,\ m_{33}(q) = (m_1 + m_2) l_1 \cos^2(\theta_{1y}),\\
&m_{34}(q) = 0,\ m_{35}(q) = m_2 l_1 l_2 \cos(\theta_{1y}) \cos(\theta_{2y}) \cos(\theta_{1x} - \theta_{2x}),\\
&m_{36}(q) = m_2 l_1 l_2 \sin(\theta_{2y}) \cos(\theta_{1y}) \sin(\theta_{1x} - \theta_{2x}),\ m_{37}(q) = 0,\\
&m_{38}(q) = m_2 l_1 \cos(\theta_{2y}) \cos(\theta_{1y}) \sin(\theta_{2x} - \theta_{1x})
\end{aligned} \tag{F.4}$$

$$\begin{aligned}
&m_{41}(q) = m_{14}(q),\ m_{42}(q) = m_{24}(q),\ m_{43}(q) = m_{34}(q) = 0,\\
&m_{44}(q) = (m_1 + m_2) l_1^2,\\
&m_{45}(q) = m_2 l_1 l_2 \sin(\theta_{1y}) \cos(\theta_{2y}) \sin(\theta_{2x} - \theta_{1x}),\\
&m_{46}(q) = m_1 l_1 l_2 \sin(\theta_{1x}) \sin(\theta_{1y}) \sin(\theta_{2x}) \sin(\theta_{2y})\\
&+m_2 l_1 l_2 [\cos(\theta_{1y}) \cos(\theta_{2y}) + \cos(\theta_{1x}) \sin(\theta_{1y}) \cos(\theta_{2x}) \sin(\theta_{2y})],\\
&m_{47}(q) = 0,\\
&m_{48}(q) = m_2 l_1 [\cos(\theta_{1y}) \sin(\theta_{2y}) - \cos(\theta_{2y}) \sin(\theta_{1y}) \cos(\theta_{1x} - \theta_{2x})]
\end{aligned} \tag{F.5}$$

$$\begin{aligned}
&m_{51}(q) = m_{15}(q),\ m_{52}(q) = m_{25}(q),\ m_{53}(q) = m_{35}(q),\ m_{54}(q) = m_{45}(q),\\
&m_{55}(q) = m_2 l_2^2 \cos^2(\theta_{2y}),\ m_{56}(q) = 0,\\
&m_{57}(q) = m_2 l_2 \cos(\theta_{1y}) \cos(\theta_{2y}) \sin(\theta_{1x} - \theta_{2x}),\\
&m_{58}(q) = 0
\end{aligned} \tag{F.6}$$

$$\begin{aligned}
&m_{61}(q) = m_{16}(q),\ m_{62}(q) = m_{26}(q),\ m_{63}(q) = m_{36}(q),\\
&m_{64}(q) = m_{46}(q),\ m_{65}(q) = m_{56}(q),\\
&m_{66}(q) = m_2 l_2^2,\ m_{67}(q) = m_2 l_2 [\cos(\theta_{2y}) \sin(\theta_{1y})\\
&- \sin(\theta_{2y}) \cos(\theta_{1y}) \cos(\theta_{1x} - \theta_{2x})],\\
&m_{68}(q) = 0
\end{aligned} \tag{F.7}$$

$$\begin{aligned}
&m_{71}(q) = m_{17}(q),\ m_{72}(q) = m_{27}(q),\ m_{73}(q) = m_{37}(q),\ m_{74}(q) = m_{47}(q),\\
&m_{75}(q) = m_{57}(q),\ m_{76}(q) = m_{67}(q),\ m_{77}(q) = m_1 + m_2,\\
&m_{78}(q) = m_2 [\sin(\theta_{1y}) \sin(\theta_{2y}) + \cos(\theta_{1y}) \cos(\theta_{2y}) \cos(\theta_{1x} - \theta_{2x})]
\end{aligned} \tag{F.8}$$

$$\begin{aligned}
&m_{81}(q) = m_{18}(q),\ m_{82}(q) = m_{28}(q),\ m_{83}(q) = m_{38}(q),\\
&m_{84}(q) = m_{48}(q),\ m_{85}(q) = m_{58}(q),\\
&m_{86}(q) = m_{68}(q),\ m_{87}(q) = m_{78}(q),\ m_{88}(q) = m_2
\end{aligned} \tag{F.9}$$

Notice that the conclusion in item 5 of Lemma 1 still holds for the submatrix $M_{ll}(q) = \begin{pmatrix} m_{77} & m_{78} \\ m_{87} & m_{88} \end{pmatrix}$, which is singular at the vertical posture and if $m_1 = 0$. The nonlinear inertial generalized forces are defined from the matrix $C(q, \dot{q})$ of Christoffel's symbols as (given row by row):

$$\begin{aligned}
C_{1\bullet}(q, \dot{q}) = \ & (0,\ 0,\ c_{13} = (m_1 + m_2)[- l_1 \sin(\theta_{1x}) \cos(\theta_{1y}) \dot{\theta}_{1x}\\
&- l_1 \cos(\theta_{1x}) \sin(\theta_{1y}) \dot{\theta}_{1y} + \cos(\theta_{1x}) \cos(\theta_{1y}) \dot{l}_1)],\\
&c_{14} = -(m_1 + m_2)[l_1 \cos(\theta_{1x}) \sin(\theta_{1y}) \dot{\theta}_{1x}\\
&+ \sin(\theta_{1x}) \sin(\theta_{1y}) \dot{l}_1 + l_1 \sin(\theta_{1x}) \cos(\theta_{1y}) \dot{\theta}_{1y}],\\
&c_{15} = m_2 [- l_2 \sin(\theta_{2x}) \cos(\theta_{2y}) \dot{\theta}_{2x} - l_2 \cos(\theta_{2x}) \sin(\theta_{2y}) \dot{\theta}_{2y}\\
&+ \cos(\theta_{2x}) \cos(\theta_{2y}) \dot{l}_2],\\
&c_{16} = -m_2 [l_2 \cos(\theta_{2x}) \sin(\theta_{2y}) \dot{\theta}_{2x} + l_2 \sin(\theta_{2x}) \cos(\theta_{2y}) \dot{\theta}_{2y}\\
&+ \sin(\theta_{2x}) \sin(\theta_{2y}) \dot{l}_2],\\
&c_{17} = (m_1 + m_2)[\cos(\theta_{1x}) \cos(\theta_{1y}) \dot{\theta}_{1x} - \sin(\theta_{1x}) \sin(\theta_{1y}) \dot{\theta}_{1y}],\\
&c_{18} = m_2 [\cos(\theta_{2x}) \cos(\theta_{2y}) \dot{\theta}_{2x}\\
&- \sin(\theta_{2x}) \sin(\theta_{2y}) \dot{\theta}_{2y}]
\end{aligned} \tag{F.10}$$

$$\begin{aligned}
C_{2\bullet}(q, \dot{q}) = \ & (0,\ 0,\ 0,\ c_{24} = (m_1 + m_2)[-l_1 \sin(\theta_{1y}) \dot{\theta}_{1y} + \cos(\theta_{1y}) \dot{l}_1],\\
&0,\ \ c_{26} = -m_2 l_2 \sin(\theta_{2y}) \dot{\theta}_{2y}\\
&+ m_2 \cos(\theta_{2y}) \dot{l}_2,\ c_{27} = (m_1 + m_2) \cos(\theta_{1y}) \dot{\theta}_{1y},\\
&c_{28} = m_2 \cos(\theta_{2y}) \dot{\theta}_{2y})
\end{aligned} \tag{F.11}$$

$$\begin{aligned}
C_{3\bullet}(q, \dot{q}) = \ & (0,\ 0,\ c_{33} = -(m_1 + m_2) l_1 \cos(\theta_{1y}) \sin(\theta_{1y}) \dot{\theta}_{1y}\\
&+ \tfrac{1}{2}(m_1 + m_2) \cos^2(\theta_{1y}) \dot{l}_1,\\
&c_{34} = -(m_1 + m_2) l_1 \cos(\theta_{1y}) \sin(\theta_{1y}) \dot{\theta}_{1y},\\
&c_{35} = m_2 l_1 l_2 \cos(\theta_{1y}) \cos(\theta_{1y}) \sin(\theta_{1x} - \theta_{2x}) \dot{\theta}_{2x}\\
&- m_2 l_1 l_2 \cos(\theta_{1y}) \sin(\theta_{2y}) \cos(\theta_{1x} - \theta_{2x}) \dot{\theta}_{2y}\\
&+ m_2 l_1 \cos(\theta_{1y}) \cos(\theta_{2y}) \cos(\theta_{1x} - \theta_{2x}) \dot{l}_2,\\
&c_{36} = \tfrac{1}{2}(m_2 - m_1) l_1 l_2 \cos(\theta_{1x}) \sin(\theta_{1y}) \sin(\theta_{2x}) \sin(\theta_{2y}) \dot{\theta}_{1y}\\
&- m_2 l_1 l_2 \cos(\theta_{1y}) \sin(\theta_{2y}) \cos(\theta_{1x} - \theta_{2x}) \dot{\theta}_{2x}\\
&+ m_2 l_1 l_2 \cos(\theta_{2y}) \cos(\theta_{1y}) \sin(\theta_{1x} - \theta_{2x}) \dot{\theta}_{2y}\\
&+ m_2 l_1 \sin(\theta_{2y}) \cos(\theta_{1y}) \sin(\theta_{1x} - \theta_{2x}) \dot{l}_2,\ c_{37}\\
&= \tfrac{1}{2}(m_1 + m_2) \cos^2(\theta_{1y}) \dot{\theta}_{1x},\\
&c_{38} = m_2 l_1 \cos(\theta_{1y}) \cos(\theta_{2y}) \cos(\theta_{1x} - \theta_{2x}) \dot{\theta}_{2x}\\
&+ m_2 l_1 \sin(\theta_{2y}) \cos(\theta_{1y}) \sin(\theta_{1x} - \theta_{2x}) \dot{\theta}_{2y})
\end{aligned} \tag{F.12}$$

$$\begin{aligned}
C_{4\bullet}(q, \dot{q}) = \ & (0,\ 0,\ \ c_{43} = (m_1 + m_2) l_1 \cos(\theta_{1y}) \sin(\theta_{1y}) \dot{\theta}_{1y},\\
&c_{44} = m(_1 + m_2) l_1 \dot{l}_1,\\
&c_{45} = m_2 l_1 l_2 \sin(\theta_{1y}) \cos(\theta_{2y}) \cos(\theta_{1x} - \theta_{2x}) \dot{\theta}_{2x}\\
&- m_2 l_1 l_2 \sin(\theta_{1y}) \sin(\theta_{2y}) \sin(\theta_{2x}) \cos(\theta_{1x}) \dot{\theta}_{2y}\\
&+ \tfrac{m_1 + m_2}{2} l_1 l_2 \sin(\theta_{1x}) \sin(\theta_{1y}) \cos(\theta_{2x}) \sin(\theta_{2y}) \dot{\theta}_{2y}\\
&+ m_2 l_1 \sin(\theta_{1y}) \cos(\theta_{2y}) \sin(\theta_{2x} - \theta_{1x}) \dot{l}_2,\\
&c_{46} = \tfrac{m_1 + m_2}{2} l_1 l_2 \cos(\theta_{1x}) \sin(\theta_{1y}) \sin(\theta_{2x}) \sin(\theta_{2y}) \dot{\theta}_{1x}\\
&+ \tfrac{1}{2} m_1 l_1 l_2 \sin(\theta_{1x}) \sin(\theta_{1y}) \cos(\theta_{2x}) \sin(\theta_{2y}) \dot{\theta}_{2x}\\
&- \tfrac{1}{2} m_2 l_1 l_2 \sin(\theta_{1y}) \sin(\theta_{2y}) \sin(\theta_{2x} - \theta_{1x}) \dot{\theta}_{2x}\\
&+ m_1 l_1 l_2 \sin(\theta_{1x}) \sin(\theta_{1y}) \sin(\theta_{2x}) \cos(\theta_{2y}) \dot{\theta}_{2y}\\
&- m_2 l_1 l_2 \cos(\theta_{1y}) \sin(\theta_{2y}) \dot{\theta}_{2y}\\
&+ m_2 l_1 l_2 \cos(\theta_{1x}) \sin(\theta_{1y}) \cos(\theta_{2x}) \cos(\theta_{2y}) \dot{\theta}_{2y}\\
&+ \tfrac{m_1 - m_2}{2} l_2 \sin(\theta_{1x}) \sin(\theta_{1y}) \sin(\theta_{2x}) \sin(\theta_{2y}) \dot{l}_1\\
&+ \tfrac{m_1 + m_2}{2} l_1 \sin(\theta_{2y}) \sin(\theta_{1y}) \sin(\theta_{1x}) \sin(\theta_{2x}) \dot{l}_2
\end{aligned}$$

$$
\begin{aligned}
&+ m_2 l_1 \cos(\theta_{1y})\cos(\theta_{2y})\dot{l}_2 + m_2 l_1 \cos(\theta_{1x})\sin(\theta_{1y})\\
&\cos(\theta_{2x})\sin(\theta_{2y})\dot{l}_2\ ,\quad c_{47} = (m_1+m_2)l_1\dot{\theta}_{1y}\\
&+ \tfrac{m_1-m_2}{2} l_2 \sin(\theta_{2y})\sin(\theta_{1y})\sin(\theta_{1x})\sin(\theta_{2x})\dot{\theta}_{2y}\ ,\\
&c_{48} = m_2 l_1 \cos(\theta_{1y})\cos(\theta_{2y})\dot{\theta}_{2y}\\
&+m_2 l_1 \sin(\theta_{2y})\sin(\theta_{1y})\cos(\theta_{1x})\cos(\theta_{2x})\dot{\theta}_{2y}\\
&+\tfrac{m_1+m_2}{2} l_1 \sin(\theta_{1x})\sin(\theta_{1y})\sin(\theta_{2x})\sin(\theta_{2y})\dot{\theta}_{2y})
\end{aligned}
\tag{F.13}
$$

$$
\begin{aligned}
C_{5\bullet}(q,\dot{q}) = \quad & (0,\ 0,\ c_{53} = -m_2 l_1 l_2 \cos(\theta_{1y})\cos(\theta_{2y})\sin(\theta_{1x}-\theta_{2x})\dot{\theta}_{1x}\\
&-m_2 l_1 l_2 \sin(\theta_{1y})\cos(\theta_{2y})\cos(\theta_{1x}-\theta_{2x})\dot{\theta}_{1y}\\
&+ m_2 l_2 \cos(\theta_{1y})\cos(\theta_{2y})\cos(\theta_{1x}-\theta_{2x})\dot{l}_1,\\
&c_{54} = -m_2 l_1 l_2 \sin(\theta_{1y})\cos(\theta_{2y})\cos(\theta_{1x}-\theta_{2x})\dot{\theta}_{1x}\\
&+m_2 l_1 l_2 \cos(\theta_{1y})\cos(\theta_{2y})\sin(\theta_{2x}-\theta_{1x})\dot{\theta}_{1y}\\
&+ \tfrac{m_2-m_1}{2} l_1 l_2 \sin(\theta_{1x})\sin(\theta_{1y})\sin(\theta_{2y})\cos(\theta_{2x})\dot{\theta}_{2y}\\
&+m_2 l_2 \sin(\theta_{1y})\cos(\theta_{2y})\sin(\theta_{2x}-\theta_{1x})\dot{l}_1\ ,\\
&c_{55} = -m_2 l_2^2 \cos(\theta_{2y})\sin(\theta_{2y})\dot{\theta}_{2y} + m_2 l_2 \cos^2(\theta_{2y})\dot{l}_2\ ,\\
&c_{56} = \tfrac{m_2-m_1}{2} l_1 l_2 \sin(\theta_{1y})\sin(\theta_{2y})\cos(\theta_{2x})\sin(\theta_{1x})\dot{\theta}_{1y}\\
&-m_2 l_2^2 \cos(\theta_{2y})\sin(\theta_{2y})\dot{\theta}_{2x}\ ,\\
&c_{57} = m_2 l_2 \cos(\theta_{1y})\cos(\theta_{2y})\cos(\theta_{1x}-\theta_{2x})\dot{\theta}_{1x}\\
&-m_2 l_2 \sin(\theta_{1y})\cos(\theta_{2y})\sin(\theta_{1x}-\theta_{2x})\dot{\theta}_{1y}\ ,\\
&c_{58} = -m_2 l_2 \cos^2(\theta_{2y})\dot{\theta}_{2x})
\end{aligned}
\tag{F.14}
$$

$$
\begin{aligned}
C_{6\bullet}(q,\dot{q}) = \quad & (0,\ 0,\ c_{63} = m_2 l_1 l_2 \sin(\theta_{2y})\cos(\theta_{1y})\cos(\theta_{1x}-\theta_{2x})\dot{\theta}_{1x}\\
&-m_2 l_1 l_2 \sin(\theta_{2y})\sin(\theta_{1y})\sin(\theta_{1x})\cos(\theta_{2x})\dot{\theta}_{1y}\\
&+ \tfrac{1}{2}(m_1+m_2) l_1 l_2 \cos(\theta_{1x})\sin(\theta_{1y})\sin(\theta_{2x})\sin(\theta_{2y})\dot{\theta}_{1y}\\
&+m_2 l_2 \sin(\theta_{2y})\cos(\theta_{1y})\sin(\theta_{1x}-\theta_{2x})\dot{l}_1\ ,\\
&c_{64} = -m_2 l_1 l_2 \sin(\theta_{1x})\sin(\theta_{1y})\cos(\theta_{2x})\sin(\theta_{1y})\dot{\theta}_{1x}\\
&+\tfrac{m_1+m_2}{2} l_1 l_2 \cos(\theta_{1x})\sin(\theta_{1y})\sin(\theta_{2x})\sin(\theta_{2y})\dot{\theta}_{1x}\\
&+m_1 l_1 l_2 \sin(\theta_{1x})\cos(\theta_{1y})\sin(\theta_{2x})\sin(\theta_{2y})\dot{\theta}_{1y}\\
&-m_2 l_1 l_2 \sin(\theta_{1y})\cos(\theta_{2y})\dot{\theta}_{1y}\\
&+ m_2 l_1 l_2 \cos(\theta_{1x})\cos(\theta_{1y})\cos(\theta_{2x})\sin(\theta_{2y})\dot{\theta}_{1y}\\
&+\tfrac{m_1-m_2}{2} l_1 l_2 \sin(\theta_{1y})\sin(\theta_{2y})\cos(\theta_{2x})\sin(\theta_{1x})\dot{\theta}_{2x}\\
&+m_2 l_2 \cos(\theta_{1x})\sin(\theta_{1y})\cos(\theta_{2x})\sin(\theta_{2y})\dot{l}_1\\
&+m_2 l_2 \cos(\theta_{1y})\cos(\theta_{2y})\dot{l}_1\\
&+\tfrac{m_1+m_2}{2} l_2 \sin(\theta_{2y})\sin(\theta_{1y})\sin(\theta_{1x})\sin(\theta_{2x})\dot{l}_1\\
&+\tfrac{m_1-m_2}{2} l_1 \sin(\theta_{1x})\sin(\theta_{1y})\sin(\theta_{2x})\sin(\theta_{2y})\dot{l}_2\ ,\\
&c_{65} = \tfrac{m_1-m_2}{2} l_1 l_2 \sin(\theta_{1y})\sin(\theta_{2y})\cos(\theta_{2x})\sin(\theta_{1x})\dot{\theta}_{1y}\\
&+m_2 l_2^2 \cos(\theta_{2y})\sin(\theta_{2y})\dot{\theta}_{2x}\ ,\\
&c_{66} = m_2 l_2 \dot{l}_2\ ,\ c_{67} = m_2 l_2 \cos(\theta_{1y})\sin(\theta_{2y})\sin(\theta_{1x}-\theta_{2x})\dot{\theta}_{1x}\\
&+m_2 l_2 \cos(\theta_{2y})\cos(\theta_{1y})\dot{\theta}_{1y}\\
&+ m_2 l_2 \cos(\theta_{1x})\sin(\theta_{1y})\cos(\theta_{2x})\sin(\theta_{2y})\dot{\theta}_{1y}\\
&+\tfrac{m_1+m_2}{2} l_2 \sin(\theta_{2y})\sin(\theta_{1y})\sin(\theta_{1x})\sin(\theta_{2x})\dot{\theta}_{1y}\\
&c_{67} = m_2 l_2 \cos(\theta_{1y})\sin(\theta_{2y})\sin(\theta_{1x}-\theta_{2x})\dot{\theta}_{1x}\\
&+m_2 l_2 \cos(\theta_{2y})\cos(\theta_{1y})\dot{\theta}_{1y}\\
&+ m_2 l_2 \cos(\theta_{1x})\sin(\theta_{1y})\cos(\theta_{2x})\sin(\theta_{2y})\dot{\theta}_{1y}\\
&+\tfrac{m_1+m_2}{2} l_2 \sin(\theta_{2y})\sin(\theta_{1y})\sin(\theta_{1x})\sin(\theta_{2x})\dot{\theta}_{1y}\ ,\\
&c_{68} = m_2 l_2 \dot{\theta}_{2y} + \tfrac{m_1-m_2}{2} l_1 \sin(\theta_{2y})\sin(\theta_{1y})\sin(\theta_{1x})\sin(\theta_{2x})\dot{\theta}_{1y})
\end{aligned}
\tag{F.15}
$$

$$
\begin{aligned}
C_{7\bullet}(q,\dot{q}) = \quad & (0,\ 0,\ c_{73} = -\tfrac{1}{2}(m_1+m_2)\cos^2(\theta_{1y})\dot{\theta}_{1x},\\
&c_{74} = -(m_1+m_2)l_1\dot{\theta}_{1y}\\
&- \tfrac{m_1-m_2}{2} l_2 \sin(\theta_{2y})\sin(\theta_{1y})\sin(\theta_{1x})\sin(\theta_{2x})\dot{\theta}_{2y},\\
&c_{75} = -m_2 l_2 \cos(\theta_{1y})\cos(\theta_{2y})\cos(\theta_{1x}-\theta_{2x})\dot{\theta}_{2x}\\
&-m_2 l_2 \cos(\theta_{1y})\sin(\theta_{2y})\sin(\theta_{1x}-\theta_{2x})\dot{\theta}_{2y}\\
&+ m_2 \cos(\theta_{1y})\cos(\theta_{2y})\sin(\theta_{1x}-\theta_{2y})\dot{l}_2\ ,\\
&c_{76} = \tfrac{m_2-m_1}{2} l_2 \sin(\theta_{2y})\sin(\theta_{1y})\sin(\theta_{1x})\sin(\theta_{2x})\dot{\theta}_{1y}\\
&- m_2 l_2 \cos(\theta_{1y})\sin(\theta_{2y})\sin(\theta_{1x}-\theta_{2x})\dot{\theta}_{2x}\\
&-m_2 l_2 \sin(\theta_{2y})\sin(\theta_{1y})\dot{\theta}_{2y}\\
&- m_2 l_2 \cos(\theta_{2y})\cos(\theta_{1y})\cos(\theta_{1x}-\theta_{2x})\dot{\theta}_{2y}\\
&+m_2 \cos(\theta_{2y})\sin(\theta_{1y})\dot{l}_2\\
&- m_2 \sin(\theta_{2y})\cos(\theta_{1y})\cos(\theta_{1x}-\theta_{2x})\dot{l}_2\ ,\ c_{77} = 0,\\
&c_{78} = m_2 \cos(\theta_{1y})\cos(\theta_{2y})\sin(\theta_{1x}-\theta_{2x})\dot{\theta}_{2x}\\
&- m_2 \cos(\theta_{1y})\sin(\theta_{2y})\cos(\theta_{1x}-\theta_{2x})\dot{\theta}_{2y})
\end{aligned}
\tag{F.16}
$$

$$
\begin{aligned}
C_{8\bullet}(q,\dot{q}) = \quad & (0,\ 0,\ c_{83} = -m_2 l_1 \cos(\theta_{2y})\cos(\theta_{1y})\cos(\theta_{1x}-\theta_{2x})\dot{\theta}_{1x}\\
&-m_2 l_1 \cos(\theta_{2y})\sin(\theta_{1y})\sin(\theta_{2x}-\theta_{1x})\dot{\theta}_{1y}\\
&+ m_2 \cos(\theta_{2y})\cos(\theta_{1y})\sin(\theta_{2x}-\theta_{1x})\dot{l}_1,\\
&c_{84} = m_2 l_1 \cos(\theta_{2y})\sin(\theta_{1y})\sin(\theta_{1x}-\theta_{2x})\dot{\theta}_{1x}\\
&- m_2 l_1 \sin(\theta_{1y})\sin(\theta_{2y})\dot{\theta}_{1y}\\
&-m_2 l_1 \cos(\theta_{2y})\cos(\theta_{1y})\cos(\theta_{1x}-\theta_{2x})\dot{\theta}_{1y}\\
&+\tfrac{m_2-m_1}{2} l_1 \sin(\theta_{1x})\sin(\theta_{1y})\\
&\sin(\theta_{2x})\sin(\theta_{1y})\dot{\theta}_{2y} + m_2 \cos(\theta_{1y})\sin(\theta_{2y})\dot{l}_1\\
&-m_2 \cos(\theta_{2y})\sin(\theta_{1y})\cos(\theta_{1x}-\theta_{2x})\dot{l}_1,\\
&c_{85} = m_2 l_2 \cos^2(\theta_{2y})\dot{\theta}_{2x}\ ,\\
&c_{86} = \tfrac{m_2-m_1}{2} l_1 \sin(\theta_{2y})\sin(\theta_{1y})\sin(\theta_{2x})\sin(\theta_{1x})\dot{\theta}_{1y} - m_2 l_2 \dot{\theta}_{2y}\ ,\\
&c_{87} = -m_2 \cos(\theta_{1y})\cos(\theta_{2y})\sin(\theta_{1x}-\theta_{2x})\dot{\theta}_{1x}\\
&+m_2 \cos(\theta_{1y})\sin(\theta_{2y})\dot{\theta}_{1y}\\
&- m_2 \cos(\theta_{2y})\sin(\theta_{2y})\cos(\theta_{1x}-\theta_{2x})\dot{\theta}_{1y}\ ,\ c_{88} = 0)
\end{aligned}
\tag{F.17}
$$

The gravity potential energy is given by:

$$
\begin{aligned}
&U_g(q) = -m_1 g l_1 \cos(\theta_{1x})\cos(\theta_{1y}) - m_2 g[l_1 \cos(\theta_{1x})\cos(\theta_{1y})\\
&+ l_2 \cos(\theta_{2x})\cos(\theta_{2y})],
\end{aligned}
\tag{F.18}
$$

so that the gravity generalized force is equal to:

$$
-\frac{\partial U_g}{\partial q} = \begin{pmatrix}
0\\ 0\\ -(m_1+m_2)g l_1 \sin(\theta_{1x})\cos(\theta_{1y})\\ -(m_1+m_2)g l_1 \cos(\theta_{1x})\sin(\theta_{1y})\\ m_2 g l_2 \sin(\theta_{2x})\cos(\theta_{2y})\\ m_2 g l_2 \cos(\theta_{2x})\sin(\theta_{2y})\\ (m_1+m_2)g\cos(\theta_{1x})\cos(\theta_{1y})\\ m_2 g \cos(\theta_{2x})\cos(\theta_{2y})
\end{pmatrix}
\tag{F.19}
$$

The vector of torque inputs is $Q = (F_x, F_y, 0, 0, 0, 0, F_{l_1}, F_{l_2})^\top$, where F_{l_1} corresponds to a winch mechanism at the attachment joint between link 1 and the cart, while F_{l_2} corresponds to a winch mechanism mounted in joint with mass m_1 (see Fig. 3(b)). As alluded to in Section 2.2, an even more complete model incorporates the 3D dynamics of the payload (considered as a rigid body). This adds three orientation angles (Euler or else), yielding an 11-degree-of-freedom system. The analytical calculations of the matrix $C(q,\dot{q})$ using Christoffel's symbols thus involve $11^3 \times 3 = 3993$ partial derivatives $\frac{\partial m_{ij}}{\partial q_k}$. Certainly the use of a formal calculus tool becomes mandatory at this stage.

Table G.14
Main parameters of the HOISTING TOOLBOX.

Variable	Value
file name `main_run.m`:running the main simulation and updating the results	
`Method`	The default value is `"all"` meaning that the simulations will be done for all controllers. Alternatively, by selecting an integer value for this variable it is possible to conduct the simulation for a single controller. The integer value corresponds to the row of Table 11
`model_select`	The default value is `"rigid"` meaning that the lumped mass model introduced in Section 5 will be used. Alternatively, it is possible to replace this value with `"flexible"` to use the built-in MATLAB flexible beam model for the cable (this should be used with caution).
file name `parameters.m`: used to modify the parameters of the simulation	
	`traj_type`: used to select a trajectory, `load_type`: used to select the payload type, `matched_disurbance_flag` and `load_disturbance_flag`: select disturbances, `initial_sway_type`: select initial sway `SNR_value`: SNR of feedback noise

Appendix G. Some technical results for control

The above calculations are not useful for numerical simulation sake, since available multibody toolboxes allow the construction of such dynamical systems automatically. However, they may be necessary to extend the stability analyses relying on zero-state detectability, LaSalle's invariance principle, in order to extend the results obtained for $N = 1$ (in 2D and 3D)and $N = 2$ (in 2D), see Section 3.3.4. Consider Appendix A. Let us further split the matrix $M_{x\theta l}(q) = \begin{pmatrix} M_{xl}(q) \\ M_{\theta l}(q) \end{pmatrix}$, so that:

$$M(q) = \begin{pmatrix} M_{xx} & \bar{M}_{x\theta} & M_{xl} \\ \bar{M}_{x\theta}^{\top} & M_{\theta\theta} & M_{\theta l} \\ M_{xl}^{\top} & M_{\theta l}^{\top} & M_{ll} \end{pmatrix} \tag{G.1}$$

Item 4 in Lemma 1 allows us to perform Spong's transformation for actuated and unactuated coordinates (Reyhanoglu et al., 1999). Indeed $\ddot{\theta} = M_{\theta\theta}^{-1}(-\bar{M}_{x\theta}^{\top}\ddot{x} - M_{\theta l}\ddot{l} - NL(q,\dot{q}))$, where $NL(q,\dot{q})$ stands for generic nonlinearities. Hence:

$$\underbrace{(M_{xx} - \bar{M}_{x\theta}M_{\theta\theta}^{-1}\bar{M}_{x\theta}^{\top})}_{\triangleq \mathcal{M}_x}\ddot{x} + \underbrace{(M_{ll} - \bar{M}_{x\theta}M_{\theta\theta}^{-1}M_{\theta l})}_{\triangleq \mathcal{M}_{xl}}\ddot{l}$$
$$- \bar{M}_{x\theta}M_{\theta\theta}^{-1}NL(q,\dot{q}) + NL(q,\dot{q}) = F_x \tag{G.2}$$

$$(M_{xl}^{\top} - M_{\theta l}^{\top}M_{\theta\theta}^{-1}\bar{M}_{x\theta}^{\top})\ddot{x} + \underbrace{(M_{ll} - M_{\theta l}^{\top}M_{\theta\theta}^{-1}M_{\theta l})}_{\triangleq \mathcal{M}_l}\ddot{l}$$
$$- M_{\theta l}^{\top}M_{\theta\theta}^{-1}NL(q,\dot{q}) + NL(q,\dot{q}) = F_l \tag{G.3}$$

where $\mathcal{M}_x \succ 0$ and $\mathcal{M}_l \succ 0$ from the Schur complement Theorem (but, in view of Lemma 1, $\mathcal{M}_l$ becomes singular at the vertical posture and if the payload is much heavier than the cable and the hook). Rearranging the matrix in (G.1) and applying again the Schur complement Theorem, it follows that:

Lemma 2. *Let us consider (G.2) (G.3), then:*

$$\mathcal{M}(q) \triangleq \begin{pmatrix} \mathcal{M}_x(q) & \mathcal{M}_{xl}(q) \\ \mathcal{M}_{xl}^{\top}(q) & \mathcal{M}_l(q) \end{pmatrix} = \mathcal{M}^{\top}(q) \succ 0 \tag{G.4}$$

Consequently the system in (G.2) (G.3) with state $(x, \dot{x}, l^{\top}, \dot{l}^{\top})^{\top}$ and input $(F_x, F_l)^{\top}$ is controllable (if some basic conditions hold to guarantee $M_{ll} \succ 0$), linearizable by state feedback. Then the crucial point concerns the integrability properties of the system of unactuated coordinates (Reyhanoglu et al., 1999):

$$\ddot{\theta} = M_{\theta\theta}^{-1}(-\bar{M}_{x\theta}^{\top}\ddot{x} - M_{\theta l}\ddot{l} - NL(q,\dot{q})) \tag{G.5}$$

Usually such dynamics are nonintegrable and thus can be interpreted as second-order nonholonomic constraints, which do not reduce the state-space dimension (Reyhanoglu et al., 1999). From Lemma 1 the term $M_{\theta l}(q)$ vanishes at the vertical cable's posture and is proportional to θ_i and sums of angles in a neighborhood of it. Thus around the vertical posture only $\bar{M}_{x\theta}^{\top}\ddot{x}$ remains available as a control input to this subdynamics, and some control action may also exist through $NL(q,\dot{q})$. Said otherwise:

Proposition 2. *Let $q = (x, \theta_1, \ldots, \theta_N, l_1, \ldots, l_N)^{\top}$. The only way to control the θ dynamics (G.5) in the neighborhood of the cable's vertical posture, is through $\ddot{x}$ and/or some nonlinear velocity couplings.*

It is not difficult to extend these results to the case where only l_1 varies, and also to the 3D double-pendulum in Appendix F. It is noteworthy that the nonlinear forces in (D.4) could be interesting for control purposes, by choosing suitable $\frac{\partial m_1}{\partial l_1}$ when a winch is mounted on a fixed reference frame outside the OC's moving structure. To the best of the authors' knowledge, this is an open issue.

Appendix H. Hoisting toolbox

A set of scripts and files have been developed in this work to conduct all the necessary numerical simulations and optimizations.[2] The controllers listed in Table 11 are implemented in the toolbox and a set of optimization algorithms have been used in the toolbox in order to optimize the parameters of the controllers. Moreover, it can generate and compare the results using plots and tables compatible with LaTeX. The toolbox contains many functions and scripts and files. But, for a normal usages, user only needs to consider two script files named `main_run.m` and `parameters.m` and modify it according to Table G.14. In addition, other parameters can be modified in the toolbox to get customized results as explained in detail in the corresponding files.

References

Abdel-Rahman, E., & Nayfeh, A. (2002). Pendulation reduction in boom cranes using cable length manipulation. *Nonlinear Dynamics*, *27*(3), 255–269.

Abdel-Rahman, E. M., Nayfeh, A. H., & Masoud, Z. N. (2003). Dynamics and control of cranes: A review. *Journal of Vibration and Control*, *9*(7), 863–908.

Abdullahi, A., Mohamed, Z., Abidin, M. Z., Akmeliawati, R., Husain, A., Bature, A., et al. (2016). Negative imaginary theorem with an application to robust control of a crane system. *Jurnal Teknologi*, *78*(6–11), 33–39.

[2] A MATLAB installation is required in order to use the toolbox. The toolbox is available on https://github.com/Mojallizadeh/HoistingToolbox under GPL license, and therefore it is possible to modify it to get customized results. All the results presented in this paper are easily reproducible thanks to this toolbox.

Abdullahi, A. M., Mohamed, Z., Selamat, H., Pota, H. R., Zainal Abidin, M., Ismail, F., et al. (2018). Adaptive output-based command shaping for sway control of a 3D overhead crane with payload hoisting and wind disturbance. *Mechanical Systems and Signal Processing*, *98*, 157–172.

Acary, V., & Brogliato, B. (2008). *Lecture notes in applied and computational mechanics*, *Numerical methods for nonsmooth dynamical systems. Applications in mechanics and electronics*. (35), Berlin Heidelberg: Springer-Verlag.

Acary, V., Brogliato, B., & Orlov, Y. (2012). Chattering-free digital sliding-mode control with state observer and disturbance rejection. *IEEE Transactions on Automatic Control*, *57*(5), 1087–1101.

Ackermann, J. (2012). *Robust control: Systems with uncertain physical parameters*. Springer Science & Business Media.

Al-Garni, A., Moustafa, K., & Javeed Nizami, S. (1995). Optimal control of overhead cranes. *Control Engineering Practice*, *3*(9), 1277–1284.

Alghanim, K. A., Alhazza, K. A., & Masoud, Z. N. (2015). Discrete-time command profile for simultaneous travel and hoist maneuvers of overhead cranes. *Journal of Sound and Vibration*, *345*, 47–57.

Alhazza, K., Masoud, Z., & Alotaibi, N. (2016). A smooth wave-form shaped command with flexible maneuvering time: Analysis and experiments. *Asian Journal of Control*, *18*(4), 1376–1384.

Alli, H., & Singh, T. (1998). Passive control of overhead cranes. In *Proceedings of the 1998 IEEE international conference on control applications, vol. 2* (pp. 1046–1050).

Almutairi, N. B., & Zribi, M. (2009). Sliding mode control of a three-dimensional overhead crane. *Journal of Vibration and Control*, *15*(11), 1679–1730.

Alshaya, A., & Alghanim, K. (2020). Command shaping for sloshing suppression of a suspended liquid container. *Journal of Dynamic Systems, Measurement, and Control*, *142*(12), Article 121003.

Antipov, A., & Krasnova, S. (2022). Using of sigmoid functions in the control system of the overhead crane. In *2022 16th international conference on stability and oscillations of nonlinear control systems (Pyatnitskiy's conference)* (pp. 1–4).

Arena, A., Casalotti, A., Lacarbonara, W., & Cartmell, M. P. (2013). Three-dimensional modeling of container cranes. In *International design engineering technical conferences and computers and information in engineering conference*: *vol. 7A*, *9th international conference on multibody systems, nonlinear dynamics, and control* (pp. 1–10).

Arena, A., Casalotti, A., Lacarbonara, W., & Cartmell, M. (2015). Dynamics of container cranes: three-dimensional modeling, full-scale experiments, and identification. *International Journal of Mechanical Sciences*, *93*, 8–21.

Artola, M., Wynn, A., & Palacios, R. (2021). Modal-based nonlinear model predictive control for 3D very flexible structures. *IEEE Transactions on Automatic Control*.

Aschemann, H. (2009). Passivity-based trajectory control of an overhead crane by interconnection and damping assignment. In H. Ulbrich, & L. Ginzinger (Eds.), *Motion and vibration control* (pp. 21–30). Springer Netherlands.

Auernig, J., & Troger, H. (1987). Time optimal control of overhead cranes with hoisting of the load. *Automatica*, *23*(4), 437–447.

Balachandran, B., Li, Y.-Y., & Fang, C.-C. (1999). A mechanical filter concept for control of non-linear crane-load oscillations. *Journal of Sound and Vibration*, *228*(3), 651–682.

Bartolini, G., Orani, N., Pisano, A., & Usai, E. (2000). Load swing damping in overhead cranes by sliding mode technique. In *Proceedings of the 39th IEEE conference on decision and control, vol. 2* (pp. 1697–1702).

Bartolini, G., Pisano, A., & Usai, E. (2002). Second-order sliding-mode control of container cranes. *Automatica*, *38*(10), 1783–1790.

Bartolini, G., Pisano, A., & Usai, E. (2003). Output-feedback control of container cranes: A comparative analysis. *Asian Journal of Control*, *5*(4), 578–593.

Bauer, D., Schaper, U., Schneider, K., & Sawodny, O. (2014). Observer design and flatness-based feedforward control with model predictive trajectory planning of a crane rotator. In *2014 American control conference* (pp. 4020–4025).

Bernstein, D. (2009). *Matrix mathematics. Theory, facts and formulas* (2nd ed.). Princeton University Press.

Bernstein, D. (2018). *Scalar, vector, and matrix mathematics. Theory, facts and formulas* (Revised and expanded ed.). Princeton University Press.

Bertrand, C., Acary, V., Lamarque, C.-H., & Svadkoohi, A. T. (2020). A robust and efficient numerical finite element method for cables. *International Journal for Numerical Methods in Engineering*, *121*(18), 4157–4186.

Bockstedte, A., & Kreuzer, E. (2005). Hoisting manipulation by modal coupling control for underactuated cranes. In *IUTAM symposium on vibration control of nonlinear mechanisms and structures* (pp. 121–130). Springer.

Bonnabel, S., & Claeys, X. (2020). The industrial control of tower cranes: An operator-in-the-loop approach [applications in control]. *IEEE Control Systems Magazine*, *40*(5), 27–39.

Boustany, F., & d'Andrea Novel, B. (1992). Adaptive control of an overhead crane using dynamic feedback linearization and estimation design. In *Proceedings 1992 IEEE international conference on robotics and automation, vol. 3* (pp. 1963–1968).

Brogliato, B. (2016). *Communications and control engineering*, *Nonsmooth mechanics. Models, dynamics and control* (3rd ed.). Springer Int. Publishing Switzerland.

Brogliato, B. (2022). *Lagrange dynamics of lumped-mass multibody models of overhead cranes in 2D and 3D operational spaces*: *Research report*, INRIA, https://hal-lara.archives-ouvertes.fr/LJK-MAD-TRIPOP/hal-03674652v2.

Brogliato, B., Lozano, R., Maschke, B., & Egeland, O. (2020a). *Communications and control engineering, Dissipative systems analysis and control. Theory and applications* (3rd ed.). Cham, CH: Springer Nature Switzerland AG.

Brogliato, B., Lozano, R., Maschke, B., & Egeland, O. (2020b). Passivity-based control. In *Dissipative systems analysis and control* (pp. 491–573). Springer.

Brogliato, B., Ortega, R., & Lozano, R. (1995). Global tracking controllers for flexible-joint manipulators: a comparative study. *Automatica*, *31*(7), 941–956.

Brogliato, B., & Polyakov, A. (2021). Digital implementation of sliding-mode control via the implicit method: A tutorial. *International Journal of Robust and Nonlinear Control*, *31*(9), 3528–3586.

Brogliato, B., Polyakov, A., & Efimov, D. (2020). The implicit discretization of the super-twisting sliding-mode control algorithm. *IEEE Transactions on Automatic Control*, *65*(8), 3707–3713.

Carricato, M. (2013). Direct geometrico-static problem of underconstrained cable-driven parallel robots with three cables. *ASME Journal of Mechanisms and Robotics*, *5*(3), Article 031008.

Carricato, M., & Merlet, J. (2013). Stability analysis of underconstrained cable-driven parallel robots. *IEEE Transactions on Robotics*, *29*(1), 288–296.

Cartmell, M., Morrish, L., Alberts, T. E., & Taylor, A. J. (1996). Controlling the nonlinear dynamics of gantry cranes. *Machine Vibration*, *5*(4), 197–210.

Cartmell, M., Morrish, L., & Taylor, A. (1998). Dynamics of spreader motion in a gantry crane. *Proceedings of the Institution of Mechanical Engineers IMechE Part C*, *212*, 85–105.

Caverly, R., Forbes, J., & Mohammadshahi, D. (2014). Dynamic modelling and passivity-based control of a single degree of freedom cable-actuated system. *IEEE Transactions on Control Systems Technology*, *23*(3), 898–909.

Chang, C.-Y., & Chiang, K.-H. (2008). The nonlinear 3-D crane control with an intelligent operating method. In *2008 SICE annual conference* (pp. 2917–2921).

Chen, Q., Cheng, W., Liu, J., & Du, R. (2022). Partial state feedback sliding mode control for double-pendulum overhead cranes with unknown disturbances. *Proceedings of the Institution of Mechanical Engineers, Part C (Mechanical Engineering Science)*, *236*(8), 3902–3911.

Chen, H., Fang, Y., & Sun, N. (2016). Optimal trajectory planning and tracking control method for overhead cranes. *IET Control Theory & Applications*, *10*(6), 692–699.

Chen, H., Fang, Y., & Sun, N. (2016). A swing constraint guaranteed MPC algorithm for underactuated overhead cranes. *IEEE/ASME Transactions on Mechatronics*, *21*(5), 2543–2555.

Chen, H., Gao, B., & Zhang, X. (2005). Dynamical modelling and nonlinear control of a 3D crane. In *2005 international conference on control and automation, vol. 2* (pp. 1085–1090).

Chen, W., & Saif, M. (2008). Output feedback controller design for a class of MIMO nonlinear systems using high-order sliding-mode differentiators with application to a laboratory 3-D crane. *IEEE Transactions on Industrial Electronics*, *55*(11), 3985–3997.

Chen, H., & Sun, N. (2020). Nonlinear control of underactuated systems subject to both actuated and unactuated state constraints with experimental verification. *IEEE Transactions on Industrial Electronics*, *67*(9), 7702–7714.

Chen, H., Xuan, B., Yang, P., & Chen, H. (2019). A new overhead crane emergency braking method with theoretical analysis and experimental verification. *Nonlinear Dynamics*, *98*(3), 2211–2225.

Chen, J.-y., Yang, W.-l., Ni, H.-y., & Yan, W.-x. (2020). A hierarchical sliding mode control method for bridge crane system. In *2020 IEEE international conference on high voltage engineering and application* (pp. 1–4).

Chentouf, B., & Han, Z. J. (2020). On the stabilization of an overhead crane system with dynamic and delayed boundary conditions. *IEEE Transactions on Automatic Control*, *65*(10), 4273–4280.

Chentouf, B., & Mansouri, S. (2022). Stabilization of an overhead crane system with infinite memory in the boundary control. *IEEE Transactions on Automatic Control*, DOI: 10.1109/TAC.2022.3206250.

Choe, B., Choi, M. G., & Ko, H.-S. (2005). Simulating complex hair with robust collision handling. In *Proceedings of the 2005 ACM SIGGRAPH/eurographics symposium on computer animation* (pp. 153–160). New York, NY, USA: Association for Computing Machinery.

Chunshien Li, Chun-Yi Lee, & Kuo-Hsiang Cheng (2004). Pseudoerror-based self-organizing neuro-fuzzy system. *IEEE Transactions on Fuzzy Systems*, *12*(6), 812–819.

Chwa, D. (2009). Nonlinear tracking control of 3-D overhead cranes against the initial swing angle and the variation of payload weight. *IEEE Transactions on Control Systems Technology*, *17*(4), 876–883.

Chwa, D. (2017). Sliding-mode-control-based robust finite-time antisway tracking control of 3-D overhead cranes. *IEEE Transactions on Industrial Electronics*, *64*(8), 6775–6784.

Collado, J., Lozano, R., & Fantoni, I. (2000). Control of convey-crane based on passivity. In *Proceedings of the 2000 American control conference, vol. 2* (pp. 1260–1264).

Crépeau, E., & Prieur, C. (2006). Control of a clamped-free beam by a piezoelectric actuator. *ESAIM. Control, Optimisation and Calculus of Variations*, *12*(3), 545–563.

Cui, L., & Zheng, D. (2019). Visual servoing of a flexible gantry crane with a sway range constraint. *IEEE Control Systems Letters*, *3*(1), 138–143.

Cuong, H. M., & Tuan, L. A. (2023). Robust control of rubber–tyred gantry cranes with structural elasticity. *Applied Mathematical Modelling*, *117*, 741–761.

Damaren, C. J. (1999). Passivity and noncollocation in the control of flexible multibody systems. *Journal of Dynamic Systems, Measurement, and Control*, *122*(1), 11–17.

Damaren, C. (2000). On the dynamics and control of flexible multibody systems with closed loops. *International Journal of Robotics Research*, *19*(3), 238–253.

d'Andréa-Novel, B., & Coron, J.-M. (2000). Exponential stabilization of an overhead crane with flexible cable via a back-stepping approach. *Automatica*, *36*(4), 587–593.

Di Leva, R., Carricato, M., Gattringer, H., & Müller, A. (2022). Sloshing dynamics estimation for liquid-filled containers performing 3-dimensional motions: modeling and experimental validation. *Multibody System Dynamics*, *15*(7), 1049–1077.

Diwold, J., Kolar, B., & Schöberl, M. (2022). Discrete-time flatness-based control of a gantry crane. *Control Engineering Practice*, *119*, Article 104980.

Ebeid, A. M., Moustafa, K. A. F., & Emara-Shabaik, H. E. (1992). Electromechanical modelling of overhead cranes. *International Journal of Systems Science*, *23*(12), 2155–2169.

Egeland, O., & Gravdahl, J. (2002). *Modeling and simulation for automatic control*. Marine Cybernetics A.S., Corrected second printing 2003.

Engelberg, S. (2021). Input shaping: A tutorial introduction [lecture notes]. *IEEE Control Systems Magazine*, *41*(2), 45–51.

Fang, Y., Dixon, W., Dawson, D., & Zergeroglu, E. (2001). Nonlinear coupling control laws for a 3-DOF overhead crane system. In *Proceedings of the 40th IEEE conference on decision and control (cat. no.01CH37228), vol. 4* (pp. 3766–3771).

Fang, Y., Dixon, W., Dawson, D., & Zergeroglu, E. (2003). Nonlinear coupling control laws for an underactuated overhead crane system. *IEEE/ASME Transactions on Mechatronics*, *8*(3), 418–423.

Fang, Y., Ma, B., Wang, P., & Zhang, X. (2012). A motion planning-based adaptive control method for an underactuated crane system. *IEEE Transactions on Control Systems Technology*, *20*(1), 241–248.

Fang, Y., Zergeroglu, E., Dixon, W. E., & Dawson, D. M. (2001). Nonlinear coupling control laws for an overhead crane system. In *Proceedings of the 2001 IEEE international conference on control applications* (CCA'01), (pp. 639–644).

Faravelli, L., Fuggini, C., & Ubertini, F. (2010). Toward a hybrid control solution for cable dynamics: Theoretical prediction and experimental validation. *Structural Control and Health Monitoring*, *17*, 386–403.

Faravelli, L., & Ubertini, F. (2009). Nonlinear state observation for cable dynamics. *Journal of Vibration and Control*, *15*(7), 1049–1077.

Fatehi, M. H., Eghtesad, M., & Amjadifard, R. (2014). Modelling and control of an overhead crane system with a flexible cable and large swing angle. *Journal of Low Frequency Noise, Vibration and Active Control*, *33*(4), 395–409.

Fliess, M., Lévine, J., Martin, P., & Rouchon, P. (1995). Flatness and defect of non-linear systems: introductory theory and examples. *International Journal of Control*, *61*(6), 1327–1361.

Fliess, M., Levine, J., & Rouchon, P. (1991). A simplified approach of crane control via a generalized state-space model. In *[1991] Proceedings of the 30th IEEE conference on decision and control, vol. 1* (pp. 736–741).

Fotland, G., & Haugen, B. (2022). Numerical integration algorithms and constraint formulations for ALE-ANCF cable element. *Mechanism and Machine Theory*, *170*, Article 104659.

Garrido, S., Abderrahim, M., Gimenez, A., Diez, R., & Balaguer, C. (2008). Anti-swinging input shaping control of an automatic construction crane. *IEEE Transactions on Automation Science and Engineering*, *5*(3), 549–557.

Gattulli, V. (2007). Advanced control strategies in cable dynamics. In B. Topper (Ed.), *Civil engineering computations: Tools and techniques* (pp. 243–269). Stirlinghshire, Scotland: Saxe-Coburg Publications.

Gattulli, V., Martinelli, L., Perotti, F., & Vestroni, F. (2004). Nonlinear oscillations of cables under harmonic loading using analytical and finite element models. *Computer Methods in Applied Mechanics and Engineering*, *93*(1–2), 69–85.

Giacomelli, M., Colombo, D., Faroni, M., Schmidt, O., Simoni, L., & Visioli, A. (2019). Comparison of linear and nonlinear MPC on operator-in-the-loop overhead cranes. In *2019 7th international conference on control, mechatronics and automation* (pp. 221–225).

Giacomelli, M., Faroni, M., Gorni, D., Marini, A., Simoni, L., & Visioli, A. (2018a). Model predictive control for operator-in-the-loop overhead cranes. In *2018 IEEE 23rd international conference on emerging technologies and factory automation, vol. 1* (pp. 589–596).

Giacomelli, M., Faroni, M., Gorni, D., Marini, A., Simoni, L., & Visioli, A. (2018b). MPC-PID control of operator-in-the-loop overhead cranes: A practical approach. In *2018 7th international conference on systems and control* (pp. 321–326).

Golovin, I., Maksakov, A., Shysh, M., & Palis, S. (2022). Discrepancy-based control for positioning of large gantry crane. *Mechanical Systems and Signal Processing*, *163*, Article 108199.

Gu, X., & Xu, W. (2022). Moving sliding mode controller for overhead cranes suffering from matched and unmatched disturbances. *Transactions of the Institute of Measurement and Control*, *44*(1), 60–75.

Gueners, D., Bouzgarrou, B., & Chanal, H. (2021). Cable behaviour influence on cable-driven parallel-robots vibrations: Experimental characterization and simulation. *ASME Journal of Mechanisms and Robotics*, *13*, 041003–1–17.

Guo, Q., Chai, L., & Liu, H. (2023). Anti-swing sliding mode control of three-dimensional double pendulum overhead cranes based on extended state observer. *Nonlinear Dynamics*, *111*, 391–410.

Hamdy, M., Shalaby, R., & Sallam, M. (2018). A hybrid partial feedback linearization and deadbeat control scheme for a nonlinear gantry crane. *Journal of the Franklin Institute*, *355*(14), 6286–6299.

Hayajneh, M. T., Radaideh, S. M., AL-Oqla, F. M., & Nejdawi, I. (2008). Reductions of pendulations of overhead cranes under the effect of air resistance by a cable manipulation manner. In *2008 5th international symposium on mechatronics and its applications* (pp. 1–6).

Hazlerigg, A. (1972). Automatic control of crane operations. *IFAC Proceedings Volumes*, *5*(1, Part 1), 250–258.

He, W., & Ge, S. S. (2016). Cooperative control of a nonuniform gantry crane with constrained tension. *Automatica*, *66*, 146–154.

He, W., Zhang, S., & Ge, S. S. (2014). Adaptive control of a flexible crane system with the boundary output constraint. *IEEE Transactions on Industrial Electronics*, *61*(8), 4126–4133.

Hičár, M., & Ritók, J. (2006). Robust crane control. *Acta Polytechnica Hungarica*, *3*(2), 91–101.

Hong, K.-T., Huh, C.-D., & Hong, K.-S. (2003). Command shaping control for limiting the transient sway angle of crane systems. *International Journal of Control, Automation and Systems*, *1*(1), 43–53.

Hong, K.-S., & Ngo, Q. H. (2012). Dynamics of the container crane on a mobile harbor. *Ocean Engineering*, *53*, 16–24.

Hong, K.-S., & Shah, U. H. (2019). *Advances in industrial control*, *Dynamics and control of industrial cranes*. Springer.

Hong, D., Tang, J., & Ren, G. (2011). Dynamic modeling of mass-flowing linear medium with large amplitude displacement and rotation. *Journal of Fluids and Structures*, *27*, 1137–1148.

Hu, Q., & Xu, W. (2022). AUDE-based model reference adaptive dynamic sliding mode control for overhead cranes. *International Core Journal of Engineering*, *8*(4), 16–34.

Huang, J., Xu, W., Zhao, W., & Yuan, H. (2022). An improved method for swing measurement based on monocular vision to the payload of overhead crane. *Transactions of the Institute of Measurement and Control*, *44*(1), 50–59.

Huber, O., Acary, V., & Brogliato, B. (2016). Lyapunov stability and performance analysis of the implicit discrete sliding mode control. *IEEE Transactions on Automatic Control*, *61*(10), 3016–3030.

Huston, R., & Kamman, J. (1981). A representation of fluid forces in finite segment cable models. *Computers and Structures*, *14*, 281–287.

Huston, R., & Kamman, J. (1982). Validation of finite segment cable models. *Computers and Structures*, *15*, 653–660.

Huston, R., Passerello, C., & Harlow, M. (1978). Dynamics of multi-rigid-body systems. *Journal of Applied Mechanics*, *45*, 889–894.

Ibrahim, R. (2005). *Liquid sloshing dynamics. Theory and applications*. Cambridge University Press.

Isa, A. I., Hamza, M. F., Adamu, Y. A., & Adamu, J. K. (2022). Position and swing angle control of nonlinear gantry crane system. In *Recent trends in mechatronics towards industry 4.0* (pp. 37–47). Springer.

Jaulin, L., & Walter, É. (1996). Guaranteed tuning, with application to robust control and motion planning. *Automatica*, *32*(8), 1217–1221.

Kamman, J., & Huston, R. (1985). Modeling of submerged cable dynamics. *Computers and Structures*, *20*(103), 623–629.

Kamman, J., & Huston, R. (2001). Multibody dynamics modeling of variable length cable systems. *Multibody System Dynamics*, *5*, 211–221.

Karkoub, M. A., & Zribi, M. (2001). Robust control schemes for an overhead crane. *Journal of Vibration and Control*, *7*(3), 395–416.

Khalid, A., Huey, J., Singhose, W., Lawrence, J., & Frakes, D. (2005). Human operator performance testing using an input-shaped bridge crane. *Journal of Dynamic Systems, Measurement, and Control*, *128*(4), 835–841.

Khalilpour, S. A., Khorrambakht, R., Damirchi, H., Taghirad, H. D., & Cardou, P. (2021). Tip-trajectory tracking control of a deployable cable-driven robot via output redefinition. *Multibody System Dynamics*, *52*, 31–58.

Khorshid, E., & Al-Fadhli, A. (2021). Optimal command shaping design for a liquid slosh suppression in overhead crane systems. *Journal of Dynamic Systems, Measurement, and Control*, *143*(2), Article 021005.

Kim, C., & Hong, K. (2009). Boundary control of container cranes from the perspective of controlling an axially moving string system. *International Journal of Control, Automation, and Systems*, *7*(3), 437–445.

Kim, G.-H., & Hong, K.-S. (2019). Adaptive sliding-mode control of an offshore container crane with unknown disturbances. *IEEE/ASME Transactions on Mechatronics*, *24*(6), 2850–2861.

Kim, Y.-S., Hong, K.-S., & Sul, S.-K. (2004). Anti-sway control of container cranes: inclinometer, observer, and state feedback. *International Journal of Control, Automation and Systems*, *2*(4), 435–449.

Kim, G.-H., Yoon, M., Jeon, J. Y., & Hong, K.-S. (2022). Data-driven modeling and adaptive predictive anti-swing control of overhead cranes. *International Journal of Control, Automation and Systems*, *20*(8), 2712–2723.

Kimiaghalam, B., Homaifar, A., Bikdash, M., & Dozier, G. (1999). Genetic algorithms solution for unconstrained optimal crane control. In *Proceedings of the 1999 congress on evolutionary computation, vol. 3* (pp. 2124–2130).

Klaassens, J., Honderd, G., El Azzouzi, A., Cheok, K. C., & Smid, G. (1999). 3D modeling visualization for studying controls of the jumbo container crane. In *Proceedings of the 1999 American control conference (cat. no. 99CH36251), vol. 3* (pp. 1754–1758).

Knierim, K., Krieger, K., & Sawodny, O. (2010). Flatness based control of a 3-DOF overhead crane with velocity controlled drives. *IFAC Proceedings Volumes*, *43*(18), 363–368.

Kolonic, F., Poljugan, A., & Petrovic, I. (2006). Tensor product model transformation-based controller design for gantry crane control system–an application approach. *Acta Polytechnica Hungarica*, *3*(4), 95–112.

Krupa, F., Nemcik, J., Ozana, S., & Slanina, Z. (2022). NMPC design and embedded application for overhead crane: Case study. *IFAC-PapersOnLine*, *55*(4), 356–361.

Kuo-Kai Shyu, Cheng-Lung Jen, & Li-Jen Shang (2005). Design of sliding-mode controller for anti-swing control of overhead cranes. In *31st annual conference of IEEE industrial electronics society, 2005* (pp. 147–152).

Le, H. X., Kim, T. D., Hoang, Q.-D., Pham, M. V., Nguyen, T. V., Pham, H. V., et al. (2022). Adaptive fuzzy backstepping hierarchical sliding mode control for six degrees of freedom overhead crane. *International Journal of Dynamics and Control*, *10*, 2174–2192.

Le, T. A., Kim, G.-H., Kim, M. Y., & Lee, S.-G. (2012). Partial feedback linearization control of overhead cranes with varying cable lengths. *International Journal of Precision Engineering and Manufacturing*, *13*(4), 501–507.

Le, T. A., Lee, S.-G., & Moon, S.-C. (2014). Partial feedback linearization and sliding mode techniques for 2D crane control. *Transactions of the Institute of Measurement and Control*, *36*(1), 78–87.

Le Gall, P., Prieur, C., & Rosier, L. (2007). Output feedback stabilization of a clamped-free beam. *International Journal of Control*, *80*(8), 1201–1216.

Lee, H.-H. (1998). Modeling and control of a three-dimensional overhead crane. *Journal of Dynamic Systems, Measurement, and Control*, *120*(4), 471–476.

Lee, H.-H. (2004). A new design approach for the anti-swing trajectory control of overhead cranes with high-speed hoisting. *International Journal of Control*, *77*(10), 931–940.

Lee, H.-H., & Cho, S.-K. (2001). A new fuzzy-logic anti-swing control for industrial three-dimensional overhead cranes. In *Proceedings 2001 ICRA. IEEE international conference on robotics and automation (cat. no.01CH37164), vol. 3* (pp. 2956–2961).

Lee, H.-H., Cho, S.-K., & Cho, J.-S. (1997). A new anti-swing control of overhead cranes. *IFAC Proceedings Volumes*, *30*(13), 115–120.

Lee, S.-G., Dang, V.-H., Moon, S., Kim, B., et al. (2013). Partial feedback linearization control of a three-dimensional overhead crane. *International Journal of Control, Automation and Systems*, *11*(4), 718–727.

Lee, L.-H., Huang, C.-H., Ku, S.-C., Yang, Z.-H., & Chang, C.-Y. (2014). Efficient visual feedback method to control a three-dimensional overhead crane. *IEEE Transactions on Industrial Electronics*, *61*(8), 4073–4083.

Lee, H.-H., Liang, Y., & Segura, D. (2006). A sliding-mode antiswing trajectory control for overhead cranes with high-speed load hoisting. *Journal of Dynamic Systems, Measurement and Control*, *128*(4), 842–845.

Lhachemi, H., Prieur, C., & Trélat, E. (2022). Proportional integral regulation control of a one-dimensional semilinear wave equation. *SIAM Journal on Control and Optimization*, *60*(1), 1–21.

Li, M., Chen, H., & Zhang, R. (2022). An input dead zones considered adaptive fuzzy control approach for double pendulum cranes with variable rope lengths. *IEEE/ASME Transactions on Mechatronics*, *27*(5), 3385–3396.

Li, G., Ma, X., Li, Z., & Li, Y. (2022). Optimal trajectory planning strategy for underactuated overhead crane with pendulum-sloshing dynamics and full-state constraints. *Nonlinear Dynamics*, *109*, 815–835.

Liang, Y., & Koh, K. (1997). Concise anti-swing approach for fuzzy crane control. *Electronics Letters*, *33*(2), 167–168.

Lin, F., Chou, P., Chen, C., & Lin, Y. (2012). Three-degree-of-freedom dynamic model-based intelligent nonsingular terminal sliding mode control for a gantry position stage. *IEEE Transactions on Fuzzy Systems*, *20*(5), 971–985.

Liu, R., Li, S., & Ding, S. (2012). Nested saturation control for overhead crane systems. *Transactions of the Institute of Measurement and Control*, *34*(7), 862–875.

Liu, Y., & Yu, H. (2013). A survey of underactuated mechanical systems. *IET Control Theory & Applications*, *7*(7), 921–935.

Lozano, R., & Brogliato, B. (1992). Adaptive control of robot manipulators with flexible joints. *IEEE Transactions on Automatic Control*, *37*(2), 174–181.

Lu, B., Fang, Y., & Sun, N. (2017a). Enhanced-coupling adaptive control for double-pendulum overhead cranes with payload hoisting and lowering. *Automatica*, *101*, 241–251.

Lu, B., Fang, Y., & Sun, N. (2017b). Sliding mode control for underactuated overhead cranes suffering from both matched and unmatched disturbances. *Mechatronics*, *47*, 116–125.

Lu, B., Fang, Y., & Sun, N. (2018). Nonlinear control for underactuated multi-rope cranes: Modeling, theoretical design and hardware experiments. *Control Engineering Practice*, *76*, 123–132.

Lv, N., Liu, J., & Jia, Y. (2021). Coordinated control of flexible cables with human-like dual manipulators. *Transactions of the ASME. Journal of Dynamic Systems, Measurement and Control*, *143*, Article 081006.

Lv, N., Liu, J., Xia, H., Ma, J., & Yang, X. (2020). A review of techniques for modeling flexible cables. *Computer-Aided Design*, *122*, Article 102826.

Ma, L., Lou, X., & Jia, J. (2023). Neural-network-based boundary control for a gantry crane system with unknown friction and output constraint. *Neurocomputing*, *518*, 271–281.

Ma, L., Lou, X., Wu, W., & Huang, X. (2022). Neural network-based boundary control of a gantry crane system subject to input deadzone and external disturbance. *Nonlinear Dynamics*, *108*, 3449–3466.

Maghsoudi, M. J., Mohamed, Z., Husain, A., & Tokhi, M. (2016). An optimal performance control scheme for a 3D crane. *Mechanical Systems and Signal Processing*, *66–67*, 7F56–768.

Maghsoudi, M. J., Mohamed, Z., Sudin, S., Buyamin, S., Jaafar, H., & Ahmad, S. (2017). An improved input shaping design for an efficient sway control of a nonlinear 3D overhead crane with friction. *Mechanical Systems and Signal Processing*, *92*, 364–378.

Manson, G. A. (1982). Time-optimal control of an overhead crane model. *Optimal Control Applications & Methods*, *3*(2), 115–120.

Merlet, J. (2017). Simulation of discrete-time controlled cable-driven parallel robots on a trajectory. *IEEE Transactions on Robotics*, *33*(3), 675–688.

Miao, X., Zhao, B., Wang, L., & Ouyang, H. (2022). Trolley regulation and swing reduction of underactuated double-pendulum overhead cranes using fuzzy adaptive nonlinear control. *Nonlinear Dynamics*, *109*, 837–847.

Mohamed, K. T., Abdel-razak, M. H., Haraz, E. H., & Ata, A. A. (2022). Fine tuning of a PID controller with inlet derivative filter using Pareto solution for gantry crane systems. *Alexandria Engineering Journal*, *61*(9), 6659–6673.

Mojallizadeh, M. R., Brogliato, B., & Acary, V. (2021). Time-discretizations of differentiators: Design of implicit algorithms and comparative analysis. *International Journal of Robust and Nonlinear Control*, *31*(16), 7679–7723.

Mojallizadeh, M. R., Brogliato, B., & Prieur, C. (2022). *Modeling and control of overhead cranes: a survey*: *Technical report*, INRIA Grenoble-Alpes, https://hal.inria.fr/hal-03817363.

Moon, S.-C., Lee, W. G., Lee, S.-G., et al. (2013). Adaptive sliding mode control of overhead cranes with varying cable length. *Journal of Mechanical Science and Technology*, *27*(3), 885–893.

Morrish, L., Cartmell, M. P., & Taylor, A. J. (1996). Cable stretch asymmetries in multi-cable spreader suspension systems undergoing combined translations and rotations. *Proceedings of the Institution of Mechanical Engineers, Part C (Mechanical Engineering Science)*, *210*(3), 225–237.

Morrish, L., Cartmell, M. P., & Taylor, A. J. (1997). Geometry and kinematics of multicable spreader lifting gear. *Proceedings of the Institution of Mechanical Engineers, Part C (Mechanical Engineering Science)*, *211*(3), 185–194.

Moustafa, K. A. F. (1994). Feedback control of overhead cranes swing with variable rope length. In *Proceedings of 1994 American control conference, vol. 1* (pp. 691–695 vol.1).

Nayfeh, N. A., & Baumann, W. T. (2008). Nonlinear analysis of time-delay position feedback control of container cranes. *Nonlinear Dynamics*, *53*(1), 75–88.

Nayfeh, N., Masoud, Z., & Baumann, W. (2005). A comparison of three feedback controllers for container cranes. In *International design engineering technical conferences and computers and information in engineering conference*: *vol. 6*, *5th international conference on multibody systems, nonlinear dynamics, and control, Parts A, B, and C* (pp. 935–945).

Ngo, Q., & Hong, K.-S. (2012). Adaptive sliding mode control of container cranes. *IET Control Theory & Applications*, *6*(5), 662–668.

Ngo, Q. H., & Hong, K. (2012). Sliding-mode antisway control of an offshore container crane. *IEEE/ASME Transactions on Mechatronics*, *17*(2), 201–209.

Ngo, Q. H., Hong, K.-S., Kim, K. H., Shin, Y. J., & Choi, S.-H. (2008). Skew control of a container crane. In *2008 international conference on control, automation and systems* (pp. 1490–1494).

Nguyen, T. M., Do, T. H., & Duong, M. D. (2022). Anti-sway and position control for double-pendulum crane using IS-ADRC controller. *Measurement, Control, and Automation*, *3*(1), 3–9.

d'Andréa Novel, B., Boustany, F., Conrad, F., & Rao, B. (1994). Feedback stabilization of a hybrid PDE-ODE system: Application to an overhead crane. *Mathematics of Control, Signals, and Systems*, *7*(1), 1–22.

d'Andrea Novel, B., Boustany, F., & Rao, B. (1991). Control of an overhead crane: Feedback stabilization of a hybrid PDE-ODE system. In *Proceedings of the 1st European control conference, vol. 91* (pp. 2244–2249).

d'Andréa Novel, B., & Coron, J.-M. (2002). Stabilization of an overhead crane with a variable length flexible cable stabilization of an overhead crane with a variable length flexible cable. *Computational & Applied Mathematics*, *21*(1), 101–134.

d'Andréa Novel, B., Moyano, I., & Rosier, L. (2019). Finite-time stabilization of an overhead crane with a flexible cable. *Mathematics of Control, Signals, and Systems*, *31*(2), 1–19.

Oguamanam, D., Hansen, J., & Heppler, G. (1998). Dynamic response of an overhead crane system. *Journal of Sound and Vibration*, *213*(5), 889–906.

Oguamanam, D., Hansen, J., & Heppler, G. (2001). Dynamics of a three-dimensional overhead crane system. *Journal of Sound and Vibration*, *242*(3), 411–426.

Ohnishi, E., Tsuboi, I., Egusa, T., & Uesugi, M. (1981). Automatic control of an overhead crane. *IFAC Proceedings Volumes*, *14*(2), 1885–1890.

Omar, H. M. (2003). *Control of gantry and tower cranes* (Ph.D. thesis), Virginia Tech.

Omar, H. M., & Nayfeh, A. H. (2005). Gantry cranes gain scheduling feedback control with friction compensation. *Journal of Sound and Vibration*, *281*(1), 1–20.

Orsini, V. (2022). An inversion-based feedback/feedforward control for robust and precise payload positioning in gantry crane systems. *Asian Journal of Control*, http://dx.doi.org/10.1002/asjc.2811.

Ouyang, H., Hu, J., Zhang, G., Mei, L., & Deng, X. (2019). Decoupled linear model and S-shaped curve motion trajectory for load sway reduction control in overhead cranes with double-pendulum effect. *Proceedings of the Institution of Mechanical Engineers, Part C (Mechanical Engineering Science)*, *233*(10), 3678–3689.

Ouyang, H., Hu, J., Zhang, G., Mei, L., & Deng, X. (2019). Sliding-mode-based trajectory tracking and load sway suppression control for double-pendulum overhead cranes. *IEEE Access*, *7*, 4371–4379.

Ouyang, H., Wang, J., Zhang, G., Mei, L., & Deng, X. (2019). Novel adaptive hierarchical sliding mode control for trajectory tracking and load sway rejection in double-pendulum overhead cranes. *IEEE Access*, *7*, 10353–10361.

Ouyang, H., Zhao, B., & Zhang, G. (2021). Swing reduction for double-pendulum three-dimensional overhead cranes using energy-analysis-based control method. *International Journal of Robust and Nonlinear Control*, *31*(9), 4184–4202.

Ovseevich, A., & Ananievski, I. (2021). Robust feedback control for a linear chain of oscillators. *Journal of Optimization Theory and Applications*, *188*(1), 307–316.

Ovseevich, A. I., & Fedorov, A. K. (2015). Feedback control for damping a system of linear oscillators. *Automation and Remote Control*, *76*(11), 1905–1917.

Park, M., Chwa, D., & Eom, M. (2014). Adaptive sliding-mode antisway control of uncertain overhead cranes with high-speed hoisting motion. *IEEE Transactions on Fuzzy Systems*, *22*(5), 1262–1271.

Park, H., Chwa, D.-K., & Hong, K.-S. (2007). A feedback linearization control of container cranes: Varying rope length. *International Journal of Control, Automation and Systems*, *5*(4), 379–387.

Park, M., Chwa, D., & Hong, S. (2008). Antisway tracking control of overhead cranes with system uncertainty and actuator nonlinearity using an adaptive fuzzy sliding-mode control. *IEEE Transactions on Industrial Electronics*, *55*(11), 3972–3984.

Parker, G. G., Robinett, R. D., III, Driessen, B. J., & Dohrmann, C. R. (1996). Operator in-the-loop control of rotary cranes. In C. R. Crowe (Ed.), *Smart structures and materials 1996: Industrial and commercial applications of smart structures technologies, vol. 2721* (pp. 364–372). International Society for Optics and Photonics, SPIE.

Peng, K. C. C., Singhose, W., & Bhaumik, P. (2012). Using machine vision and hand-motion control to improve crane operator performance. *IEEE Transactions on Systems, Man, and Cybernetics - Part A: Systems and Humans*, *42*(6), 1496–1503.

Pesce, C. (2003). The application of Lagrange equations to mechanical systems with mass explicitly dependent on position. *ASME Journal of Applied Mechanics*, *70*, 751–756.

Pesce, C., & Casetta, L. (2007). Variable mass systems dynamics in engineering mechanics education. In *Proceedings of COBEM 2007, 19th international congress of mechanical engineering*.

Pesce, C., Tannuri, E., & Casetta, L. (2006). The Lagrange equations for systems with mass varying explicitly with position: Some applications to offshore engineering. *Journal of Brazilian Society of Mechanical Sciences and Engineering*, *28*(4), 496–504.

Pham, H. V., Hoang, Q.-D., Pham, M. V., Do, D. M., Phi, N. H., Hoang, D., et al. (2022). An efficient adaptive fuzzy hierarchical sliding mode control strategy for 6 degrees of freedom overhead crane. *Electronics*, *11*(5), 713.

Piazzi, A., & Marro, G. (1996). Robust stability using interval analysis. *International Journal of Systems Science*, *27*(12), 1381–1390.

Piazzi, A., & Visioli, A. (2002). Optimal dynamic-inversion-based control of an overhead crane. *IEE Proceedings D (Control Theory and Applications)*, *149*(6), 405–411.

Picard, E., Caro, S., Claveau, F., & Plestan, F. (2018). Pulleys and force sensors influence on payload estimation of cable-driven parallel robots. In *2018 IEEE/RSJ international conference on intelligent robots and systems* (pp. 1429–1436).

Picard, E., Caro, S., Plestan, F., & Claveau, F. (2018). Control solution for a cable-driven parallel robot with highly variable payload. In *Int. design engineering technical conferences and computers and information in engineering conference*: *vol. 5B, Proc. 42nd mechanisms and robotics conference*. paper no DETC2018-85304, V05BT07A013.

Prieur, C., Tarbouriech, S., & Gomes da Silva, J. M., Jr. (2016). Wave equation with cone-bounded control laws. *IEEE Transactions on Automatic Control*, *61*(11), 3452–3463.

Qian, D., & Yi, J. (2016). *Hierarchical sliding mode control for under-actuated cranes. design, analysis and simulation*. Springer.

Quan, W., & Chang, Q. (2020). Variable-length cable dynamics of payout reel-in with a vertically tethered underwater drill rig. *IEEE Access*, *8*, 66625–66636.

R. L. Kress, J. F. J., & Noakes, M. W. (1994). Experimental implementation of a robust damped-oscillation control algorithm on a full-sized, two-degree-of-freedom, ac induction motor-driven crane. In *5th int. symp. robotics and manufacturing* (pp. 585–592).

Ramli, L., Mohamed, Z., Abdullahi, A., Jaafar, H., & Lazim, I. (2017). Control strategies for crane systems: A comprehensive review. *Mechanical Systems and Signal Processing*, *95*, 1–23.

Rauscher, F., & Sawodny, O. (2021). Modeling and control of tower cranes with elastic structure. *IEEE Transactions on Control Systems Technology*, *29*(1), 64–79.

Ren, Y., Chen, M., & Wu, Q. (2019). Disturbance observer-based boundary control for a suspension cable system moving in the horizontal plane. *Transactions of the Institute of Measurement and Control*, *41*(2), 340–349.

Reyhanoglu, M., van der Schaft, A., McClamroch, N., & Kolmanovsky, I. (1999). Dynamics and control of a class of underactuated mechanical systems. *IEEE Transactions on Automatic Control*, *44*(9), 1663–1671.

Romero, J. G., Gandarilla, I., Santibáñez, V., & Yi, B. (2022). A constructive procedure for orbital stabilization of a class of underactuated mechanical systems. *IEEE Transactions on Control Systems Technology*, *30*(6), 2698–2706.

Sakawa, Y., & Shindo, Y. (1982). Optimal control of container cranes. *Automatica*, *18*(3), 257–266.

Sano, H., Ohishi, K., Kaneko, T., & Mine, H. (2010). Anti-sway crane control based on dual state observer with sensor-delay correction. In *2010 11th IEEE international workshop on advanced motion control* (pp. 679–684).

Sawodny, O., Aschemann, H., & Lahres, S. (2002). An automated gantry crane as a large workspace robot. *Control Engineering Practice*, *10*(12), 1323–1338.

Schindele, D., & Aschemann, H. (2011). Fast nonlinear MPC for an overhead travelling crane. *IFAC Proceedings Volumes*, *44*(1), 7963–7968.

Servin, M., & Lacoursière, C. (2008). Rigid body cable for virtual environments. *IEEE Transactions on Visualization and Computer Graphics*, *14*(4), 783–796.

Shao, X., Zhang, J., Zhang, X., Zhao, Z., & Chen, Z. (2020). A novel anti-swing and position control method for overhead crane. *Science Progress*, *103*(1), 1–24.

Shehu, M. A., Li, A., & Zeng, Y. (2022). Sliding mode control of non-linear double-pendulum overhead cranes with prescribed trolley convergence. In *Advances in guidance, navigation and control* (pp. 3217–3229). Springer.

Shen, P., & Caverly, R. J. (2020). Noncolocated passivity-based control of a 2 DOF tower crane with a flexible hoist cable. In *2020 American control conference* (pp. 5046–5051).

Shen, P.-Y., Schatz, J., & Caverly, R. J. (2021). Passivity-based adaptive trajectory control of an underactuated 3-DOF overhead crane. *Control Engineering Practice*, *112*, Article 104834.

Shi, H., Li, G., Ma, X., & Sun, J. (2019). Research on nonlin- ear coupling anti-swing control method of double pendu- lum gantry crane based on improved energy. *Symmetry*, *11*(12), 1511.

Shi, H., Yao, F., Yuan, Z., Hu, Y., Zhang, K., & Fu, L. (2022). Enhanced-coupling-based tracking control of double pendulum gantry cranes. *International Journal of Control, Automation and Systems*, 1–13.

Shi, H., Yao, F., Yuan, Z., Tong, S., Tang, Y., & Han, G. (2022). Research on nonlinear coupled tracking controller for double pendulum gantry cranes with load hoisting/lowering. *Nonlinear Dynamics*, *108*, 223–238.

Shih, M. (2022). Applications of reinforcement learning to effectively and safely control a gantry crane. *Princeton University Senior Theses 2022*.

Singhose, W., Kim, D., & Kenison, M. (2008). Input shaping control of double-pendulum bridge crane oscillations. *Journal of Dynamic Systems, Measurement, and Control*, *130*(3), Article 034504.

Singhose, W., Porter, L., Kenison, M., & Kriikku, E. (2000). Effects of hoisting on the input shaping control of gantry cranes. *Control Engineering Practice*, *8*(10), 1159–1165.

Singhose, W. E., Porter, L. J., & Seering, W. P. (1997). Input shaped control of a planar gantry crane with hoisting. In *Proceedings of the 1997 American control conference, vol. 1* (pp. 97–100).

Singhose, W., Seering, W., & Singer, N. (1990). Shaping inputs to reduce vibration: a vector diagram approach. In *Proceedings., IEEE international conference on robotics and automation, vol. 2* (pp. 922–927).

Slemrod, M. (1989). Feedback stabilization of a linear control system in Hilbert space with an a priori bounded control. *Mathematics of Control, Signals, and Systems*, *2*(3), 265–285.

Smoczek, J., & Szpytko, J. (2017). Particle swarm optimization-based multivariable generalized predictive control for an overhead crane. *IEEE/ASME Transactions on Mechatronics*, *22*(1), 258–268.

Smoczek, J., Szpytko, J., & Hyla, P. (2012). The application of an intelligent crane control system. *IFAC Proceedings Volumes*, *45*(24), 280–285.

Sonneville, V., & Brüls, O. (2014). Geometrically exact beam finite element formulated on the special Euclidean group $SE(3)$. *Computer Methods in Applied Mechanics and Engineering*, *268*, 451–474.

Spong, M. (1994). Partial feedback linearization of underactuated mechanical systems. *1*, In *Proceedings of IEEE/RSJ international conference on intelligent robots and systems, vol. 1* (pp. 314–321).

Sun, N., & Fang, Y. (2012). New energy analytical results for the regulation of underactuated overhead cranes: An end-effector motion-based approach. *IEEE Transactions on Industrial Electronics*, *59*(12), 4723–4734.

Sun, N., & Fang, Y. (2014a). An efficient online trajectory generating method for underactuated crane systems. *International Journal of Robust and Nonlinear Control*, *24*(11), 1653–1663.

Sun, N., & Fang, Y. (2014b). Nonlinear tracking control of underactuated cranes with load transferring and lowering: Theory and experimentation. *Automatica*, *50*, 2350–2357.

Sun, N., Fang, Y., Chen, H., & He, B. (2015). Adaptive nonlinear crane control with load hoisting/lowering and unknown parameters: Design and experiments. *IEEE/ASME Transactions on Mechatronics*, *20*(5), 2107–2119.

Sun, N., Fang, Y., Chen, H., & Lu, B. (2017). Amplitude-saturated nonlinear output feedback antiswing control for underactuated cranes with double-pendulum cargo dynamics. *IEEE Transactions on Industrial Electronics*, *64*(3), 2135–2146.

Sun, N., Fang, Y., & Zhang, X. (2012). An increased coupling-based control method for underactuated crane systems: theoretical design and experimental implementation. *Nonlinear Dynamics*, *70*(2), 1135–1146.

Sun, N., Fang, Y., & Zhang, X. (2013). Energy coupling output feedback control of 4-DOF underactuated cranes with saturated inputs. *Automatica*, *49*(5), 1318–1325.

Sun, N., Fang, Y., Zhang, Y., & Ma, B. (2012). A novel kinematic coupling-based trajectory planning method for overhead cranes. *IEEE/ASME Transactions on Mechatronics*, *17*(1), 166–173.

Sun, N., Wu, Y., Chen, H., & Fang, Y. (2018). An energy-optimal solution for transportation control of cranes with double pendulum dynamics: Design and experiments. *Mechanical Systems and Signal Processing*, *102*, 87–101.

Sun, N., Wu, Y., Fang, Y., & Chen, H. (2018). Nonlinear antiswing control for crane systems with double-pendulum swing effects and uncertain parameters: Design and experiments. *IEEE Transactions on Automation Science and Engineering*, *15*(3), 1413–1422.

Sun, X., & Xie, Z. (2020). Reinforcement learning-based backstepping control for container cranes. *Mathematical Problems in Engineering*, *2020*.

Sun, N., Yang, T., Fang, Y., Wu, Y., & Chen, H. (2019). Transportation control of double-pendulum cranes with a nonlinear quasi-PID scheme: Design and experiments. *IEEE Transactions on Systems, Man, and Cybernetics: Systems*, *49*(7), 1408–1418.

Sun, N., Zhang, J., Xin, X., Yang, T., & Fang, Y. (2019). Nonlinear output feedback control of flexible rope crane systems with state constraints. *IEEE Access*, *7*, 136193–136202.

Tafrishi, S., Svinin, M., & Yamamoto, M. (2021). Inverse dynamics of underactuated planar manipulators without inertial couplings singularities. *Multibody System Dynamics*, *52*, 407–429.

Tang, R., & Huang, J. (2016). Control of bridge cranes with distributed-mass payloads under windy conditions. *Mechanical Systems and Signal Processing*, *72–73*, 409–419.

Tomei, P. (1991). A simple PD controller for robots with elastic joints. *IEEE Transactions on Automatic Control*, *36*(10), 1208–1213.

Toxqui, R., Yu, W., & Li, X. (2006). Anti-swing control for overhead crane with neural compensation. In *The 2006 IEEE international joint conference on neural network proceedings* (pp. 4697–4703). IEEE.

Tran, V. P., Santoso, F., Garrat, M. A., & Anavatti, S. G. (2021a). Neural network-based self-learning of an adaptive strictly negative imaginary tracking controller for a quadrotor transporting a cable-suspended payload with minimum swing. *IEEE Transactions on Industrial Electronics*, *68*(10), 10258–10268.

Tran, V. P., Santoso, F., Garratt, M. A., & Anavatti, S. G. (2021b). Distributed artificial neural networks-based adaptive strictly negative imaginary formation controllers for unmanned aerial vehicles in time-varying environments. *IEEE Transactions on Industrial Informatics*, *17*(6), 3910–3919.

Tran, V. P., Santoso, F., Garratt, M. A., & Petersen, I. R. (2020). Adaptive second-order strictly negative imaginary controllers based on the interval type-2 fuzzy self-tuning systems for a hovering quadrotor with uncertainties. *IEEE/ASME Transactions on Mechatronics*, *25*(1), 11–20.

Tuan, L. A., Kim, G.-H., & Lee, S.-G. (2012). Partial feedback linearization control of the three dimensional overhead crane. In *2012 IEEE international conference on automation science and engineering* (pp. 1198–1203).

Tuan, L. A., & Lee, S.-G. (2013). Sliding mode controls of double-pendulum crane systems. *Journal of Mechanical Science and Technology*, *27*(6), 1863–1873.

Tuan, L. A., Lee, S.-G., Ko, D. H., & Nho, L. C. (2014). Combined control with sliding mode and partial feedback linearization for 3D overhead cranes. *International Journal of Robust and Nonlinear Control*, *24*(18), 3372–3386.

Ubertini, F. (2008). Active feedback control for cable vibrations. *Smart Structures and Systems*, *4*(4), 407–428.

Vaughan, J., Karajgikar, A., & Singhose, W. (2011). A study of crane operator performance comparing PD-control and input shaping. In *Proceedings of the 2011 American control conference* (pp. 545–550).

Vaughan, J., Kim, D., & Singhose, W. (2010). Control of tower cranes with double-pendulum payload dynamics. *IEEE Transactions on Control Systems Technology*, *18*(6), 1345–1358.

Vaughan, J., Maleki, E., & Singhose, W. (2010). Advantages of using command shaping over feedback for crane control. In *Proceedings of the 2010 American control conference* (pp. 2308–2313).

Vazquez, C., & Collado, J. (2009). Optimal delayed control for an overhead crane. In *2009 6th international conference on electrical engineering, computing science and automatic control* (pp. 1–6).

Vázquez, C., Collado, J., & Fridman, L. (2014). Super twisting control of a parametrically excited overhead crane. *Journal of the Franklin Institute*, *351*(4), 2283–2298.

Vu, M., Lobe, A., Beck, F., Weingartshofer, T., Hartl-Nesic, C., & Kugi, A. (2022). Fast trajectory planning and control of a lab-scale 3D gantry crane for a moving target in an environment with obstacles. *Control Engineering Practice*, *126*, Article 105255.

Vyhlídal, T., Kučera, V., & Hromčík, M. (2013). Signal shaper with a distributed delay: Spectral analysis and design. *Automatica*, *49*(11), 3484–3489.

Wahrburg, A., Jurvanen, J., Niemelä, M., & Holmberg, M. (2022a). Input shaping for non-zero initial conditions and arbitrary input signals with an application to overhead crane control. In *2022 IEEE 17th international conference on advanced motion control* (pp. 36–41).

Wahrburg, A., Jurvanen, J., Niemelä, M., & Holmberg, M. (2022b). On reference trajectory generation for overhead crane travel movements. *At-Automatisierungstechnik*, *70*(3), 300–311.

Wang, X., Liu, C., He, Z., et al. (2022). A parameters adaptive non-singular terminal sliding mode control method for overhead crane system. *International Journal of Frontiers in Engineering Technology*, *4*(3), 42–48.

Wang, T., Tan, N., Qiu, J., Yu, Y., Zhang, X., Zhai, Y., et al. (2021). Global-equivalent sliding mode control method for bridge crane. *IEEE Access*, *9*, 160372–160382.

Wang, T., Tan, N., Zhang, X., Li, G., Su, S., Zhou, J., et al. (2021). A time-varying sliding mode control method for distributed-mass double pendulum bridge crane with variable parameters. *IEEE Access*, *9*, 75981–75992.

Wang, L., Wu, X., & Lei, M. (2022). Feedforward-control-based nonlinear control for overhead cranes with matched and unmatched disturbances. *Proceedings of the Institution of Mechanical Engineers, Part C (Mechanical Engineering Science)*, *236*(11), 5785–5795.

Wei, L., Limin, T., & Zhengnan, J. (2017). Research on anti-swing characteristic of redundancy cable-driven parallel robot. In *2017 IEEE 2nd advanced information technology, electronic and automation control conference* (pp. 1504–1508).

Weiping, G., Diantong, L., Jianqiang, Y., & Dongbin, Z. (2004). Passivity-based-control for double-pendulum-type overhead cranes. In *2004 IEEE region 10 conference, vol. 4* (pp. 546–549).

Wen, T., Fang, Y., & Lu, B. (2022). Neural network-based adaptive sliding mode control for underactuated dual overhead cranes suffering from matched and unmatched disturbances. *Autonomous Intelligent Systems*, *2*(1), 1–15.

Wen, Y., Lou, X., Wu, W., & Cui, B. (2022). Backstepping boundary control for a class of gantry crane systems. *IEEE Transactions on Cybernetics*, http://dx.doi.org/10.1109/TCYB.2022.3188494.

Wen, J., Popa, D., Montemayor, G., & Liu, P. (2001). Human assisted impedance control of overhead cranes. In *Proceedings of the 2001 IEEE international conference on control applications (cat. no.01CH37204)* (pp. 383–387).

Wijnand, M., d´Andréa-Novel, B., & Rosier, L. (2021). Finite-time stabilization of an overhead crane with a flexible cable submitted to an affine tension. *ESAIM. Control, Optimisation and Calculus of Variations*, *27*, 94.

Winget, J., & Huston, R. (1981). Cable dynamics–A finite segment appraoch. *Computers and Structures*, *6*, 475–480.

Wu, X., & He, X. (2015). Enhanced damping-based anti-swing control method for underactuated overhead cranes. *IET Control Theory & Applications*, *9*(12), 1893–1900.

Wu, X., & He, X. (2016). Partial feedback linearization control for 3-D underactuated overhead crane systems. *ISA Transactions*, *65*, 361–370.

Wu, X., & He, X. (2017). Nonlinear energy-based regulation control of three-dimensional overhead cranes. *IEEE Transactions on Automation Science and Engineering*, *14*(2), 1297–1308.

Wu, X., He, X., Sun, N., & Fang, Y. (2014). A novel anti-swing control method for 3-D overhead cranes. In *2014 American control conference* (pp. 2821–2826).

Wu, T., Karkoub, M., Wang, H., Chen, H., & Chen, T. (2017). Robust tracking control of MIMO underactuated nonlinear systems with dead-zone band and delayed uncertainty using an adaptive fuzzy control. *IEEE Transactions on Fuzzy Systems*, *25*(4), 905–918.

Wu, Z., & Xia, X. (2014). Optimal motion planning for overhead cranes. *IET Control Theory & Applications*, *8*, 1833–1842(9).

Wu, Z., Xia, X., & Zhu, B. (2015). Model predictive control for improving operational efficiency of overhead cranes. *Nonlinear Dynamics*, *79*(4), 2639–2657.

Wu, X., Xu, K., & He, X. (2020). Disturbance-observer-based nonlinear control for overhead cranes subject to uncertain disturbances. *Mechanical Systems and Signal Processing*, *139*, Article 106631.

Xi, Z., & Hesketh, T. (2010). Discrete time integral sliding mode control for overhead crane with uncertainties. *IET Control Theory & Applications*, *4*, 2071–2081(10).

Xing, X., Yang, H., & Liu, J. (2020). Vibration control for nonlinear overhead crane bridge subject to actuator failures and output constraints. *Nonlinear Dynamics*, *101*(1), 419–438.

Yang, J., & Yang, K. (2006). Adaptive control for 3-D overhead crane systems. In *2006 American control conference*.

Yi, J., Yubazaki, N., & Hirota, K. (2003). Anti-swing and positioning control of overhead traveling crane. *Information Sciences*, *155*(1–2), 19–42.

Yoon, J., Nation, S., Singhose, W., & Vaughan, J. (2014). Control of crane payloads that bounce during hoisting. *IEEE Transactions on Control Systems Technology*, *22*(3), 1233–1238.

Yoon, J., Singhose, W., Vaughan, J., Ramirez, G., Kim, M., & Tawde, S. (2010). Dynamics and control of crane payloads that bounce and pitch during hoisting. In *Proc. ASME int. des. eng. tech. conf. comput. inf. eng. conf. DETC2009* (pp. 871–880).

Yoshida, K., & Kawabe, H. (1992). A design of saturating control with a guaranteed cost and its application to the crane control system. *IEEE Transactions on Automatic Control*, *37*(1), 121–127.

Yoshida, Y., & Tabata, H. (2008). Visual feedback control of an overhead crane and its combination with time-optimal control. In *2008 IEEE/ASME international conference on advanced intelligent mechatronics* (pp. 1114–1119). IEEE.

Yu, J., Lewis, F. L., & Huang, T. (1995). Nonlinear feedback control of a gantry crane. *6*, In *Proceedings of 1995 American control conference, vol. 6* (pp. 4310–4315).

Yu, Z., & Niu, W. (2023). Flatness-based backstepping antisway control of underactuated crane systems under wind disturbance. *Electronics*, *12*(1).

Zake, Z., Chaumette, F., Pedemonte, N., & Caro, S. (2019). Vision-based control and stability analysis of a cable-driven parallel robot. *IEEE Robotics and Automation Letters*, *4*(2), 1029–1036.

Zake, Z., Chaumette, F., Pedemonte, N., & Caro, S. (2021). Visual servoing of cable-driven parallel robots with tension management. In *2021 IEEE international conference on robotics and automation* (pp. 6861–6867).

Zhang, M. (2019). Finite-time model-free trajectory tracking control for overhead cranes subject to model uncertainties, parameter variations and external disturbances. *Transactions of the Institute of Measurement and Control*, *41*(12), 3516–3525.

Zhang, X., Fang, Y., & Sun, N. (2014). Minimum-time trajectory planning for underactuated overhead crane systems with state and control constraints. *IEEE Transactions on Industrial Electronics*, *61*(12), 6915–6925.

Zhang, S., He, X., & Chen, Q. (2020). Energy coupled–dissipation control for 3-dimensional overhead cranes. *Nonlinear Dynamics*, *99*(3), 2097–2107.

Zhang, S., He, X., Chen, Q., & Feng, Y. (2020). Improved energy dissipation control of overhead cranes. *Asian Journal of Control*, *22*(4), 1729–1735.

Zhang, S., He, X., Chen, Q., & Zhu, Z. (2019). Partially saturated coupling-based control for underactuated overhead cranes with experimental verification. *Mechatronics*, *63*, Article 102284.

Zhang, S., He, X., Zhu, H., Chen, Q., & Feng, Y. (2020). Partially saturated coupled-dissipation control for underactuated overhead cranes. *Mechanical Systems and Signal Processing*, *136*, Article 106449.

Zhang, S., He, X., Zhu, H., Li, X., & Liu, X. (2022). PID-like coupling control of underactuated overhead cranes with input constraints. *Mechanical Systems and Signal Processing*, *178*, Article 109274.

Zhang, M., Ma, X., Rong, X., Song, R., Tian, X., & Li, Y. (2018). An enhanced coupling nonlinear tracking controller for underactuated 3D overhead crane systems. *Asian Journal of Control*, *20*(5), 1839–1854.

Zhang, M., Ma, X., Rong, X., Tian, X., & Li, Y. (2016). Adaptive tracking control for double-pendulum overhead cranes subject to tracking error limitation, parametric uncertainties and external disturbances. *Mechanical Systems and Signal Processing*, *76–77*, 15–32.

Zhang, M., Ma, X., Rong, X., Tian, X., & Li, Y. (2017). Error tracking control for underactuated overhead cranes against arbitrary initial payload swing angles. *Mechanical Systems and Signal Processing*, *84*, 268–285.

Zhang, Z., Wu, Y., & Huang, J. (2017). Differential-flatness-based finite-time anti-swing control of underactuated crane systems. *Nonlinear Dynamics*, *87*, 1749–1761.

Zhang, H., Zhao, C., & Ding, J. (2022). Online reinforcement learning with passivity-based stabilizing term for real time overhead crane control without knowledge of the system model. *Control Engineering Practice*, *127*, Article 105302.

Zhang, S., Zhu, H., He, X., Feng, Y., & Pang, C. K. (2022). Passivity-based coupling control for underactuated three-dimensional overhead cranes. *ISA Transactions*, *126*, 352–360.

Zhao, Y., & Gao, H. (2012). Fuzzy-model-based control of an overhead crane with input delay and actuator saturation. *IEEE Transactions on Fuzzy Systems*, *20*(1), 181–186.

Zhao, B., Ouyang, H., & Iwasaki, M. (2021). Motion trajectory tracking and sway reduction for double-pendulum overhead cranes using improved adaptive control without velocity feedback. *IEEE/ASME Transactions on Mechatronics*, 1–10.

Zhu, X., & Wang, N. (2022). Hairpin RNA genetic algorithm based ANFIS for modeling overhead cranes. *Mechanical Systems and Signal Processing*, *165*, Article 108326.

Zhu, X., & Xu, W. (2023). Nonlinear time-varying sliding mode synchronous control of double-lift overhead cranes under unknown disturbances. *Transactions of the Institute of Measurement and Control*, *45*(1), 181–194.